West Pakistan Water and Power Development Authority

SERVICE GATES FOR TUNNELS 3 AND 4 HYDRAULIC MODEL STUDY

TARBELA DAM PROJECT
INDUS RIVER
WEST PAKISTAN

PREPARED FOR
TIPPETTS-ABBETT-McCARTHY-STRATTON
NEW YORK, NEW YORK

CIVIL ENGINEERING DEPARTMENT
ENGINEERING RESEARCH CENTER
COLORADO STATE UNIVERSITY
FORT COLLINS, COLORADO

SEPTEMBER, 1972

CER 71-72 SK34

FINAL REPORT OF THE
HYDRAULIC MODEL STUDIES OF
THE SERVICE GATES FOR
TUNNELS 3 AND 4

WEST PAKISTAN WATER AND POWER DEVELOPMENT AUTHORITY
TARBELA DAM PROJECT
INDUS RIVER
WEST PAKISTAN

Prepared for

Tippetts-Abbett-McCarthy-Stratton
New York, New York

by

S. Karaki

Colorado State University
Engineering Research Center
Civil Engineering Department
Fort Collins, Colorado

September 1972

TABLE OF CONTENTS

TABLE OF CONTENTS - Continued

LIST OF FIGURES

LIST OF FIGURES - Continued

LIST OF TABLES

PREFACE

This report describes model studies of the service gates in the irrigation release tunnels of Tarbela Dam. There were two models. The first had a linear scale ratio, model-to-prototype, of 1:69.6 and was a forerunner to studies with the larger scale model having a linear scale ratio of 1:24. Studies with the small model were conducted in November and December of 1970, and results were reported earlier. However, because that report was not printed, pertinent discussion of the small model tests is included herein.

The small model included the entire tunnel from the reservoir to the radial gates, including the intake structure, service and bulkhead gate structure and the bifurcation. The principal use of this model was to observe hydraulic conditions through the entire tunnel to be used as a guide for tests in the larger model. Tests were made with the small model to determine downpull forces on the service gates, but the model was too small to produce reliable results of hydrodynamic forces. Only the downpull forces on the service gates obtained from the large model are reported.

SUMMARY

Hydraulic model tests were conducted to determine hydrodynamic downpull for the service gates of tunnels 3 and 4 of the Tarbela Dam. This was accomplished by establishing appropriate flow parameters and pressure head coefficients for various segments of the gate. With knowledge of reservoir level and radial gate openings, hydrodynamic forces on the service gate can be calculated from the coefficients given in this report.

The pressure and hydraulic coefficients were calculated from data with steady-state flow. To be assured that unexpected hydraulic phenomena did not occur when the gates were in motion, limited tests were conducted for opening and closing of the service gates. These latter tests were approximations of the prototype conditions in that gate motion was restricted to increments primarily because of the limitation of the model test arrangement. In order to perform the tests for gates in motion in the full range from 0 to 48.8 feet of the prototype, a large constant head reservoir would have been needed for the model.

The pertinent conclusions from the study are as follows:

1. Various regimes of free flow, partially submerged and submerged gate were identified as possible conditions at the service gates from the small model. One-dimensional variables of the flow in the tunnel were grouped into nondimensional parameters. Head loss across the gate structure including the transitions is shown on Figure 51, and differential in water levels between the bulkhead gate shaft and service gate shaft is shown in Figure 52. The value H_1 can be calculated from the reservoir level, knowing the radial gate opening, and the head loss coefficients for various sections of the tunnel determined from previous model studies. Thus with H_1 known, pertinent piezometric heads used in the downpull force coefficients can be established from the curves in Figures 51 and 52.

2. The hydrodynamic downpull on various portions of the gate are expressed in terms of pressure head coefficients. The important force components acting on the gate were identified to be those acting on (a) the top seal clamp bar, (b) the bottom seal plate, (c) the bottom beam (beam 1), and (d) the top beam (beam 18). The coefficients varied with gate position and are shown graphically on Figures 53 for (a) above, 54 for (b), 58 and 59 for (c), and 62 and 63 for part (d). By use of these coefficients and the hydraulic parameters, the downpull force may be calculated.

3. Gate oscillations were small and it was concluded that they would not occur for the prototype gate because of the restraint provided by the friction of the side seals.

4. Fluctuations in water level in the service gate shaft were noted. The fluctuations in the left and right shafts were negatively correlated. The magnitudes and frequency of the oscillations were measured and analysis indicated maximum downpull due to this cause would be about 16 kips.

5. Discharge coefficients for flow into and out of the service gate shaft along the back side of the gate were determined from the small model. The coefficients are shown on Figure 70.

6. Subatmospheric pressures occurred at the top seal surface along the upstream wall of the service gate shaft because of the large velocities of flow through the gap and the sharp corner at the junction of the passage roof and the upstream wall of the gate shaft. Appropriate protective measure against possible cavitation should be provided. Low pressure areas were identified along the junction of the divider wall and floor in the downstream transition for the unsubmerged conditions.

7. The unsteady state tests indicated no unusual condition arising because of the gates in motion. Although there were two regions of downpull increase near closed (0.25 to 1 ft) and fully open (about 44.7 to 44.9 ft) in no region of gate opening was any uplift encountered.

INTRODUCTION

General Background

Two of the four tunnels of the Tarbela Dam Project are designed to release irrigation water from the reservoir which will be created by the dam. Normal regulation of flows through the tunnels is provided by radial gates located at the tunnel outlets. In the event of an emergency, the service gates located farther upstream in the tunnel may be required to close off the flow and possibly even to open for irrigation release if the radial gates are disabled at a time when water is badly needed. In either event, it is important to determine the hydrodynamic forces which act on these service gates, and to determine the general nature of the flow in the region of these gates.

Downpull is defined to be the hydrodynamic force acting on the gate parallel with the direction of gate travel and is designated positive downward, adding to the total load of the gate-hoisting mechanism. Negative downpull is thus a hydrodynamic uplift. Downpull is a consequence of non-uniform pressure distributions around the gate, which is affected by the velocity distributions of the flow in the region of the gate. Computation of downpull therefore requires determination of velocities of a complex three-dimensional flow field. At the present time calculations of velocities in the flow field is the principle difficulty; most computations are simplified using one-dimensional analysis with empirical coefficients. When reliable coefficients are not available, they must be determined from a hydrodynamic model which will create a flow field similar to that of the prototype.

A general plan of the right abutment of Tarbela Dam is shown in Figure 1, and profiles of the four tunnels are shown on Figure 2. An enlarged view of the tunnel and shaft sections of tunnels 3 and 4 are shown in Figure 3. The significant feature to be noted from these figures is that the tunnels are large, 45 feet in diameter upstream of the bulkhead and service gates, and 43.5 feet in diameter downstream for tunnels 1, 2 and 3, and 36 feet in diameter for tunnel 4. The structures which house the bulkhead and service gates of tunnels 3 and 4 are practically identical, differing only in the sill elevation by 1.68 feet. The transitions downstream from the service gate structure to the tunnels are different for tunnels 3 and 4 because of the different tunnel sizes.

The service gate assembly is shown on Figure 4, and is identical for all the tunnels. In a general way, the gates may be described as being 16 feet wide, 46.5 feet high and 4 feet thick. There are 17 sets of wheels (34 total) on each gate, each wheel being 31 inches in diameter and 14 inches wide. The estimated dead weight of the gate is 370 kips.

The seals are on the upstream face of the service gate; typical details are shown on Figure 5. The side and top seals have a thin stainless steel sheath on sealing surface. By using the water pressure on the face of the gate through appropriate piping, pressure can be applied to the back side of the seals to press against the sealing surface, thereby insuring a tight seal. There will always be contact between the side seals and seal face when the gate is between closed and fully open; fully open being defined when the bottom seal of the gate is at the level of the top of the flow passage. A gap is created however along the top seal when the gate is opened more than a few (about 3) inches. The geometry of the service gate shaft immediately above the top of the flow passage, shown in Figure 6, and the head upstream of the gate governs the velocity of the flow through the gap, hence also the pressures in that passage. It turns out that the pressure, hence the upward force on the top seal clamp bar, is an important component of the hydrodynamic force on the gate.

Scope of the Study

The study was directed to determine suitable coefficients for downpull force which could be used in a one-dimensional analysis to calculate the prototype downpull for a variety of hydraulic conditions, including various reservoir levels, tailwater levels and tunnel discharges.

The objectives of the study were:

1. To observe from the small scale model if various regimes of submergence of the gate were possible, namely;
   (a) discharge under the gate may be free and the gate unsubmerged,
   (b) tunnel may be partly full and the gate partly submerged,
   (c) tunnel may be full and the gate completely submerged.

2. To measure pressures on various parts of the gate and to express these pressures in a manner which will enable computation of the forces on the gate.

3. To conduct tests over the full range of gate positions for the various regimes of (1) above.

4. To measure downpull forces directly, if possible, for gates in motion. Tests would be limited to incremental gate motion because of the fixed flow controllers of the model.

5. To determine discharge coefficients for flow into and out of the service gate shaft for various positions of the gate.

6. To measure pressures on the walls of the gate structure at significant points.

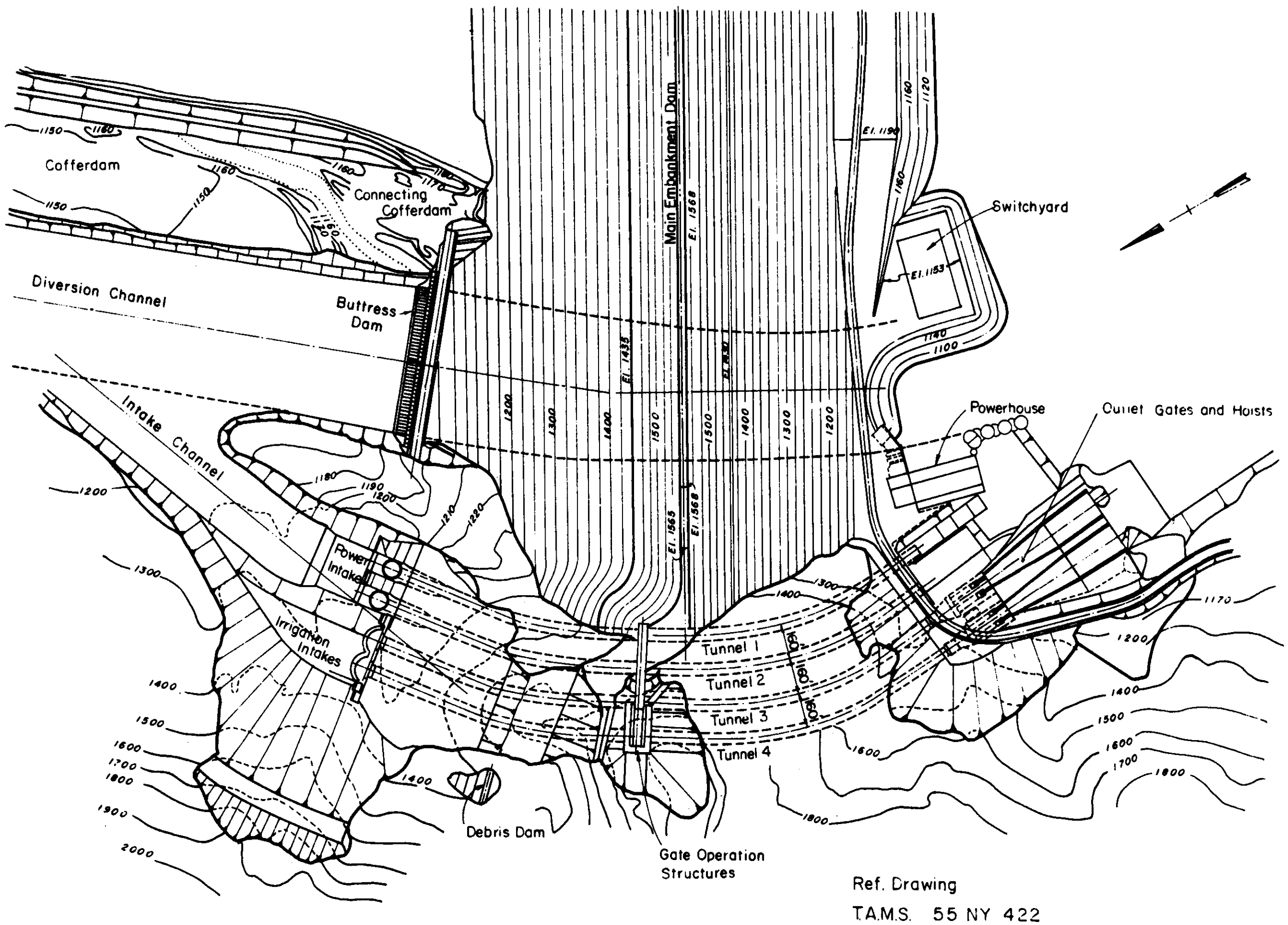

Fig. 1 General plan of right abutment showing the tunnels

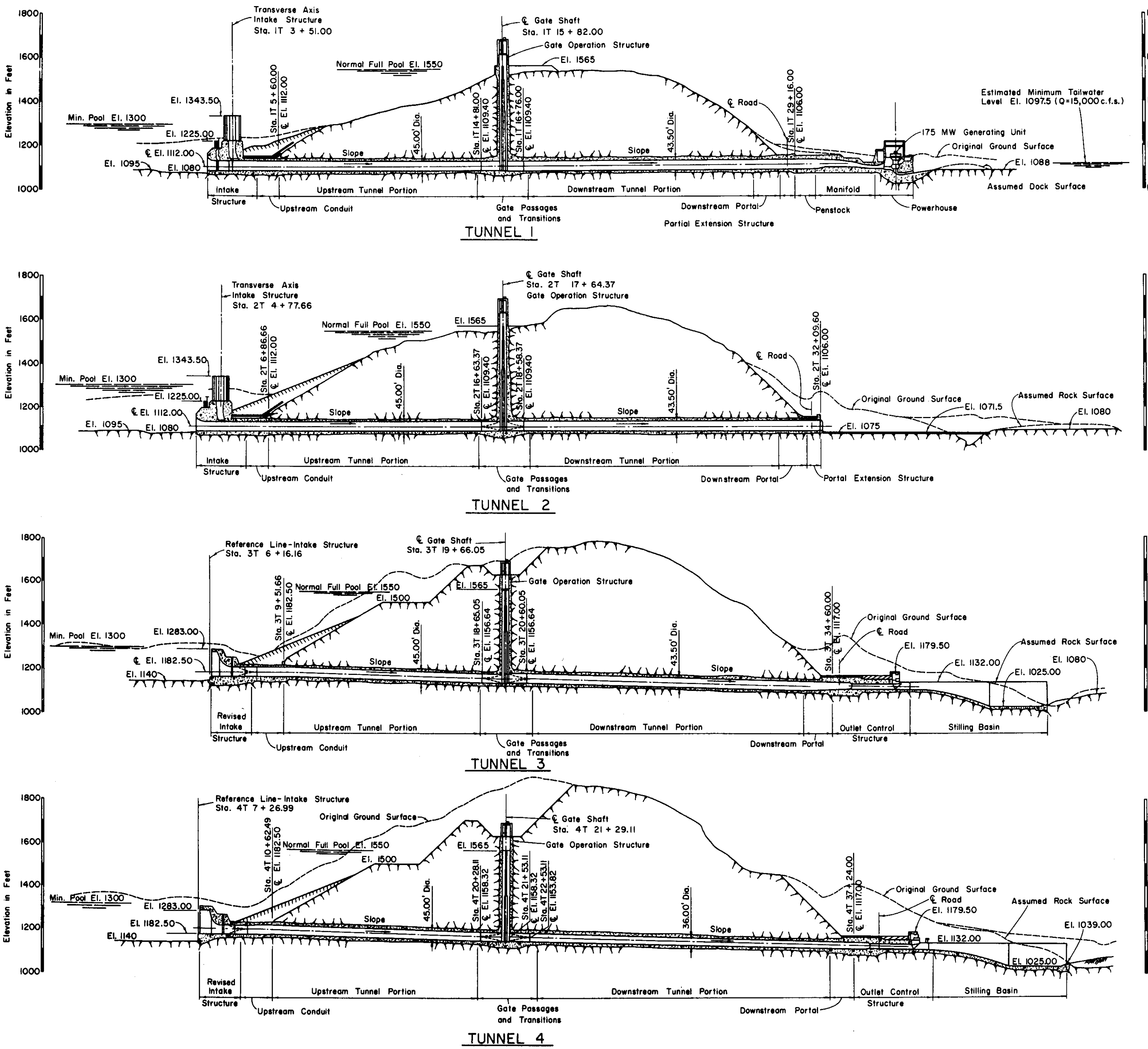

Figure 2. Tunnel profiles.

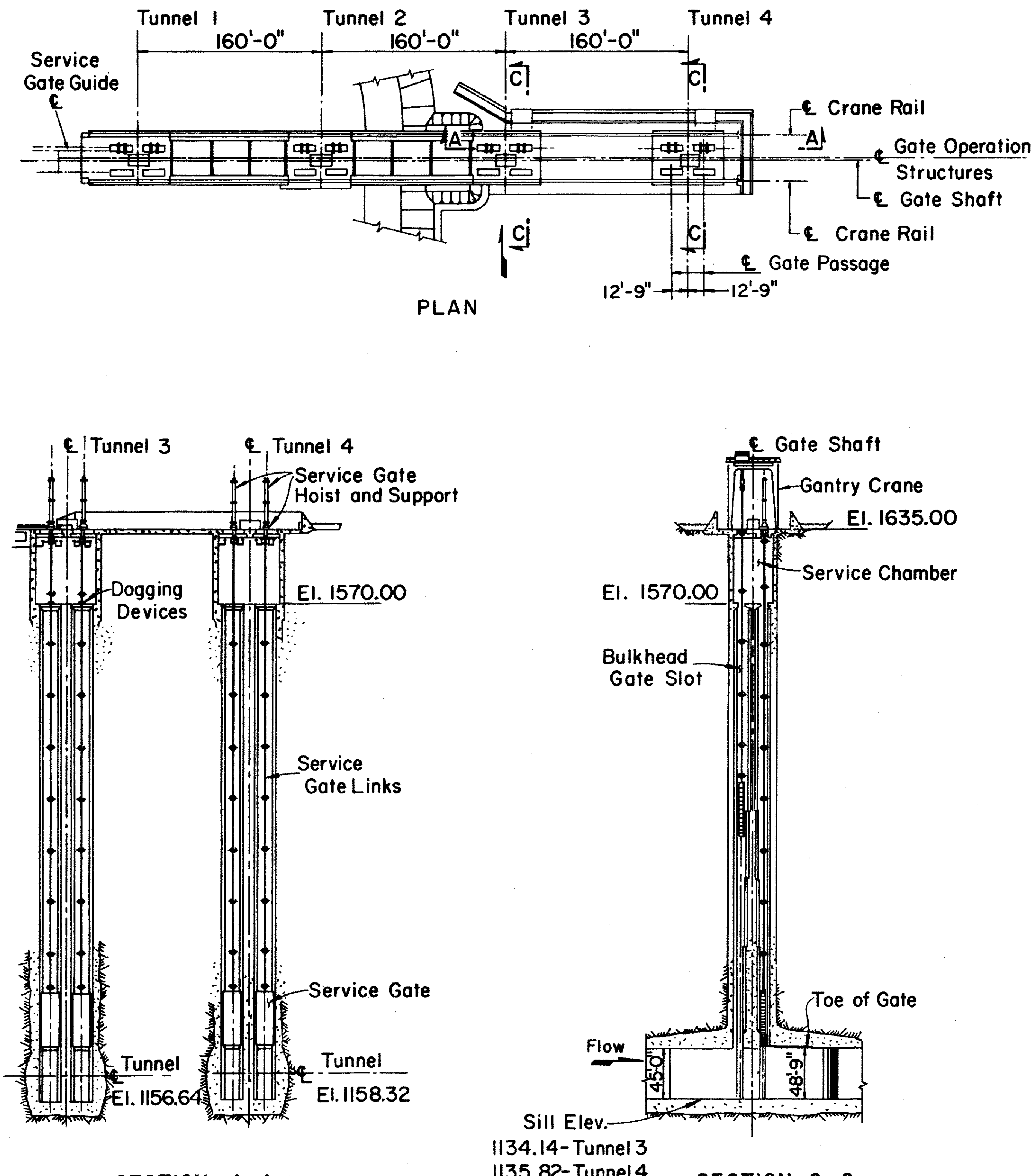

Figure 3. Tunnel gate structures - General arrangement

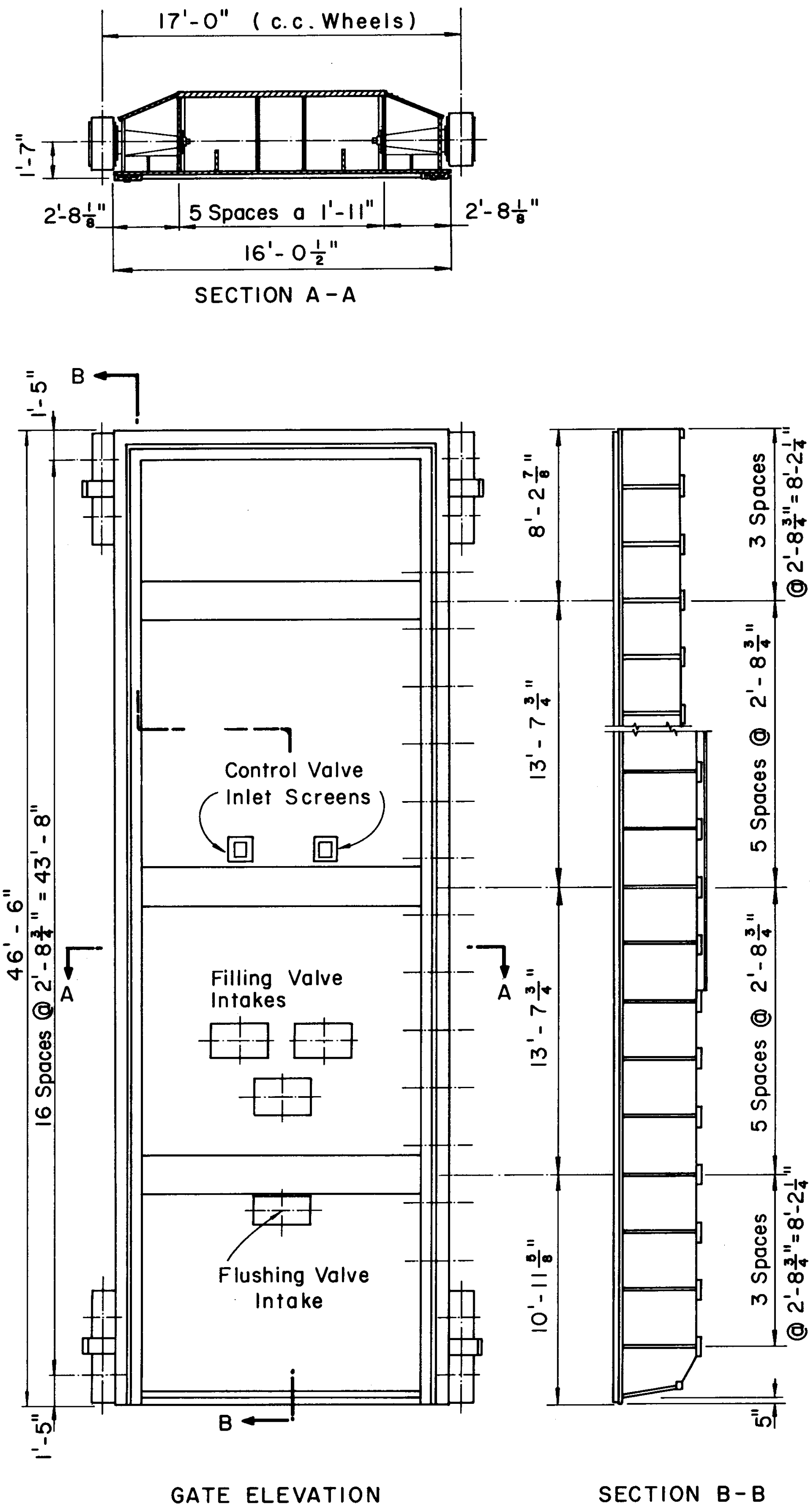

Figure 4. Service gate assembly

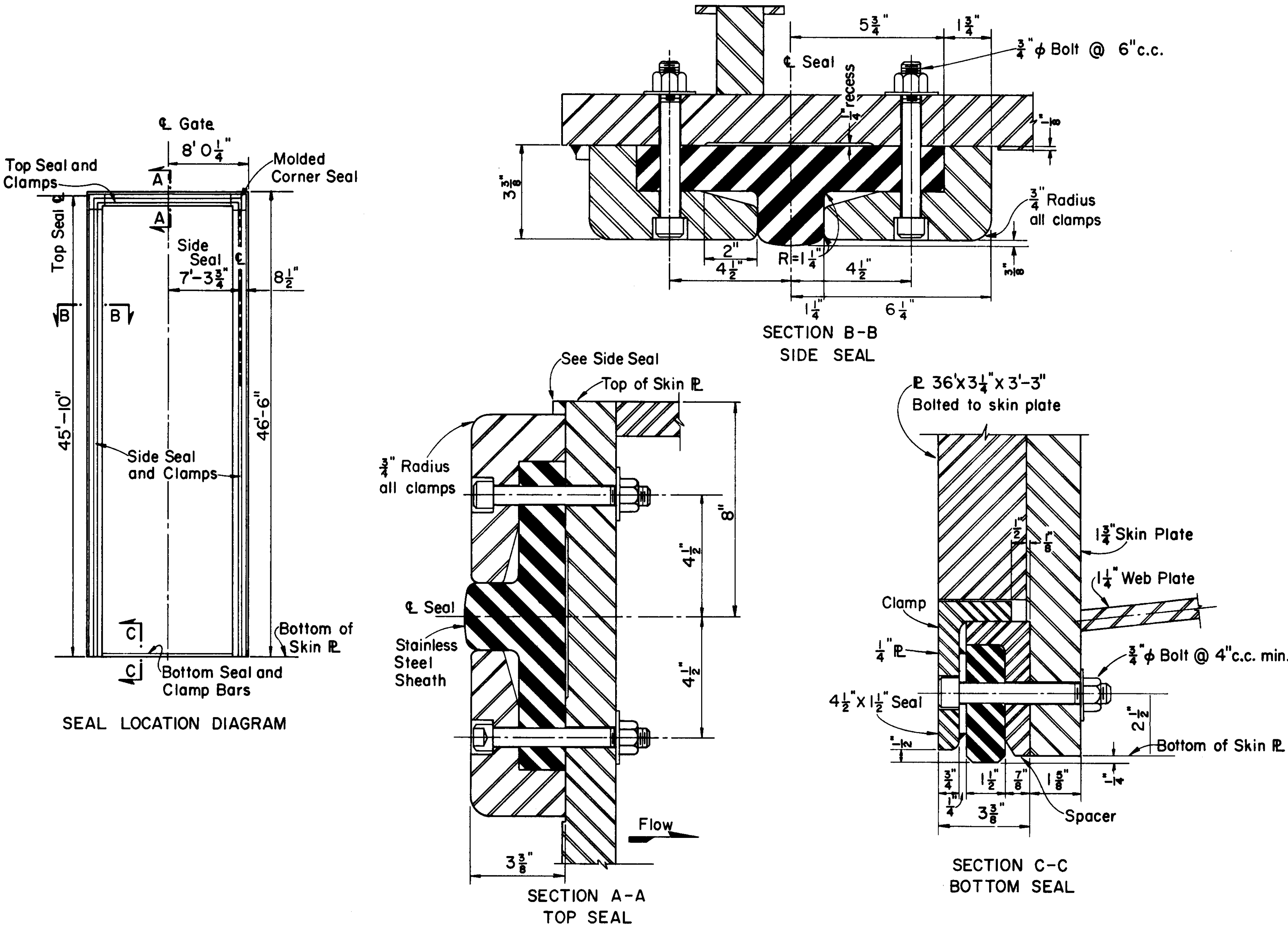

Figure 5. Service gate seal details

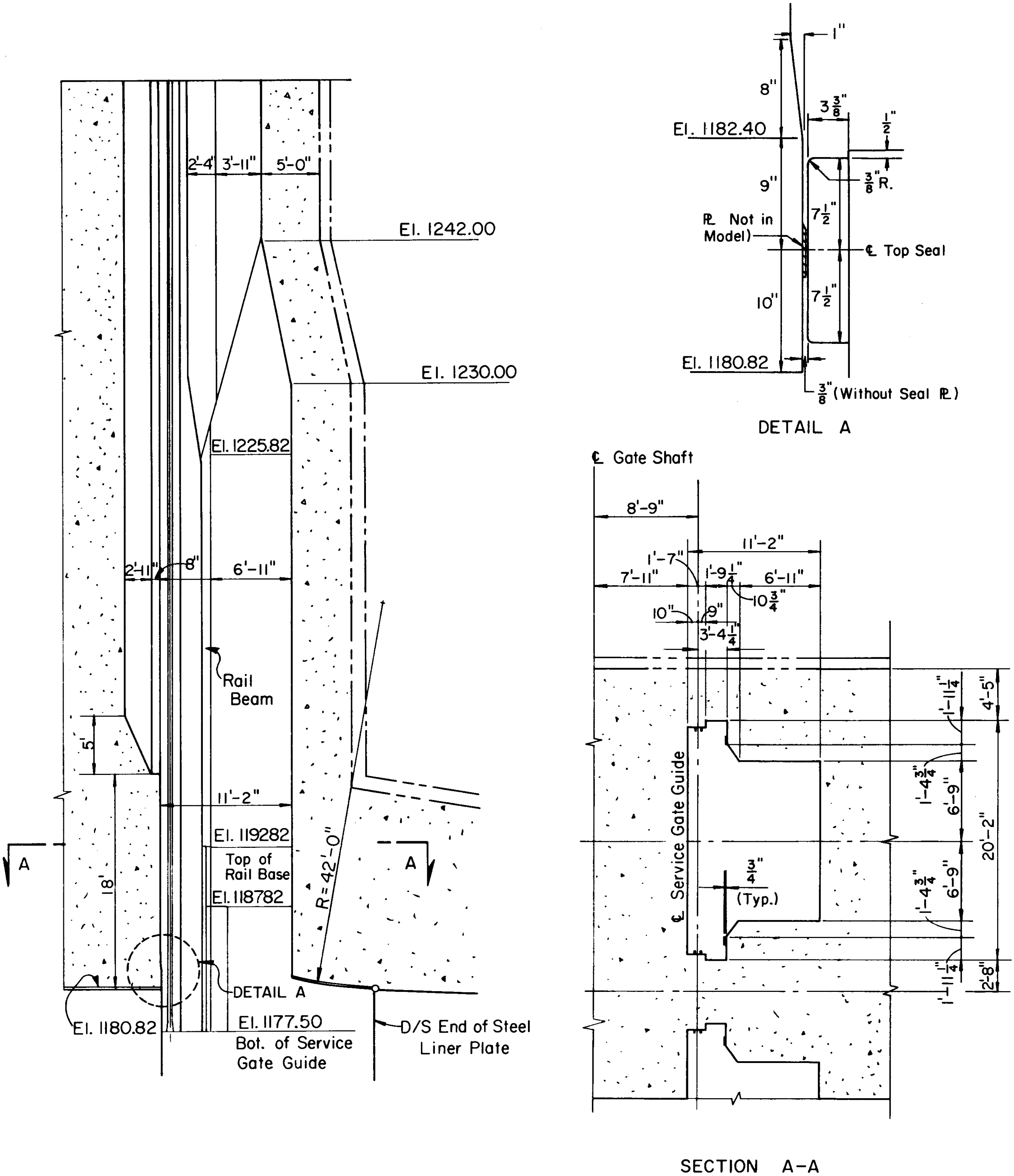

Figure 6. Gate shaft geometry

Descriptions

Small scale model (1:69.6) - The small model included the entire works of Tunnel 3; the intake structure, the gate section, the bifurcation at the end of the tunnel and the outlet control gates. A photograph of the model is shown as Figure 7, and a schematic of the model layout is shown as Figure 8. The appropriate model/prototype ratios are given in Table 1 in which the Froude criterion was used to establish the ratios.

Most of the model, which included the intake structure, the head box, the tunnels and bifurcation was constructed for prior studies. A new gate structure was constructed which included the total length of the shaft to ground level. One gate was constructed approximately to scale from a solid aluminum plate. It was approximate in the sense that the beams of the prototype were represented simply by grooves milled out of the back side of the aluminum plate, and only three sets of wheels were attached to the gate. A drawing of the model gate is shown in Figure 9. The other gate was simply a plastic plate fitted into the groove to control the flow through that side of the passage. Both gates were provided with hydraulic cylinder operators to facilitate movement.

Measurements of forces required to move the gate in this model were made with a strain-gage type force cell, but since the friction forces were large in comparison to the hydrodynamic forces, the results were inaccurate and too inconsistent to be considered of any value. Thus details of the strain-gage system will not be described.

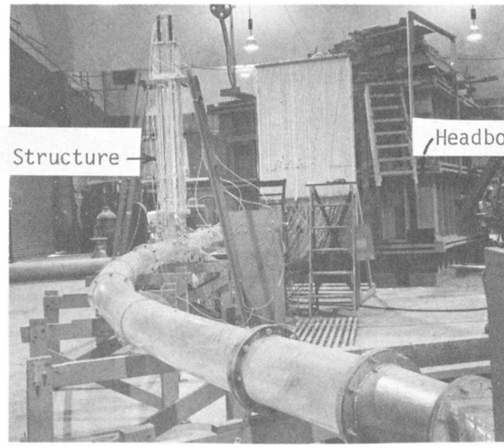

Figure 7. General view of small model

TABLE 1. MODEL-PROTOTYPE SCALE RATIOS FOR THE SMALL MODEL

Item	Scale Ratios		Absolute Magnitudes	
	Geometric	Numerical	Model	Prototype
Length	L_r	1:69.6	1 in.	5.80 ft
Velocity	$L_r^{1/2}$	1:8.343	1 ft/sec	8.343 ft/sec
Discharge	$L_r^{5/2}$	1:40413	1 cfs	40,413 cfs
Force	L_r^3	1:337,153	1 lb	337.2 Kips

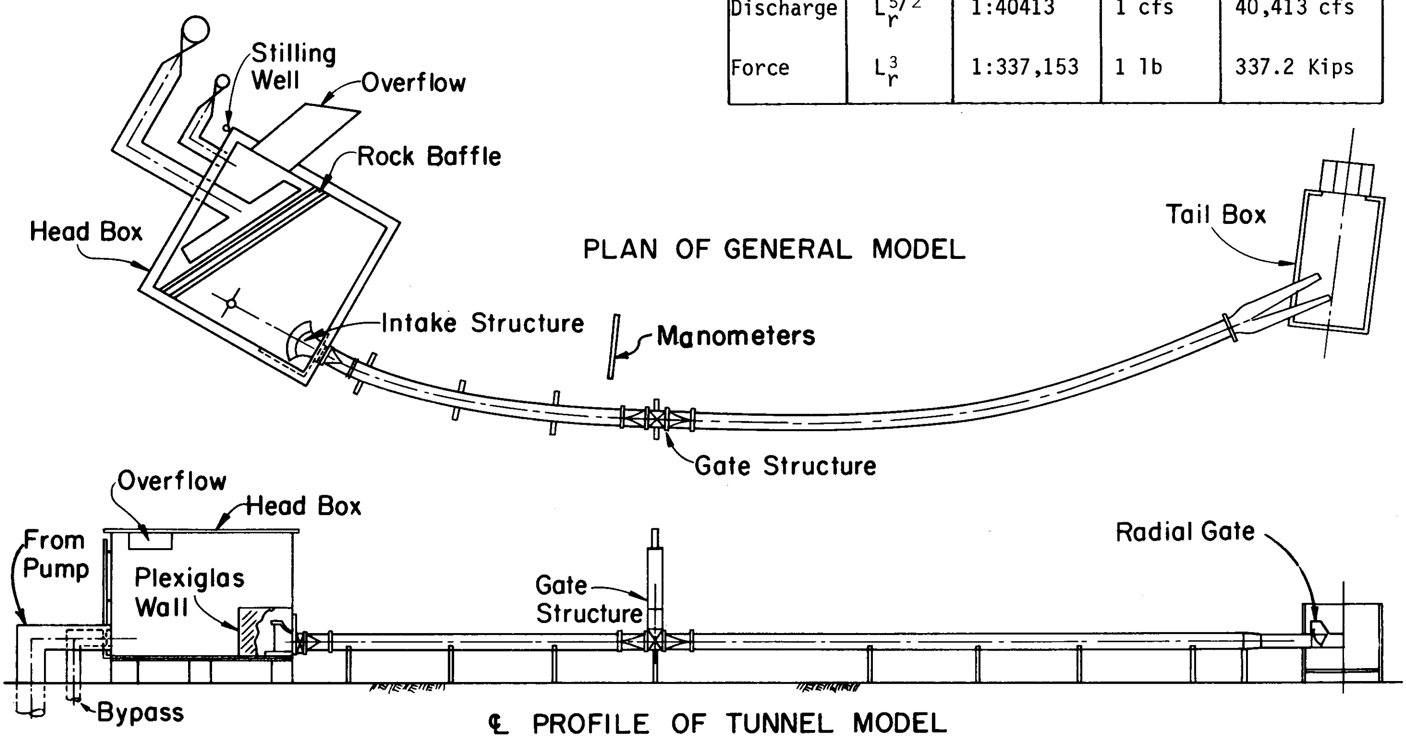

Figure 8. Schematic layout of small model

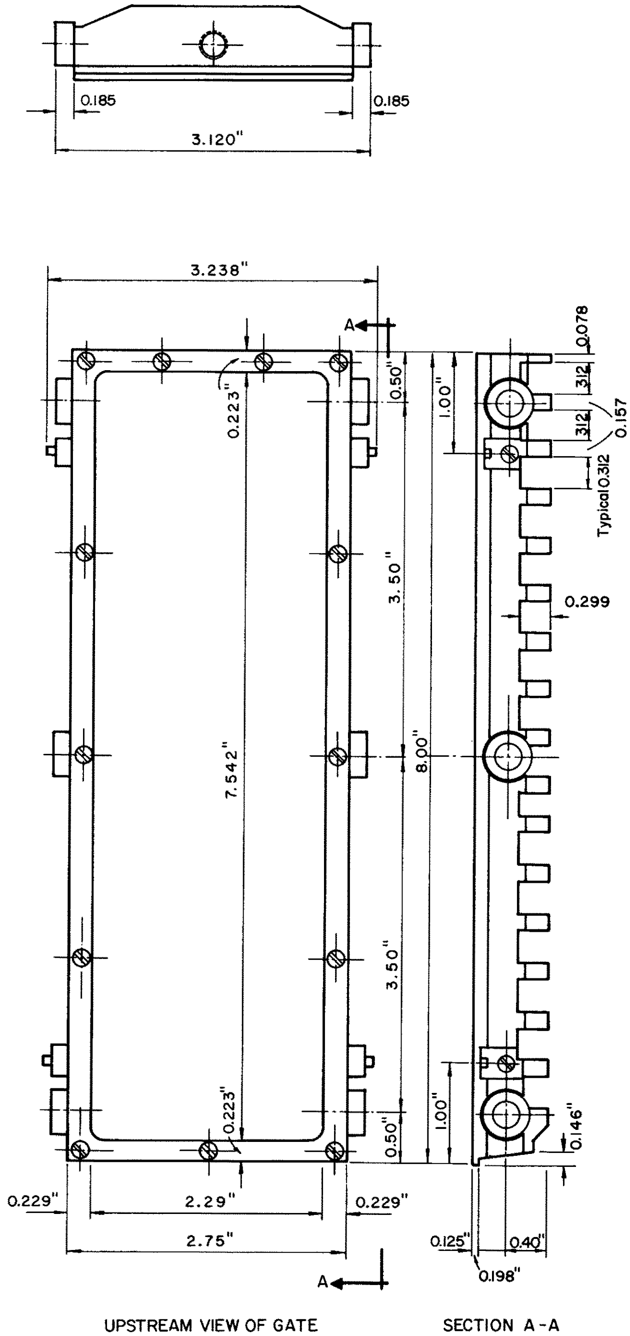

Figure 9. Model of service gate- 1:69.6 scale

Large scale model (1:24) - The large model included only portions of Tunnel 4; 480 feet of upstream tunnel, the gate structure including the transitions to the tunnels, and approximately 700 feet of downstream tunnel. A photograph of the entire model is shown in Figure 10 and a layout of the model is shown in Figure 11. Appropriate model-prototype ratios are given in Table 2.

Water was supplied to the model from Horsetooth Reservoir through a high-head, large discharge system which services the hydromachinery laboratory. The discharge was collected in a lower reservoir from which water is drawn for agricultural purposes.

Discharge through the model ranged from near zero to 39 cfs and was measured by orifices installed in the pipeline upstream from the flow control valve. Three orifices 5, 10, and 12 inches in diameter in a 14-inch diameter pipe section and a 2-inch orifice in a 3-inch pipeline were required to meter the wide discharge range. All orifices were calibrated volumetrically.

The supply head from the reservoir was approximately 220 feet, while the head needed for the model was about 18 feet. In order to dissipate the excess head, and to control the discharge, two valves in the supply line were used, the second to minimize cavitation at the first valve. In addition, a valve was placed in the downstream pipeline to regulate the hydraulic grade line in the region downstream from the service gates. The system of three valves therefore required adjustment as a set. Most of the tests in this study were conducted with steady state flow. Some tests were conducted, however, with the service gate in motion. In that event the interaction between four flow controllers in a single pipeline became a very complex system for operation. A representative constant reservoir level for the full range of motion of the service gate was not possible. Tests with the gate in motion were therefore done for incremental steps of service gate motion, requiring adjustment of the valves for each test.

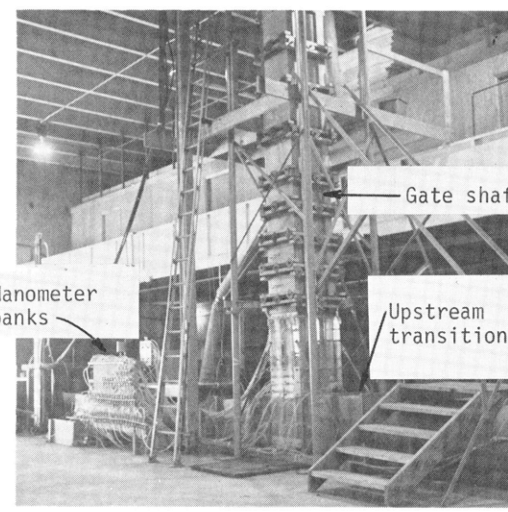

Figure 10. Large model of gate structure

TABLE 2. MODEL-PROTOTYPE SCALE RATIOS FOR THE LARGE MODEL

Item	Scale Ratios		Absolute Magnitudes	
	Geometric	Numerical	Model	Prototype
Length	L_r	1:24	1 in.	2 ft
Velocity	$L_r^{1/2}$	1:4.899	1 ft/sec	4.899 ft/sec
Discharge	$L_r^{5/2}$	1:2821.8	1 cfs	2,822 cfs
Force	L_r^3	1:13824	1 lb	13.8 Kips

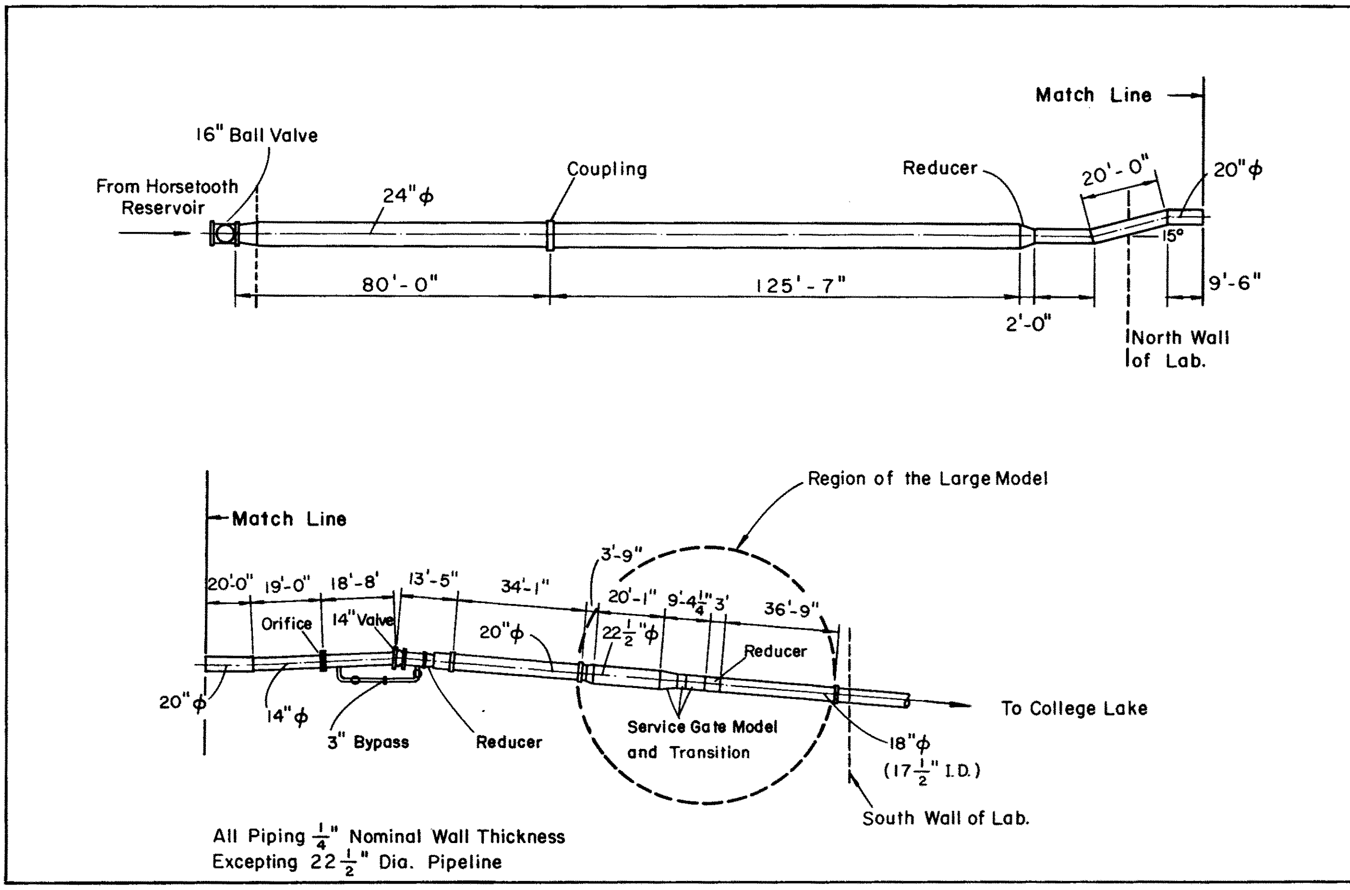

Figure 11. Schematic layout of the large model

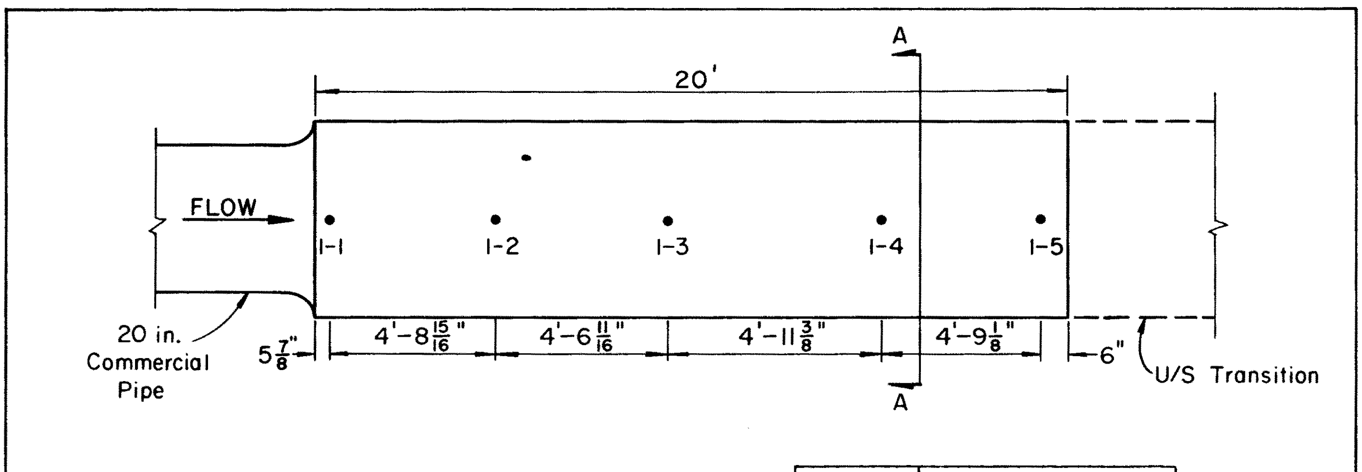

Piezo. No.	Prototype Station	Prototype Elevation
1-1	15+42.76	1157.63
1-2	16+56.66	1157.51
1-3	17+66.16	1157.59
1-4	18+84.96	1158.01
1-5	19+99.16	1158.10

Figure 12. Piezometer locations on upstream tunnel.

Construction Details of the Large Model

Upstream tunnel - A special 20-ft section of 22.5-in. I.D. pipe was rolled from 1/8-in. steel sheet for the upstream tunnel. This represented, in the prototype, a length of 480 feet. There were five sets of piezometers located along the length of pipe, each set consisting of two piezometers placed on the horizontal diameter. Locations are shown on Figure 12.

Upstream transition - The transitions (downstream as well as upstream) were constructed from 1-in. thick clear plastic sheets to permit flow visibility. The sides of the transitions were first arranged in the form of a rectangular box and the fillets were constructed from reinforcing bars, wire mesh and automobile body putty. An interim construction stage is shown in Figure 13, just prior to placement of the body putty, and in Figure 14 a further stage is shown after placement of the putty. Control of the transition shape was provided by cross-section templates as shown in Figure 14 as well as longitudinal templates. In this way, an accurate transition from round to rectangular cross-sectional shape was constructed.

The divider wall within the transition was made from 3/4-in. thick plastic with a rounded end piece as seen in Figure 15. The completed divider wall and transition is shown in the next photograph, Figure 16.

Piezometers were placed at several key locations on the transition and pier walls. These locations are shown in Figure 17. It should be pointed out that the identification of piezometers includes a prefix number as well as a sequence number. The prefix identifies the manifold bank to which the particular piezometer was connected. Three manifold banks were used, hence three prefix numbers will be noted.

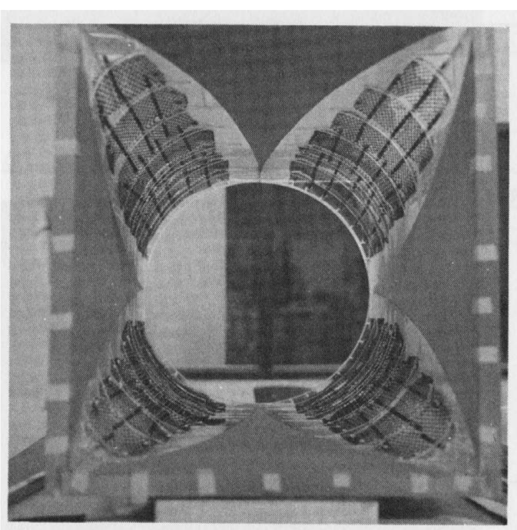

Figure 13. Interim construction stage of the downstream transition

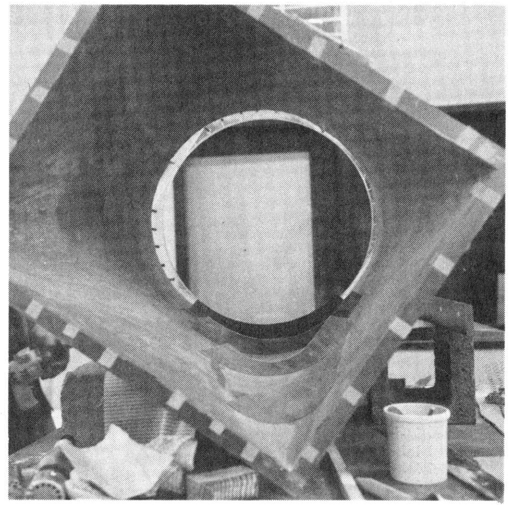

Figure 14. After placement of the body putty

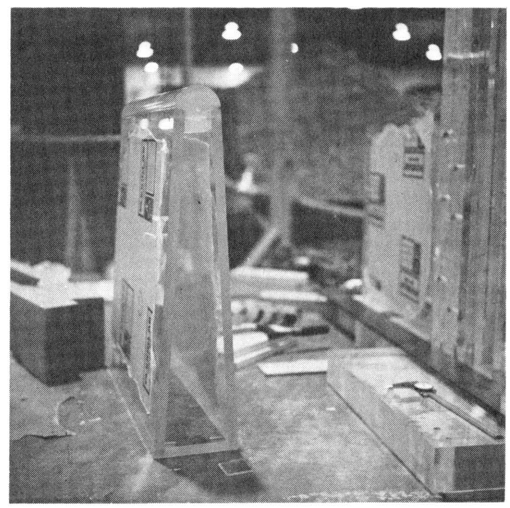

Figure 15. Divider wall

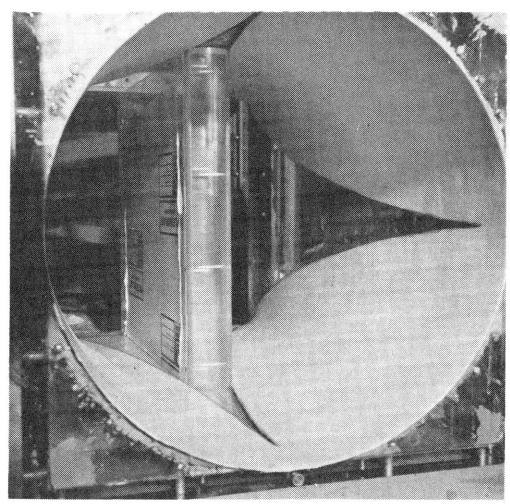

Figure 16. Completed transition

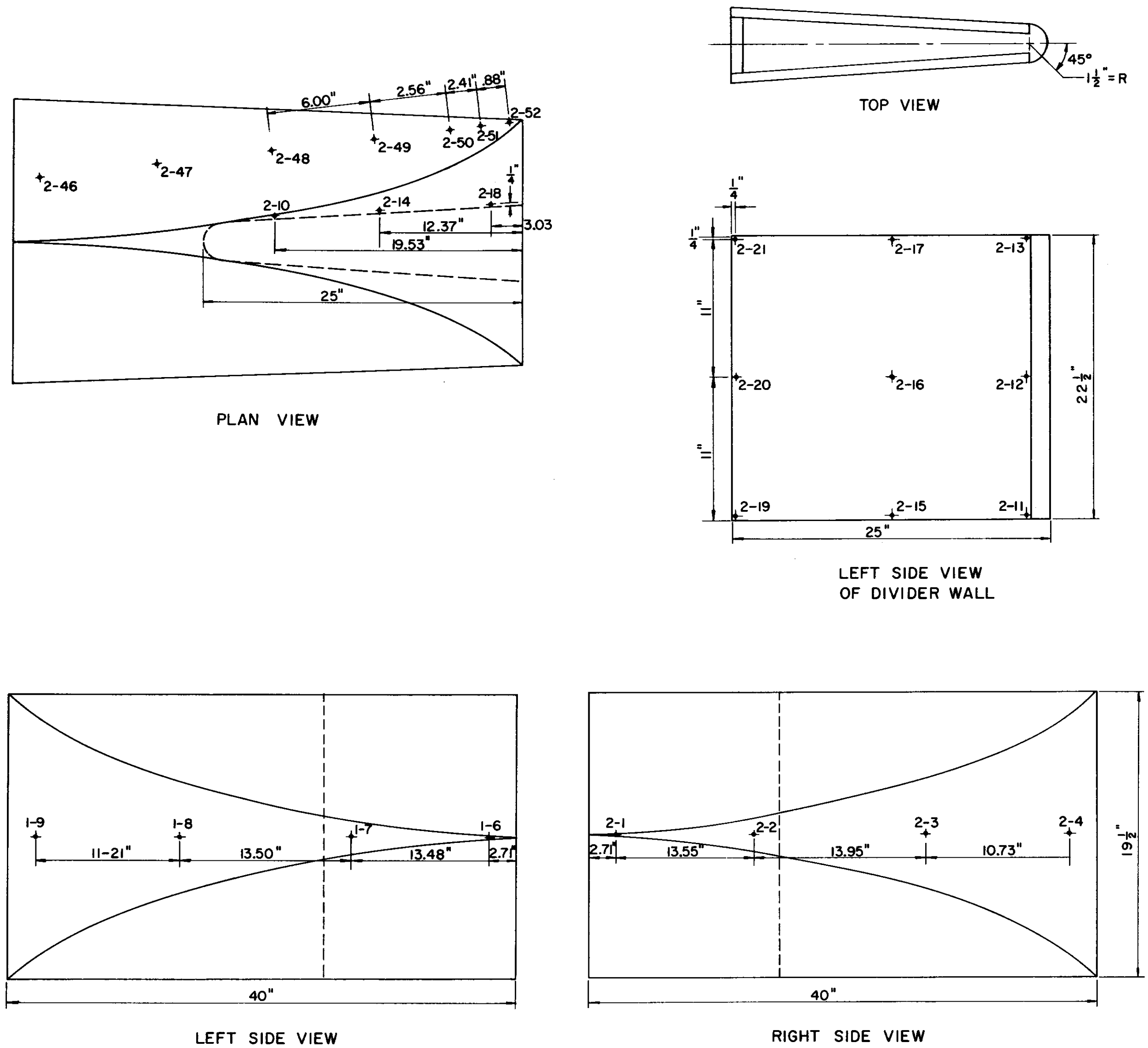

Piezo. No.	Prototype Station	Prototype Elevation	Piezo. No.	Prototype Station	Prototype Elevation	Piezo. No.	Prototype Station	Prototype Elevation
1-6	20+32.51	1158.32	2-11	20+61.53	1136.32	2-20	21+06.61	1158.34
1-7	20+54.07	1158.32	2-12	20+61.51	1158.38	2-21	21+06.61	1180.32
1-8	20+81.07	1158.32	2-13	20+61.61	1180.32	2-46	20+32.77	1146.35
1-9	21+03.49	1158.32	2-14	20+83.37	1135.82	2-47	20+54.77	1141.55
2-1	20+32.51	1158.32	2-15	20+83.11	1136.32	2-48	20+70.97	1140.51
2-2	20+54.21	1158.32	2-16	20+83.07	1158.38	2-49	20+84.85	1139.42
2-3	20+82.11	1158.32	2-17	20+83.07	1180.32	2-50	20+96.71	1138.09
2-4	21+03.57	1158.32	2-18	21+02.05	1135.82	2-51	21+01.81	1137.13
2-10	20+69.05	1135.82	2-19	21+06.65	1136.34	2-52	21+06.61	1136.24

Figure 17. Piezometer locations on the upstream transition

Gate structure and shaft - The bottom five feet of the gate structure was constructed from 3-in. thick clear plastic. Having first specified that visibility was a prime consideration, it was decided that a single plastic sheet would require the least fitting problem. The thickness of the plastic sheet was then governed by the depth of the gate grooves. The groove of the service gate was 1.67 in. deep and for the bulkhead gate it was 1.33 in. The grooves were milled out in various stages as shown in Figure 18, with hand grinding and finishing provided at places where the geometry of the cut was complex.

The center divider wall was formed by placing two pieces of the required thickness back-to-back as shown in Figure 19. The finished structure is shown in Figure 20.

The upper level of the gate shaft was constructed from wood. The internal walls separating the shafts were first constructed in the form of a cross as shown in Figure 21, then the outside walls were placed against the internal cross pieces and bolted together. An interim stage is shown in Figure 22. Numerous piezometers were placed in the walls of the flow passage as shown in Figure 23.

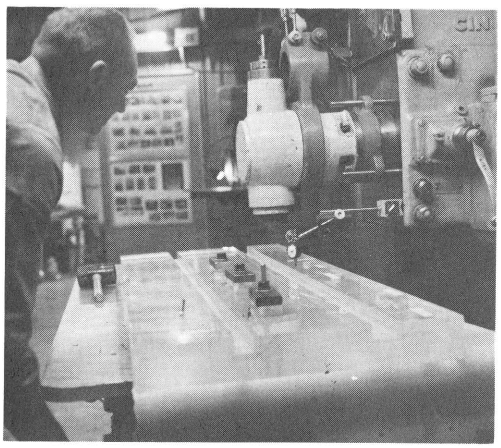

Figure 18. Wall of the gate structure

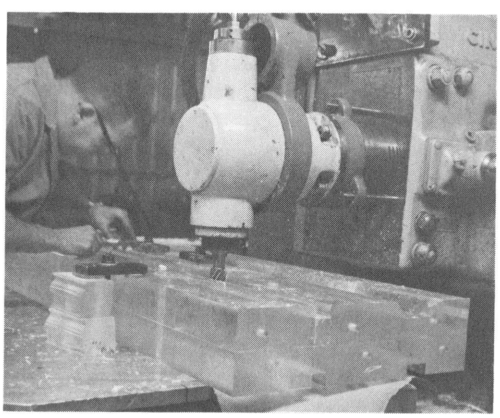

Figure 19. Center divide wall

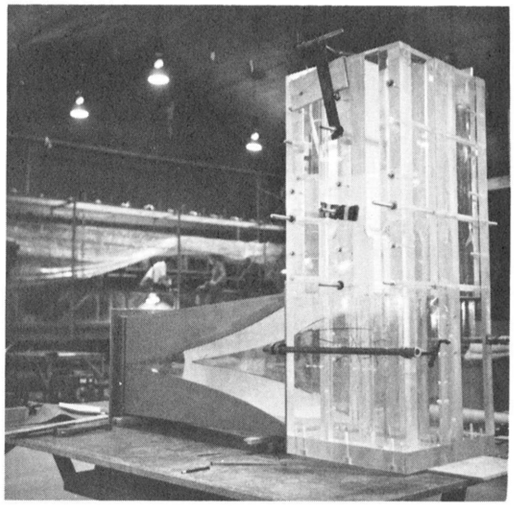

Figure 20. Completed plastic gate structure

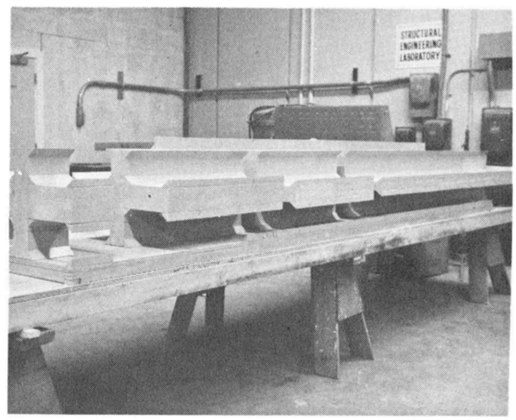

Figure 21. Internal walls of upper gate shaft

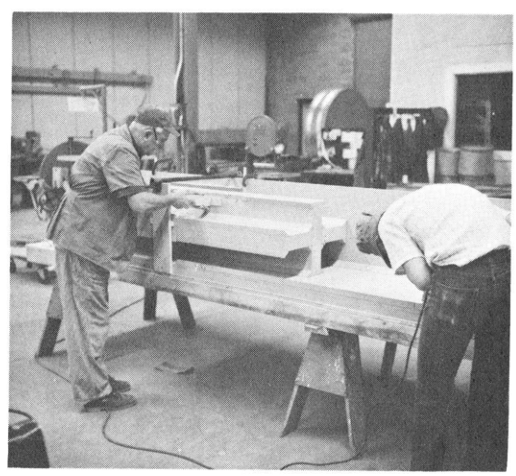

Figure 22. Assembly of upper gate shaft

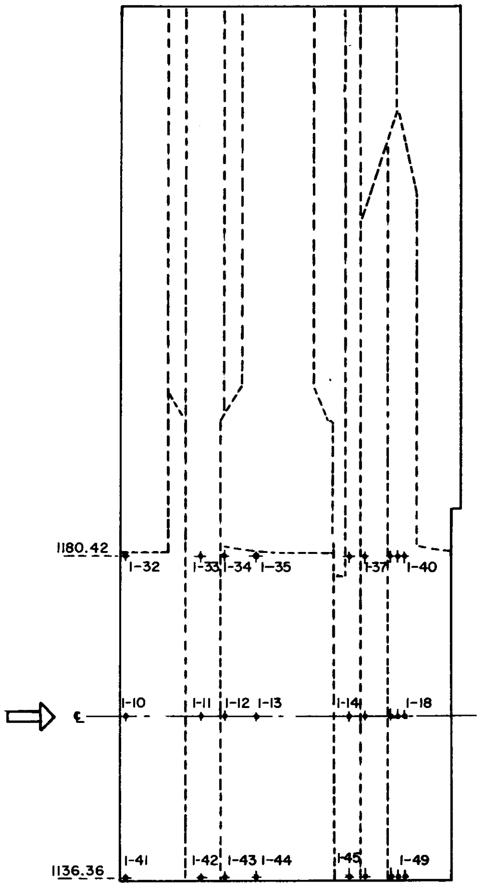

MIRROR IMAGE OF LEFT WALL

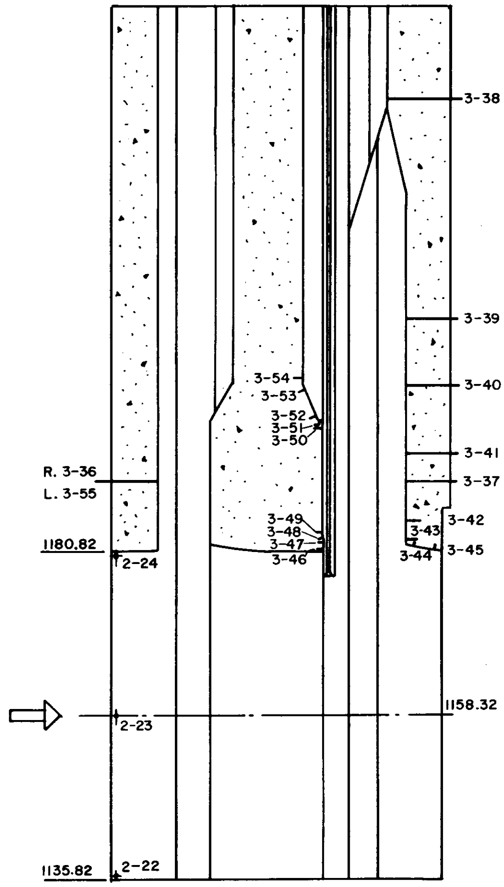

℄ LEFT PASSAGE

Piezo. No.	Prototype Station	Prototype Elevation
1-10	21+08.71	1158.36
1-11	21+18.84	1158.32
1-12	21+22.00	1158.36
1-13	21+26.21	1158.36
1-14	21+39.11	1158.34
1-15	21+41.13	1158.38
1-16	21+44.51	1158.34
1-17	21+45.55	1158.36
1-18	21+46.57	1158.32
1-32	21+08.63	1180.42
1-33	21+18.92	1180.36
1-34	21+21.90	1180.32
1-35	21+26.52	1180.28
1-36	21+39.21	1180.38
1-37	21+41.19	1180.38
1-38	21+44.57	1180.42
1-39	21+45.61	1180.42
1-40	21+46.57	1180.42
1-41	21+08.71	1136.36
1-42	21+18.92	1136.36
1-43	21+21.90	1136.36
1-44	21+26.52	1136.38
1-45	21+39.11	1136.36
1-46	21+41.09	1136.40
1-47	21+44.47	1136.42
1-48	21+45.55	1136.48
1-49	21+46.47	1136.40

Piezo. No.	Prototype Station	Prototype Elevation
2-22	21+08.61	1136.32
2-23	21+08.61	1158.34
2-24	21+08.61	1180.32
3-36	21+14.53	1190.76
3-37	21+48.61	1189.13
3-38	21+45.71	1242.02
3-39	21+48.21	1212.57
3-40	21+40.21	1203.32
3-41	21+48.21	1194.07
3-42	21+48.21	1184.82
3-43	21+48.21	1182.02
3-44	21+48.46	1181.62
3-45	21+52.61	1181.02
3-46	21+37.11	1181.07
3-47	21+37.11	1182.15
3-48	21+37.07	1182.72
3-49	21+37.03	1183.32
3-50	21+37.03	1198.57
3-51	21+36.69	1198.82
3-52	21+36.11	1199.22
3-53	21+34.31	1203.56
3-54	21+34.11	1204.12
3-55	21+14.53	1189.26

Figure 23. Piezometer locations on left passage walls

Downstream transition - The technique of constructing the downstream transition was identical with that for the upstream transition. The finished product is seen in Figure 20. Piezometers placed on the downstream transition walls and divider walls are shown in Figure 24.

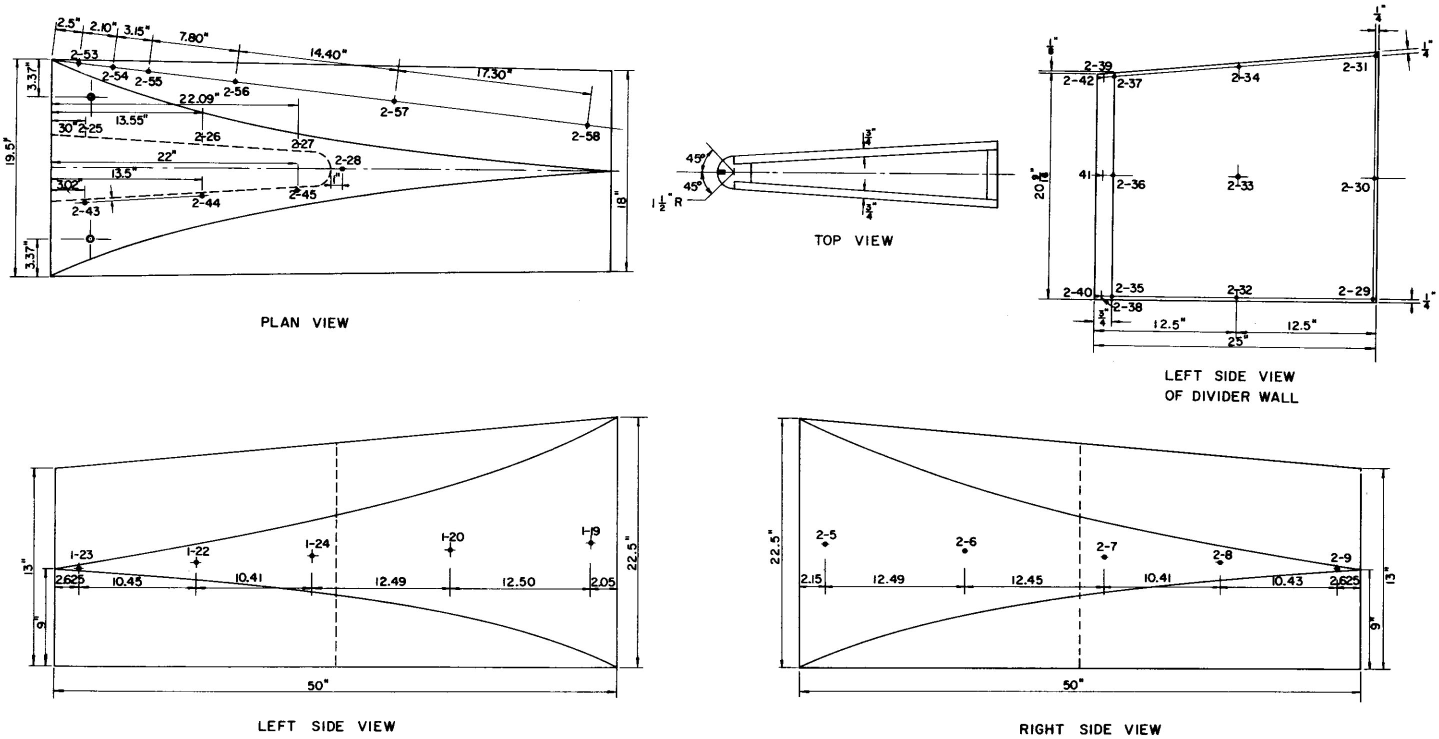

Piezo. No.	Prototype Station	Prototype Elevation	Piezo. No.	Prototype Station	Prototype Elevation	Piezo. No.	Prototype Station	Prototype Elevation
1-19	21+57.21	1158.14	2-28	22+05.11	1135.82	2-40	22+03.11	1136.22
1-20	21+82.21	1157.03	2-29	21+53.61	1136.32	2-41	22+03.11	1158.32
1-21	22+07.19	1155.92	2-30	21+53.61	1158.32	2-42	22+03.11	1175.82
1-22	22+28.01	1155.00	2-31	21+53.61	1180.32	2-43	21+59.15	1135.82
1-23	22+48.91	1154.05	2-32	21+78.11	1136.32	2-44	21+80.11	1135.82
2-5	21+57.41	1158.14	2-33	21+78.11	1158.32	2-45	21+97.11	1135.82
2-6	21+82.39	1158.03	2-34	21+78.11	1178.46	2-53	21+58.05	1136.58
2-7	22+07.29	1155.92	2.35	22+00.11	1136.22	2-54	21+64.01	1137.22
2-8	22+28.11	1155.00	2-36	22+00.11	1158.32	2-55	21+70.29	1138.10
2-9	22+48.97	1154.05	2-37	22+00.11	1176.07	2-56	21+85.95	1138.84
2-25	21+59.11	1135.82	2-38	22+02.28	1136.22	2-57	22+14.47	1140.16
2-26	21+80.21	1135.82	2-39	22+02.28	1175.92	2-58	22+49.13	1141.20
2-27	21+97.29	1135.82						

Figure 24. Piezometer locations on downstream transition

Downstream tunnel - The model pipe representing a 36-ft diameter tunnel at a scale of 1:24 is 18 inches. Commercial 18-in. pipe is however less than 18-inches I.D. The difference in size does not play an important role in this model. However, to insure that a slightly smaller diameter would not influence the hydraulic conditions in the vicinity of the gates, a four-ft section of 18-in. I.D. pipe was rolled and placed immediately adjacent to the downstream transition. From that point for a distance of 33 ft to the control valve, a commercial pipe of 17½-in. I.D. was used.

Piezometers were placed on the horizontal diameter of this pipe as shown in Figure 25. The purpose of these piezometers was to establish a hydraulic grade level near the downstream end of the transition.

Piezo. No.	Prototype Station	Prototype Elevation
1-24	22+58.11	1154.14
1-25	23+30.36	1154.06
1-26	23+54.61	1153.91
1-27	24+02.61	1153.64
1-28	25+94.61	1153.07
1-29	27+86.86	1153.05
1-30	29+78.61	1152.81
1-31	31+70.61	1151.95
2-59		1141.20
2-60		1141.20

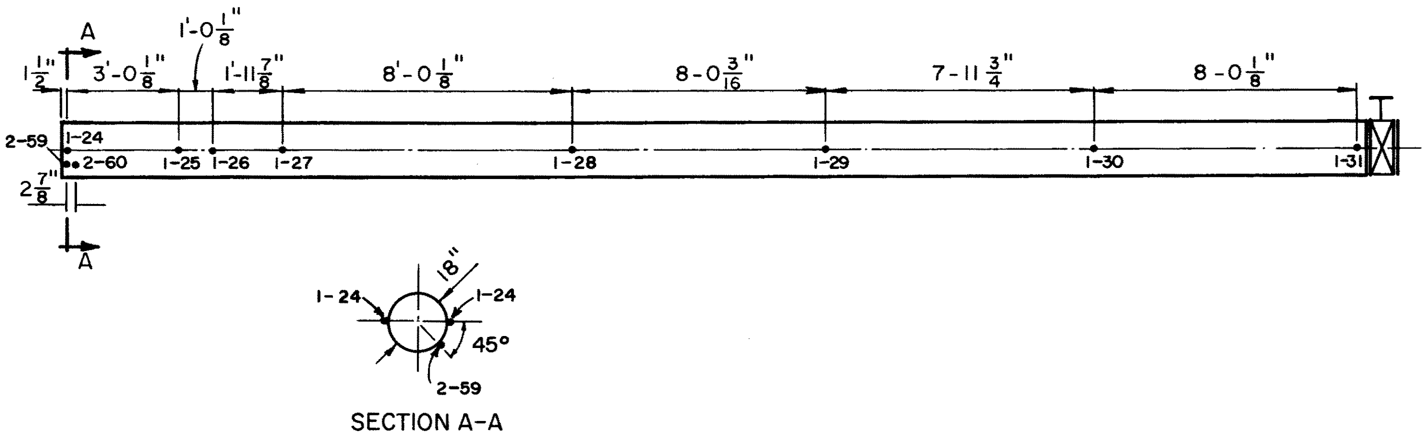

Figure 25. Piezometer locations on downstream tunnel.

Service gates - Two identical models of the service gates were constructed from brass plates. The thicknesses of the brass pieces were chosen from commerically available rolled plates to represent the thicknesses of the prototype members as closely as possible. Exceptions were made for the side and face plates of the gate. The side plate was 3/16-in. thick and the face plate was 0.102-in. thick to provide essential structural strength to the model.

The pieces of the gate were made in "egg-crate" interlaced fashion as shown in Figure 26. The face plate was fitted to it, soldering compound was placed against the joints, and the whole assembly was placed in an oven in which the temperature was raised just to the melting point of the solder. In this manner the entire gate was soldered at one time, thus avoiding warping of individual members as would have occurred if localized heat had been applied.

Hard molded rubber was glued to the face plate to form the seals. A plate was added to the bottom end of the gate and the seals were milled to the thickness desired.

The wheels of the gate were chosen from commercially available ball bearing races. Exact representation of diameter and width of the prototype wheels was not possible, so a compromise size of 32 mm diameter (1.2598 in.) by 10 mm wide (.3937 in.) bearings were chosen. The model wheel diameter was small by 0.0319 in. and the width narrower by .1896 in., but this was not considered crucial to the hydrodynamic model.

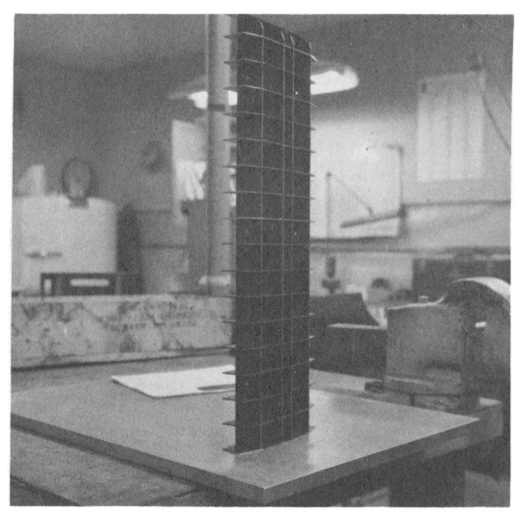

Figure 26. Assembly of service gate model

The completed model gates are shown in Figures 27 through 30. One gate was equipped with piezometers to measure pressures on the various horizontal beams of the gate. The other gate was equipped with "flush mount" pressure transducers which will be described in another section. The gate with the piezometers was placed in the left channel of the divided flow passage and the transducer-equipped gate in the right passage. Reference to right and left is made looking downstream in the direction of flow.

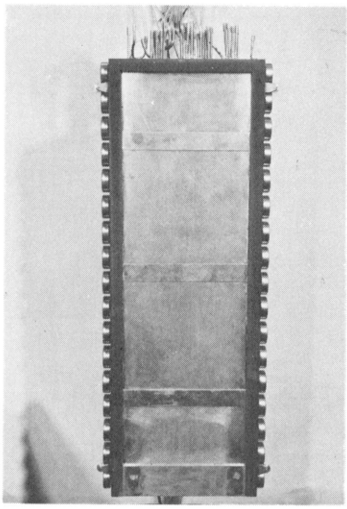

Figure 27. Upstream face of left gate

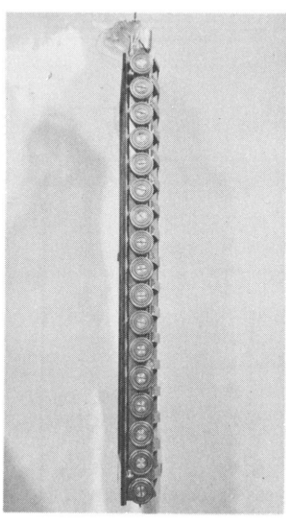

Figure 28. Side view of left gate

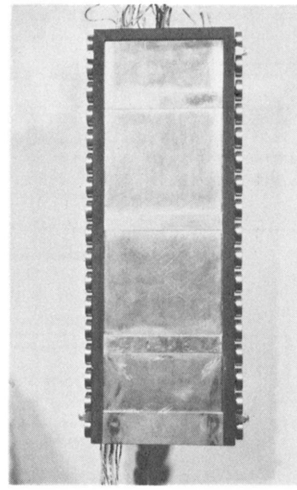

Figure 29. Upstream face of right gate

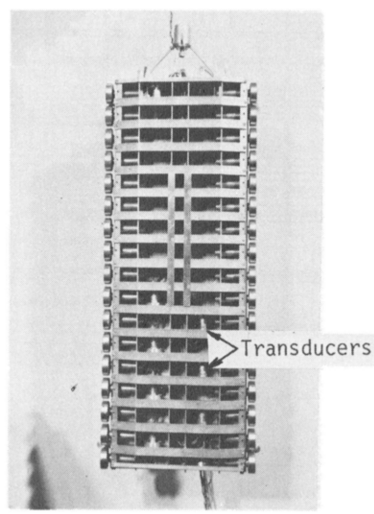

Figure 30. Downstream side of right gate

The locations of the piezometers on the left gate are indicated on Figure 31. Transducer locations are shown on Figure 32. The purpose of providing transducers on one gate was to establish local "instantaneous" pressures for tests involving gate motion. Piezometers require long lengths of tubing, wherein some attenuation of fluctuating pressure amplitudes can result and in tests involving gate motion it was desirable to measure the fluctuating pressures as well as mean pressures on the different members of the gate. The weights of the completed gate were 27.0 lbs (373 kips prototype) for the left gate and 27.2 lbs (376 kips prototype) for the right gate.

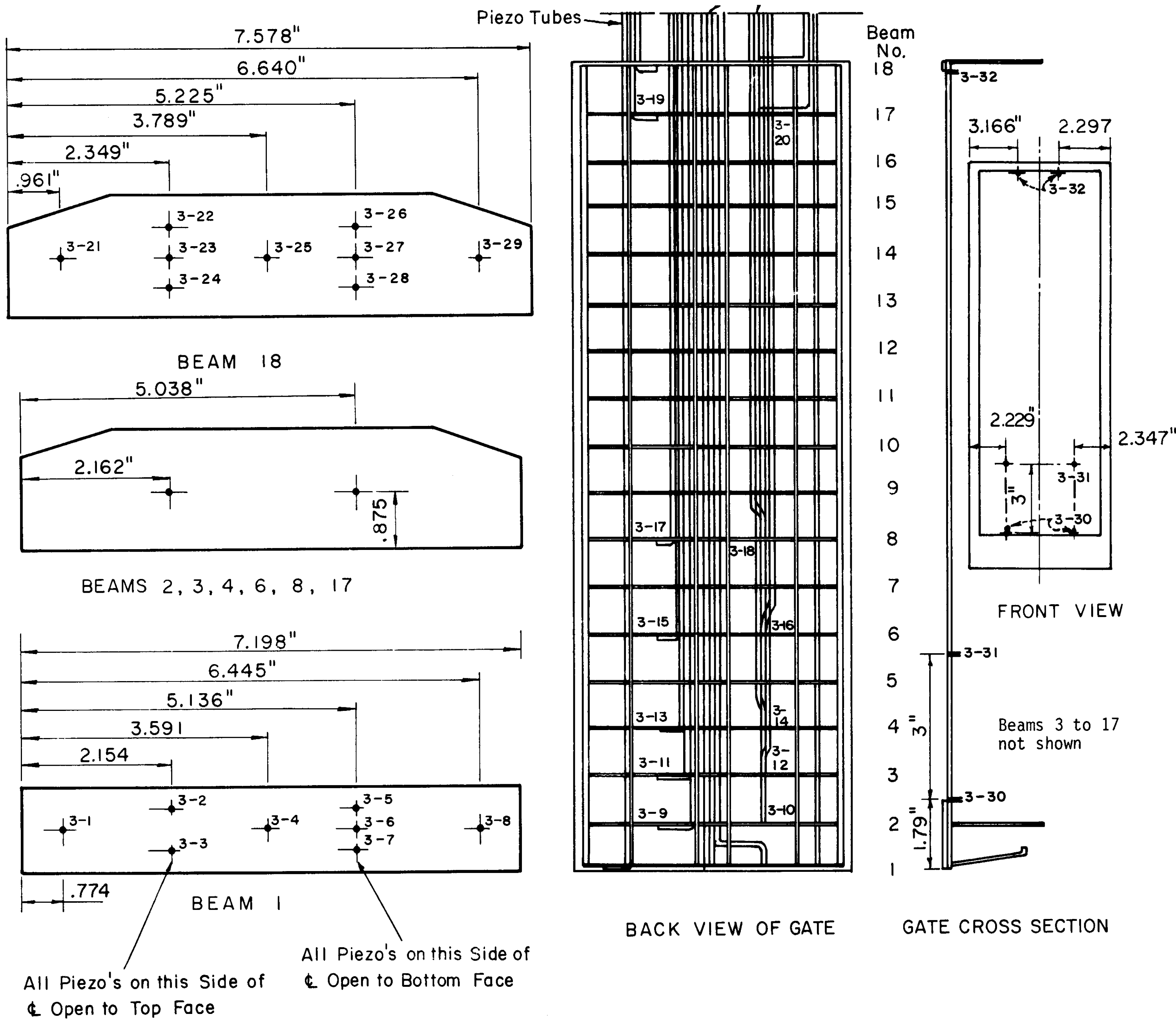

Piezo. No.	Elevation*
3-1	1136.39
3-2	1136.57
3-3	1136.43
3-4	1136.38
3-5	1136.49
3-6	1136.40
3-7	1136.30
3-8	1136.41
3-9	1138.39
3-10	1138.67
3-11	1141.48
3-12	1141.38
3-13	1144.20
3-14	1144.10
3-15	1149.63
3-16	1149.53
3-17	1155.07
3-18	1154.97
3-19	1179.65
3-20	1179.56
3-21	1182.40
3-22	1182.39
3-23	1182.40
3-24	1182.39
3-25	1182.42
3-26	1182.29
3-27	1182.31
3-28	1182.31
3-29	1182.27
3-30	1139.41
3-31	1145.41
3-32	1180.97

*Elevations are referenced to gate closed position.

Figure 31. Piezometer locations on left gate

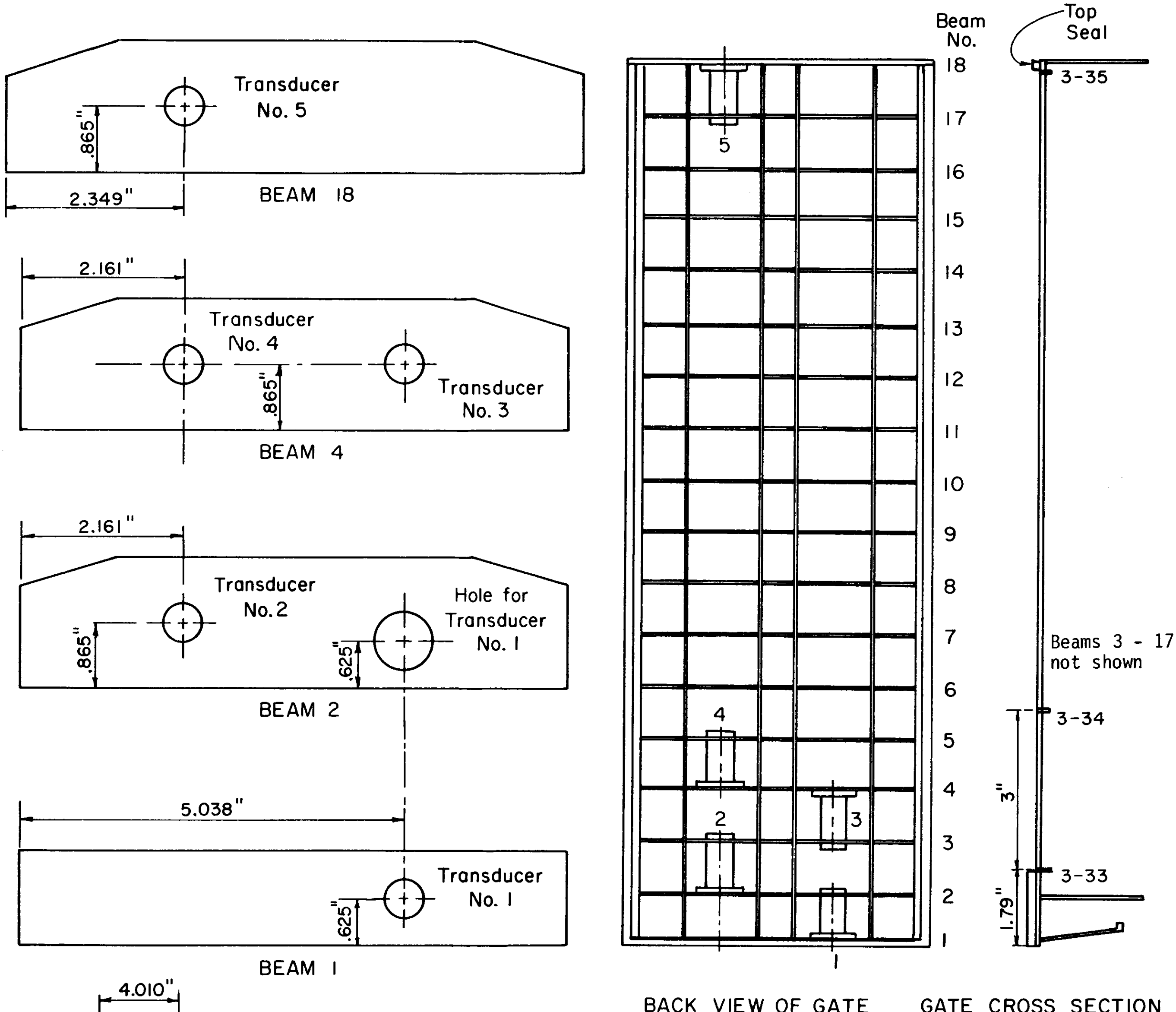

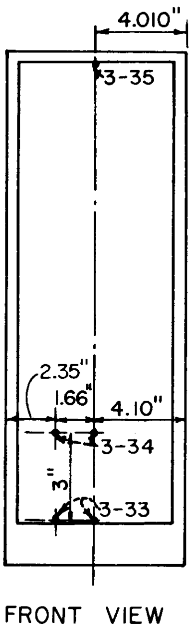

Piezo. No.	Elevation*
3-33	1139.41
3-34	1145.41
3-35	1180.97

*Elevations are referenced to gate closed position.

Transducer	Elevation*
1	1136.32
2	1138.14
3	1144.09
4	1144.19
5	1182.39

*Elevations are referenced to gate closed position

Figure 32. Piezometer locations on right gate

Gate hoists - The hydraulic prototype gate hoists have a normal stroke of 48 ft 10½ inches. The model gates were also equipped with a hydraulic cylinder with a normal stroke of 2 ft. This was about 0.44 inch shorter than the prototype hoist movement but it would raise the bottom of the gate 3 ft above the full open position.

The prototype gate links which connect the gate to the hoist are to be stainless steel tubing 10.75-in. O.D. and 1.25-in. thick. There are 16 links 45 ft and 2 links 27 ft 7-3/4 in. in length required for Tunnel 4. In the model, a 5/16-in. diameter solid steel rod was used. To establish the proper elasticity (spring constant) representative of the prototype, a special, double-spring connecting system was constructed as shown in Figure 33. The system was calibrated and the results will be discussed in a later section.

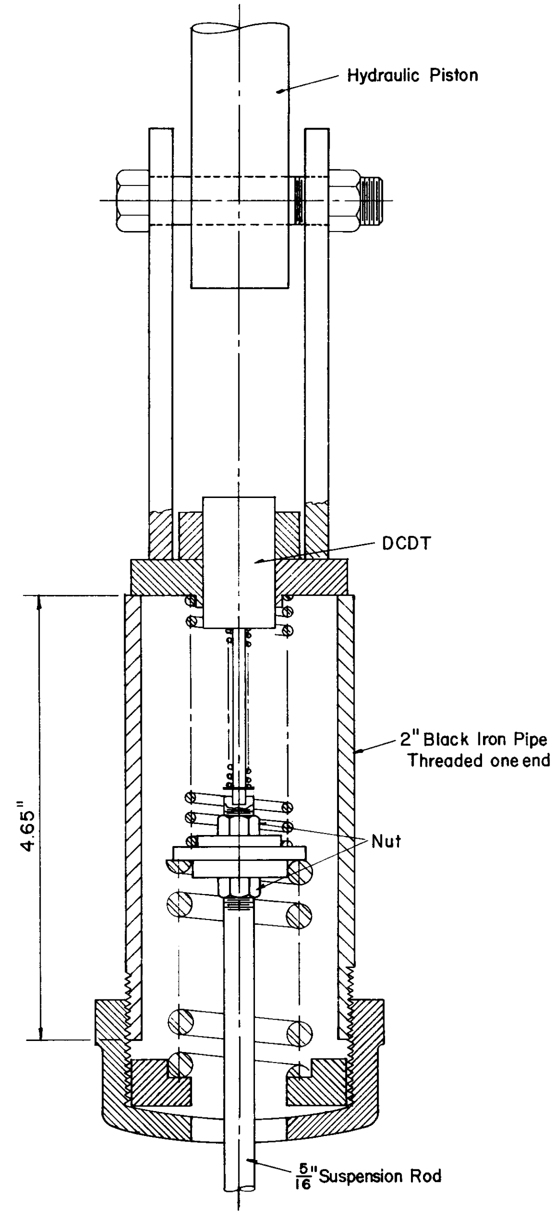

Figure 33. Model gate suspension system

Instrumentation

A number of electronic instruments were used to measure physical variables of concern in this study. Some instruments were purchased "off the shelf" while others were constructed especially for this study. A block diagram of the instrument system is shown on Figure 34. The components are discussed individually.

Gate position indicator - To determine the position of the gate, a special rack and pinion system was constructed to drive a ten-turn potentiometer as shown in Figure 35. The power supply to the potentiometer consisted of two, 1.4 volt mercury batteries, which were chosen so that the maximum output did not exceed the linear range of the record amplifiers of the Ampex tape recorder. The gate position indicator was calibrated with the total system connected, using measured gate position in the completed gate assembly. The calibrations were linear as seen in Figure 36 and they were also identical for the two gate position indicators.

Force indicator - As part of the spring suspension system (see Figure 33), a linear voltage differential transformer (LVDT) was arranged to measure the displacement of the top of the 5/16-in. suspension rod. Hydrodynamic downpull (or uplift) would register in the motion of the rod, hence register an output from the LVDT proportional to the force. A Hewlett-Packard model 7DCDT-100 displacement transducer was used. This instrument has a full scale displacement range of ±0.100 inch with full scale output of 2.8 volts with a DC excitation of 6 volts. A stable, low noise DC voltage was provided for excitation.

As the purpose of the force indicator was to measure the integrated or total hydrodynamic force on the gate, it was desirable to subtract the dead weight of the gate and suspension rod and record only the desired hydrodynamic force. A DC suppression unit was therefore provided to subtract the equivalent dead weight of the system electronically. The output was then put through an impedance matcher to prevent the tape recorder from loading the system.

The two force indicators were calibrated first for linear displacement with output voltage through the total system. The two systems were not identical as the calibration curves show in Figure 37. The systems were then calibrated for force measurement. The calibration curves are shown in Figure 38. The two calibrations thus enable determination of the spring constants for the suspension systems by dividing the slope of the displacement calibration curve by the slope of the force calibration curve. Thus the spring constants for the left suspension system was .00134 in./lb and the right suspension system was .00141 in./lb. This compares with a desired spring constant of .00144 in./lb based on calculated prototype elasticity of the suspension links.

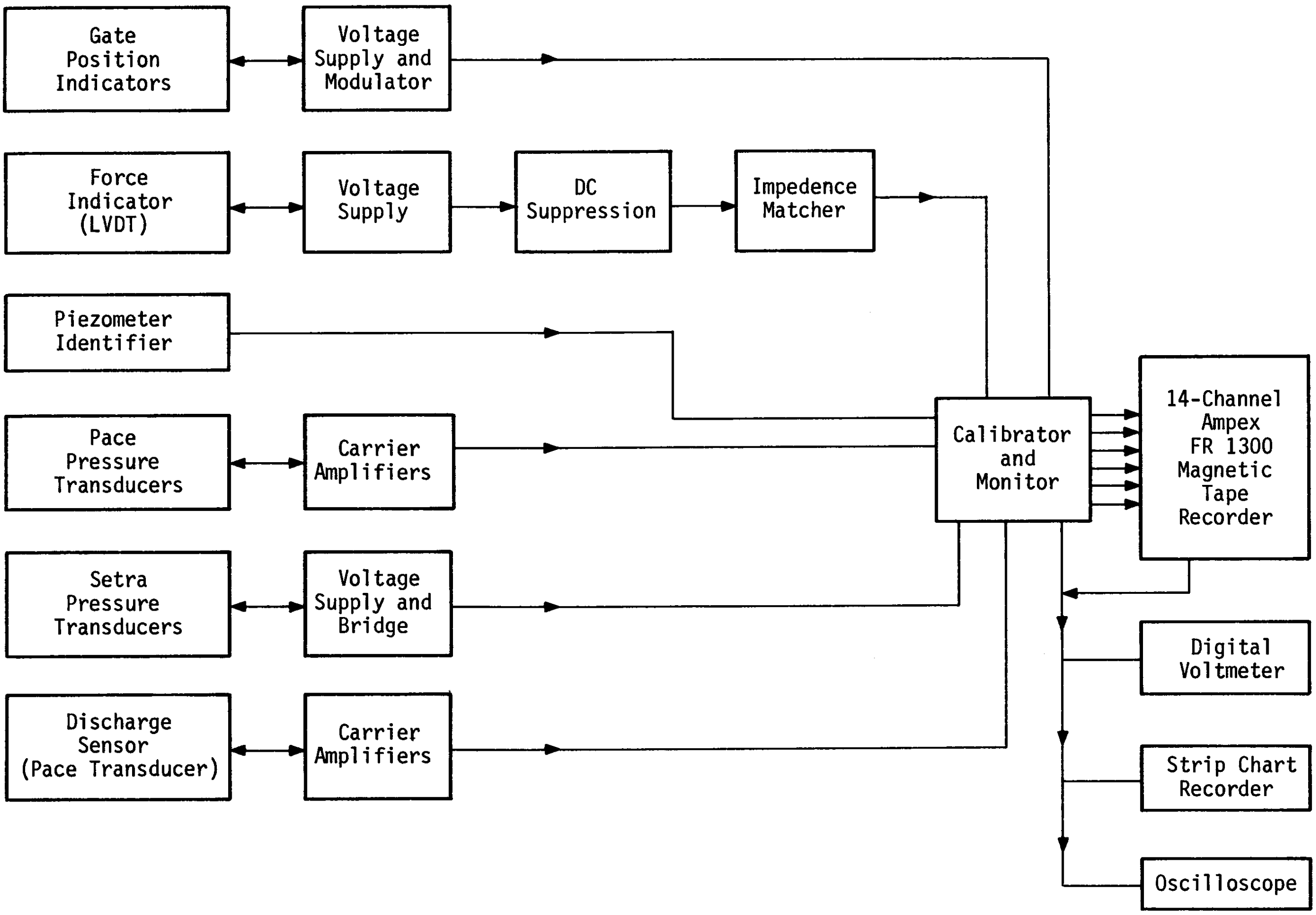

Figure 34. Block diagram of instrumentation system

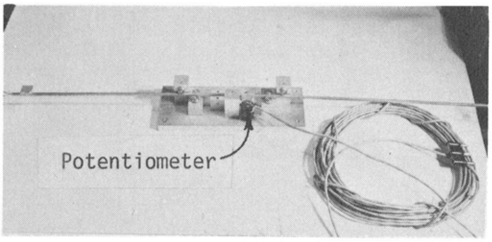

Figure 35. Gate position indicator -
Rack and pinion with potentiometer

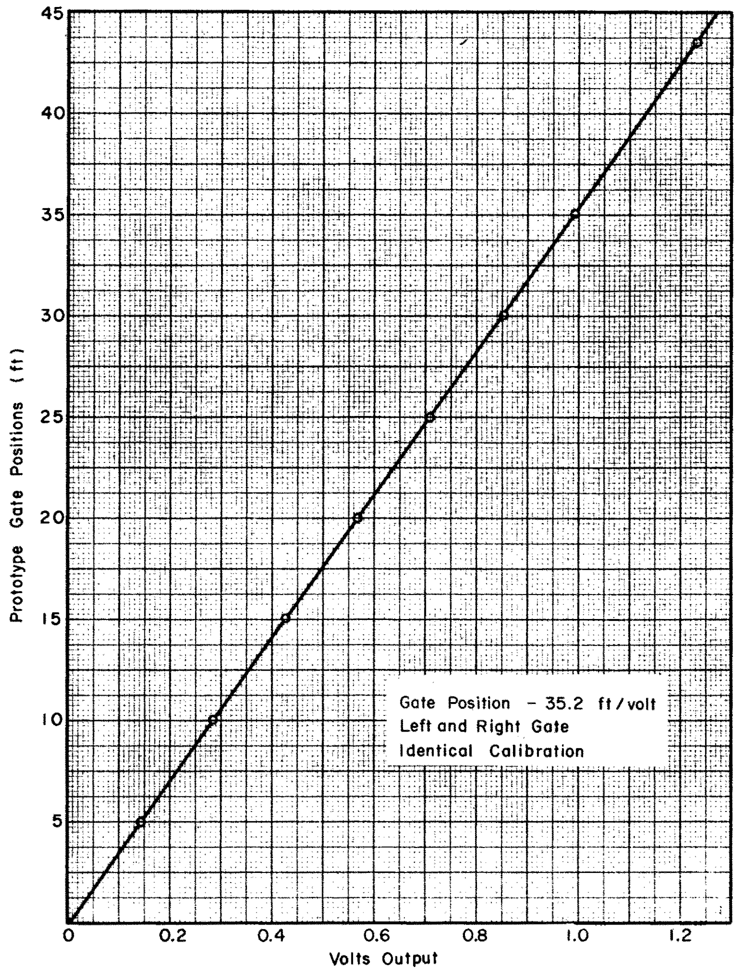

Figure 36. Calibration for gate position indicators.

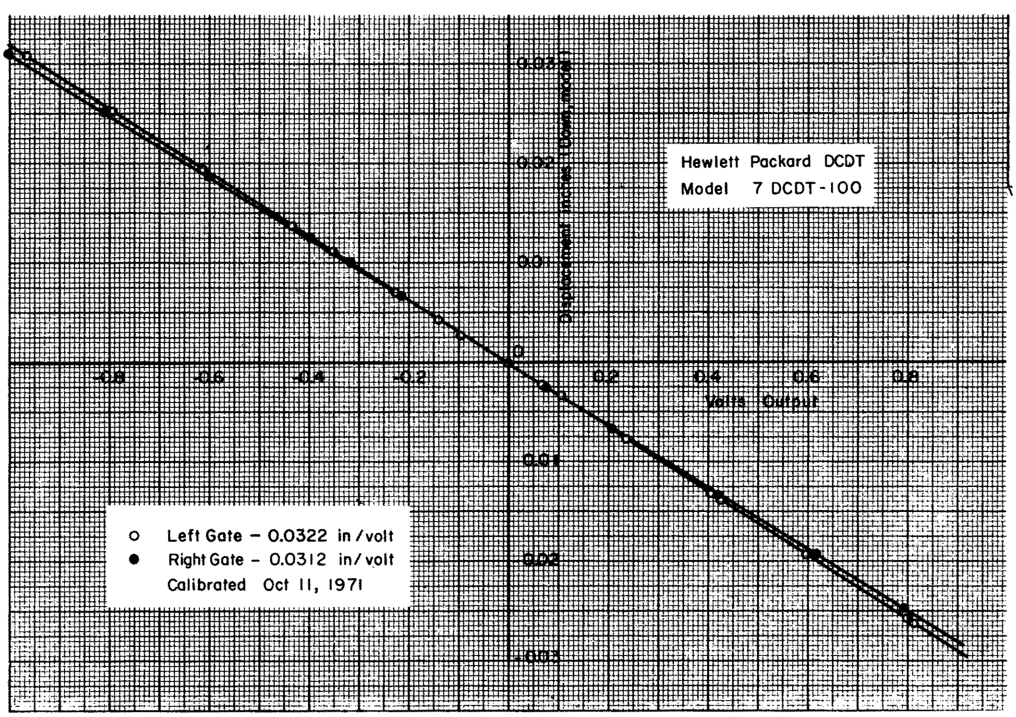

Figure 37. Displacement calibrations for LVDT's.

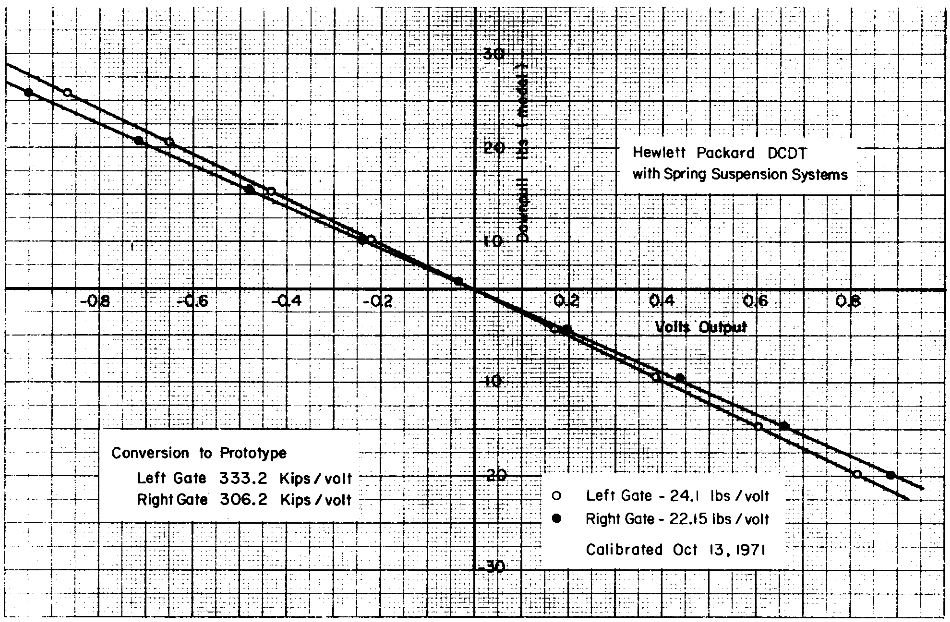

Figure 38. Force calibrations for LVDT's

Pace pressure transducers - There were a total of 164 piezometers to measure local pressures on the large model. The locations were shown on Figures 12, 17, 23, 24, and 25. Three manifold banks were used to connect groups of piezometers so that pressure at each could be measured by a pressure transducer connected to the common chamber of the manifold. A photograph of the manifolds and transducers is shown as Figure 39. The connecting tubing was 1/8-in. polyethylene tubing tested to withstand 100 psi internal pressure. Thus the tubing walls were fairly rigid and did not expand under pressures less than 10 psi experienced in this model.

The pressure transducers used were manufactured by the Pace Company. These are variable reluctance transducers and require AC excitation and carrier amplifiers. The transducers are subject to temperature drift, thus they were immersed in a water bath to maintain a fairly constant temperature. The transducers were calibrated before each test and drift was checked by comparing the output voltages before and after the test. Typical calibration curves are shown in Figure 40. Calibrations were made by connecting the transducers to a 22-ft open water column which extended from the floor of the laboratory to the ceiling. As can be seen, the outputs were linear with pressure head.

There were 49 piezometers connected to manifold bank No. 1, 60 to No. 2, and 55 to No. 3. In order to identify the piezometer at which the pressure was being measured, a piezometer identifier was arranged for each manometer bank. Identification was made by establishing voltage level changes from -1.0 to 0.8 volt corresponding to decimal numbers 0 to 9 on two consecutive channels of the tape recorder. For instance, to identify piezometer 29, a DC level of -0.6 volt on one channel and +0.8 volt on an adjacent channel served to identify the decimal number 29. Increments of 0.2 volt was arranged simply by using mercury batteries and potentiometers.

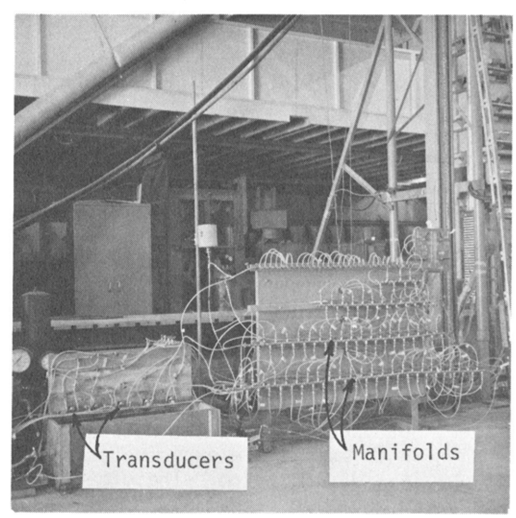

Figure 39. Manifolds and transducers for 164 piezometers

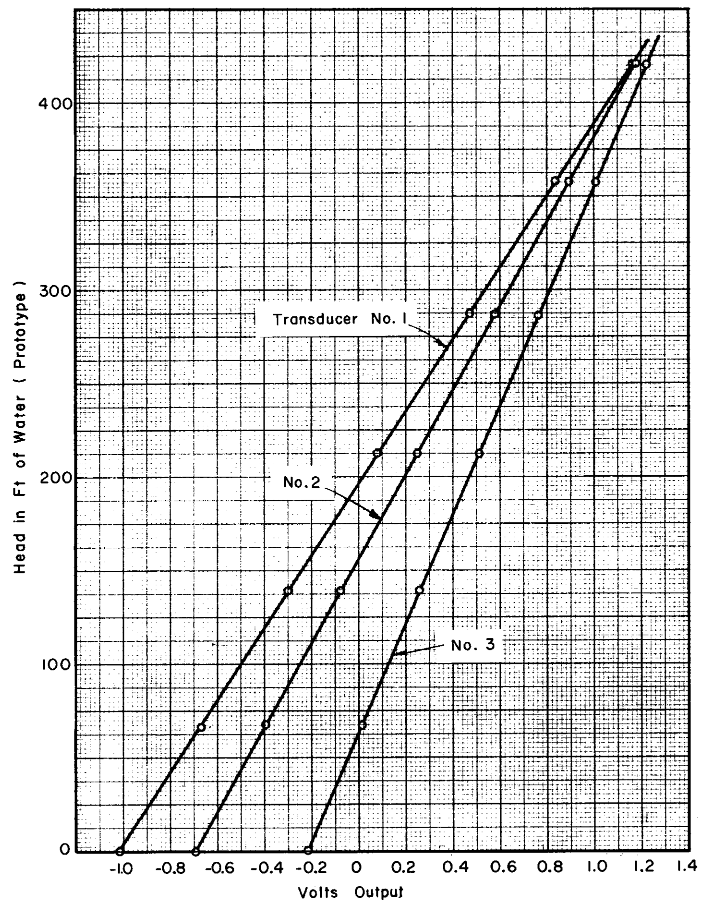

Figure 40. Typical calibration curves for the Pace transducers

Setra pressure transducers - Low range flush mounting pressure transducers were purchased from Setra Systems, Inc. The transducers are capacitance-type sensors with a thin stainless steel diaphram stretched across a stainless steel casing. The electronics are self-contained and involve a variable pulse width modulation system with a center frequency of about 500 KHz. Basically, the variable capacitance due to deflection of the diaphram from pressure variation, is converted to DC output signal. The frequency response was not specified but the natural frequency was 5 KHz which is well above expected pressure fluctuations in a water system. The dimensions of the transducers are shown on Figure 41.

Although the basic carrier amplifier system was self-contained, an additional bridge and excitation voltage supply system was required in order to make the system operational. Ten transducers were purchased, thus a 10 unit supply system was arranged. Two of the 10 transducers became erratic after a period of use and were removed from the system.

Calibrations of the transducers were made in situ before each test run. Typical calibration curves for the eight transducers are shown in Figure 42.

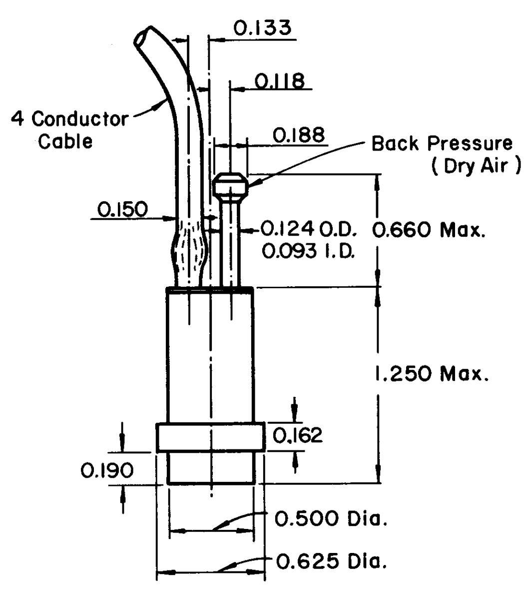

Figure 41. Setra Systems transducer

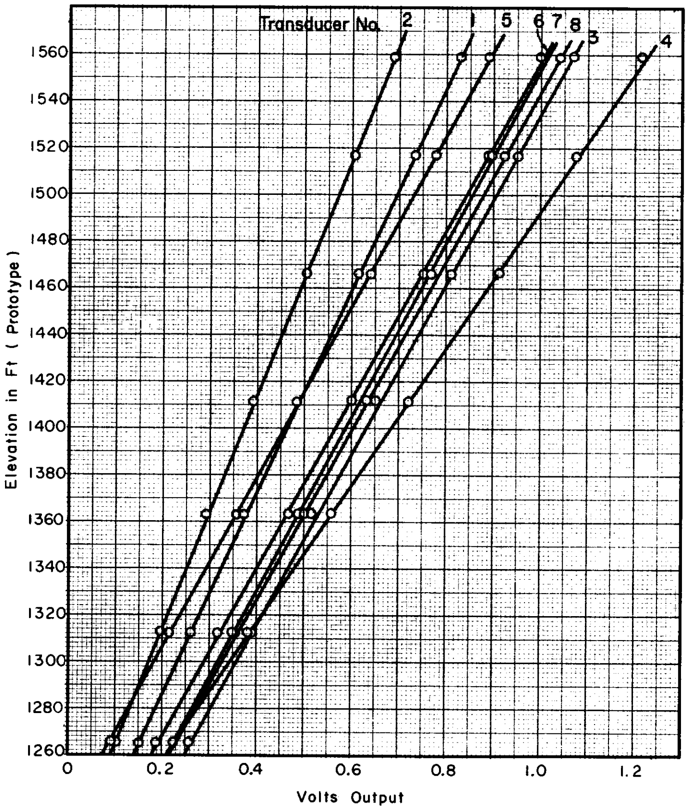

Figure 42. Typical calibrations for the Setra transducers

Discharge sensors - Orifices were used to measure the discharge. To sense the differential head across the orifices, differential pressure transducers manufactured by the Pace Company were used. As shown in the layout of Figure 11, the 2-in. orifice was placed in a 3-in. diameter by-pass line around the large gate valve. Thus, two separate transducers were used.

These differential transducers operated similarly to those used to measure the model wall pressures. The only difference was that the magnitudes of the differential pressures were greater than those which sensed wall pressures. Typical calibrations for these transducers are shown on Figure 43. The differential transducers were calibrated before each test, using a differential water manometer for small heads and mercury manometer for large heads.

Calibration and monitor - The data from this investigation were recorded on a magnetic analog tape recorder. The record was then played back, digitized and analyzed using a digital computer. The total system to determine the physical variable, say pressure or discharge, from the transducer through to the computer output involves a rather complex system. All of the transducers were arranged to produce linear output of voltage for the range of physical variables of interest. The various calibration curves were discussed in previous sections. If, however, the record amplifiers of the tape recorder are not linear, linearity of the individual transducers would be invalidated. Thus, a calibration system was needed to determine the linearity of the tape recorder with respect to input and output voltages. A unit to provide this calibration was assembled, and further, capability to monitor the transducer output was provided. Three different monitors were used, a digital voltmeter (DVM), a Mosely strip chart recorder, and an oscilloscope.

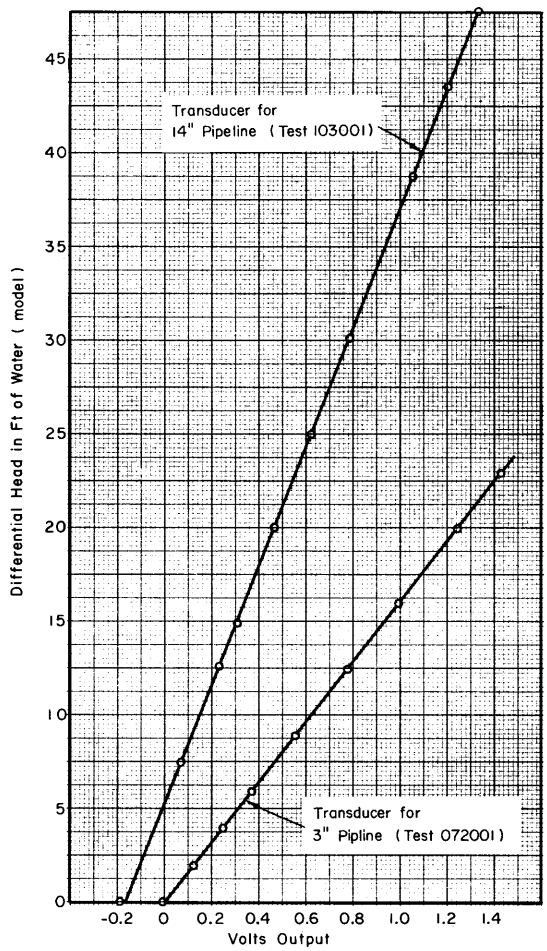

Figure 43. Typical calibrations for differential transducers

The calibrator provides simply a known input DC voltage level into the tape recorder. The digitized output from the computer then provides the appropriate scale (or calibration) to convert the recorded tape voltage to actual voltage. In view of the dependency of the transducers on linearity, a five-level calibration of the tape recorder was made before each test. It turned out that the carrier frequency (center frequency) of the record amplifiers drifted slightly from day to day and the calibration for input-output voltages were valuable in determining the physical quantities.

Analog tape recorder - A 14-channel analog FM recorder was used to record the data. The unit used was an Ampex Model FR-1300 portable tape deck. The recorder has variable tape speed capability which is associated principally with the high frequency cutoff (response) of the amplifiers. In liquid (water) flows, fluctuations of velocity or pressure greater than about 2 KHz rarely exist because of relatively large viscous damping. In the present situation, fluctuations less than 200 Hz were of interest. Thus, a low speed for the tape recorder would require the least quantity of analog tape. However, a trade-off needs to be made. The internal noise level of the tape recorder increases with decreasing tape speed, with consequent reduction of the signal to noise ratio and deterioration of the signal. It was thus decided to run the recorder at a speed of 3-7/8 inches per second (ips) with the high frequency cut off at 1.25 KHz. The noise level was still fairly high at about 10 millivolts rms.

To enable computation of expected hydrodynamic forces on the service gates, there is need to determine the one-dimensional coefficients of flow and forces (or pressures). It is appropriate to consider the physical variables of concern and to arrange them into characteristic dimensionless groups.

Dimensionless Characterizations

The geometric, hydraulic and hydrodynamic variables are identified in the definition sketch of Figure 44. In general the variables will be defined where they first appear in the following discussion.

A one-dimensional characterization of flow through the gate passage could be based on an average velocity through the passage such as V_1 , upstream of the service gate, obtained by dividing Q_0 , the flow through the passage by the normal cross-sectional area bh_0 . The width b is of course fixed at 13.5 ft and the height h_0 is 45 feet. An alternative flow characterization would be V_c , the velocity at the vena contracta of the jet flowing beneath the gate, which could be determined from discharge and gate opening provided a contraction coefficient is known. Contraction coefficients are given for standard leaf and sluice gates in many textbooks and other published literature. However, it was considered advisable to perform separate experiments to determine the contraction coefficients for the present study. The tests and results will be discussed in a later section. The velocity head $V_c^2/2g$ was used as one of the nondimensionalizing parameters in this analysis.

The unobstructed area for passage of flow beneath the gate can be expressed in terms of the total gate opening area. Since the width of the passage (or gate) is constant, this can be expressed in terms of the dimensionless gate opening ratio y/h_0 , where y is the vertical distance from the bottom seal to the sill level and can alternatively be expressed as percent of full gate opening. The other important physical dimension which governs the quantity of flow is the differential head across the gate, $H_1 - H_2 = H_4$, where H_1 is the piezometric level (water surface level) in the bulkhead gate well and H_2 the piezometric level in the service gate well, both referenced from the sill level. If the gate is only partly submerged or unsubmerged, the piezometric head on the downstream side of the gate is the depth of flow above the sill.

A significant quantity of flow can occur through the gap at the top seal, which is a function of H_1 , H_2 and y/h_0 . If H_2 is less than the height to the top of the gate, only H_1 and y/h_0 are significant. The variation in gap area can be seen from Figure 6. In general the effective flow area of this gap is different for different y/h_0 , and the velocity V_s through the gap and the pressure in that passage can develop a significant upward hydrodynamic force F_1 on the top seal clamp bar.

It is convenient to separate the components of the total hydrodynamic downpull F in terms of eight components; F_1 , upward force on the top seal clamp bar; F_2 , the downward force on top edge of the plate backing the bottom seal and extending upward for 3 feet along the gate face; F_3 , the upward force on the bottom beam (beam number 1), including the upward force on the bottom seal; F_4 , the downward force on beam 1;

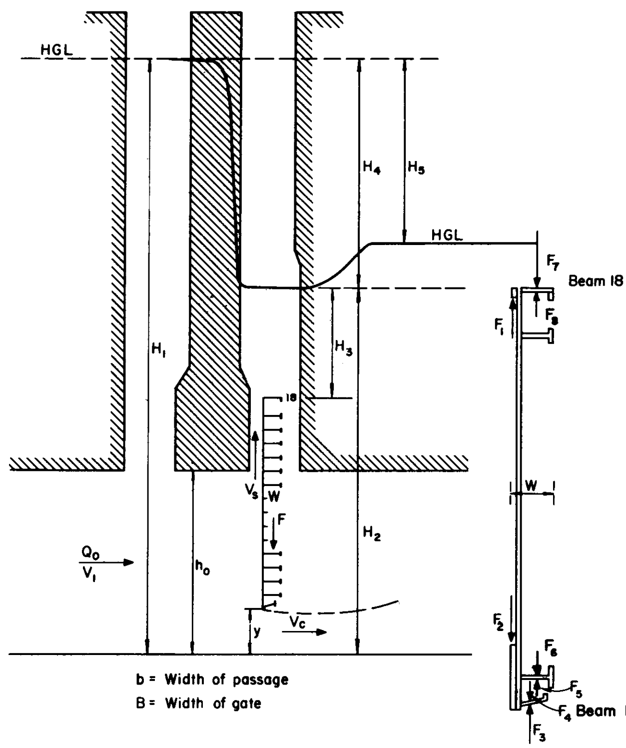

Figure 44. Definition sketch.

F_5 , the upward force on beam 2; F_6 the downward force on beam 2; F_7 the downward force on the top beam (beam number 18) and F_8 the upward force on beam 18. These forces are all determinable from measurements made with piezometers placed on the gates. The hydraulic influence on F_1 has already been discussed. F_2 is affected by the velocity distribution near the lower upstream part of the gate. It is in general, therefore, affected by H_1 (to a lesser extent by H_2) and with gate position, because the pattern of flow changes with gate position. The force F_3 is affected by the flow beneath the gate and is therefore strongly associated with H_4 and $V_c^2/2g$. The variables of the flow which affect F_4 are the same as those which affect F_3 .

The forces F_5 and F_6 represent the unbalanced forces in the vertical direction, acting on beam 2. It was found that the unbalanced forces on beams 2 through 17 were not significant as will be discussed in a later section. Forces F_7 and F_8 are directly related to the head in the service gate well above the level of the beam. Although significant difference from hydrostatic pressure distribution may not be expected, the magnitudes of F_7 and F_8 differ simply because the areas differ.

The total loss of head across the gate structure complex including the transitions may be expressed nondimensionally as a ratio $2gH_L/V^2$, where V may be V_1 , V_c , V_{36} (the velocity in the downstream tunnel) or another reference velocity in the system.

The various hydrodynamic force components can be expressed in terms of the geometry and hydraulic variables which affect the force as follows:

$$\frac{H_j - (F_i/A_i\gamma)}{V_c^2/2g} \quad \text{or alternatively} \quad \frac{H_j - (F_i/A_i\gamma)}{H_4}$$

because of the relationship between $V_c^2/2g$ and H_4. In the expressions above H_j is the piezometric head which affects the hydrodynamic force F_i most significantly, A_i is the appropriate gate area on which F_i acts, and γ is the unit weight of fluid, in this case water.

Orifice Calibrations

The four orifices used for measuring discharges in the various tests were calibrated in the volumetric test facility. Standard flange taps were used with differential manometers to measure the drop in head in Figure 45. Discharges may be written as

$$Q = C_i\sqrt{\Delta h}$$

where Q is the discharge in cfs (prototype) and Δh is the differential head in feet of water (model).

The values of C_i for the various orifices were as follows:

C_2 (2-in. orifice) = 175.0

C_5 (5-in. orifice) = 1876.5

C_{10} (10-in. orifice) = 8925.5

C_{12} (12-in. orifice) = 16652.

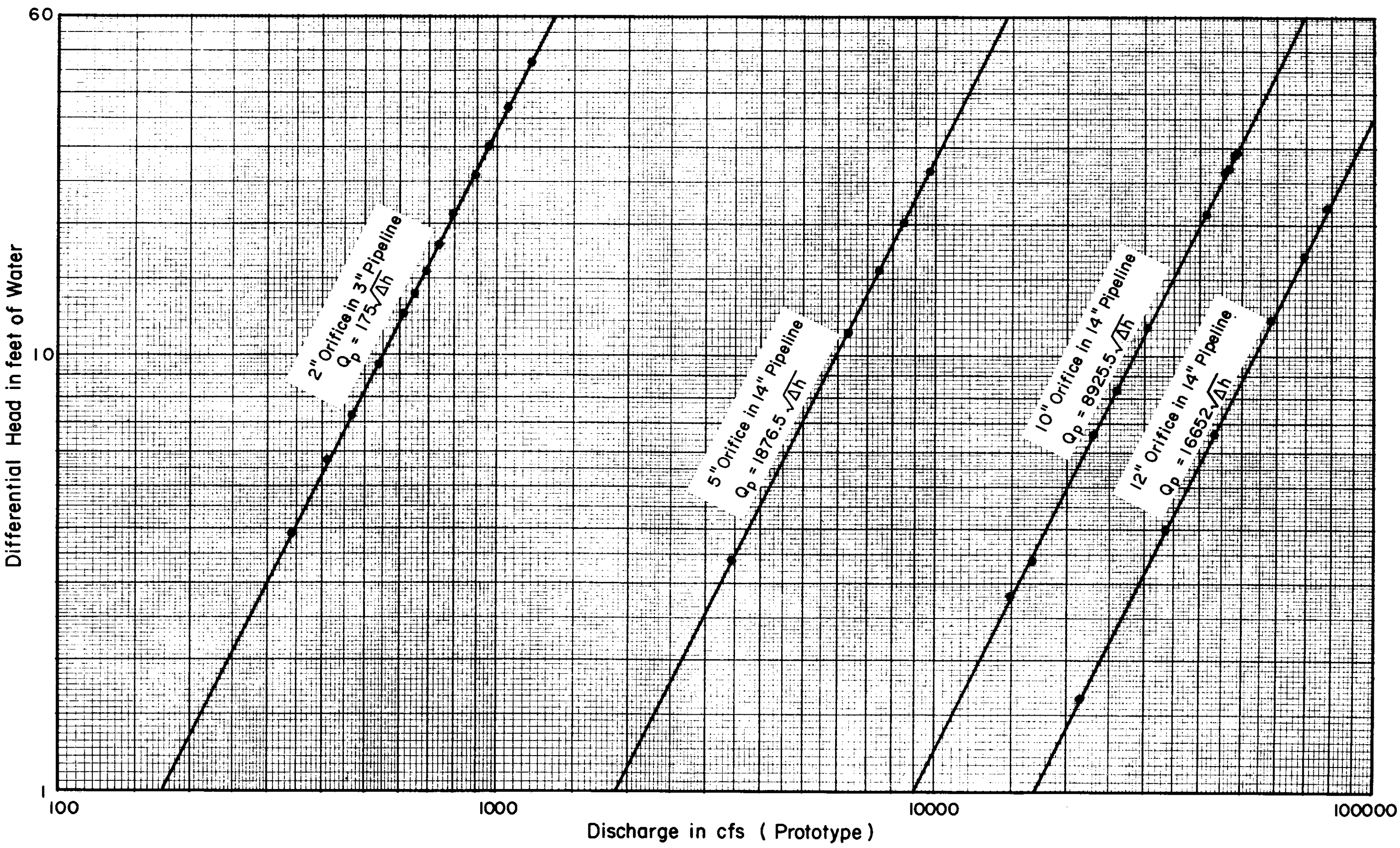

Figure 45. Calibrations for orifices used with the large model.

Gate Leakage Tests

The seals of the model gates were not in contact with the seal surface. Consequently, leakage would occur around the periphery of the gates for the model which would probably not occur, or occur to less extent in the prototype. This gap was purposely made for the model to prevent the seals from rubbing and adding additional, unknown amounts of friction forces. The model gate was therefore impeded in vertical motion only by the friction of the wheels in contact with the plastic runners, whereas in the prototype, the seals will always be in contact with the seal surface, at least for the side seals. Measurements of friction coefficients for the model gates were made and are discussed in Appendix A.

In order to determine the rate of discharge through the seal gap, here called leakage, a set of measurements was made. The leakage was determined for various gate openings at various differential heads across the gate. The discharge was measured through the 2-in. orifice in the by-pass 3-in. pipeline. The opening below the gate was blocked off with wooden blocks and sealed tightly so the measured flow is only the flow through the seal gaps. The results are shown on Figure 46.

The leakage rate is important in determining the quantity of flow under the gate to establish the contraction coefficients. As is noted in Figure 46, the leakage is logarithmically linear with differential head and may be expressed as

$$Q_L = C_L \Delta H^n ,$$

where Q_L is the prototype discharge rate,
C_L is the discharge rate when $\Delta H = 1$,
ΔH is the differential head across the gate in terms of the prototype, and
n is the slope of the line.

The values of C_L and n for different gate positions are given in Table 3 below. Curves of C_L and n are shown in Figure 47 as functions of gate opening in percent.

TABLE 3. LEAKAGE COEFFICIENTS

Gate Position (ft)	C_L	n
Closed	36.7	.526
10	38.2	.554
20	39.3	.540
25	35.5	.554
30	36.7	.526
35	39.1	.488
40	47.0	.420

There is a peculiarity of the curves for C_L and n near 40 percent gate opening which is probably associated with the change in geometry along the wall of the gate shaft. This change in geometry and its effect on leakage rate is evident from a study of Figure 6. When the gate is about 17 feet open (38.8%), there is an abrupt widening of the gap, and control of flow shifts from the top seal gap to free channel flow through an 18-ft long channel that is about 5 in. wide.

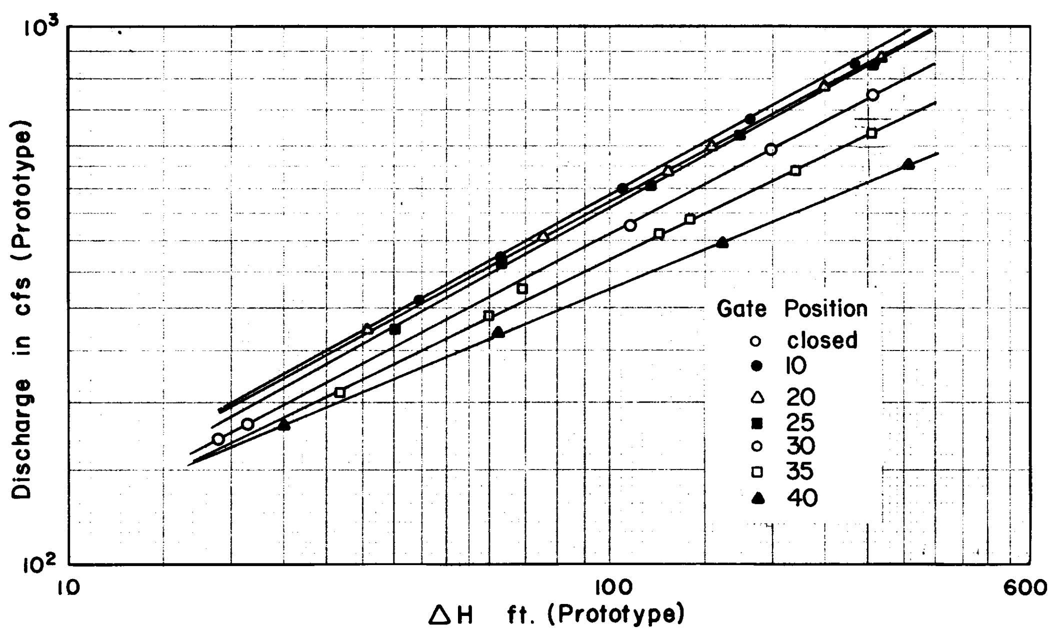

Figure 46. Model leakage rates, Q_L.

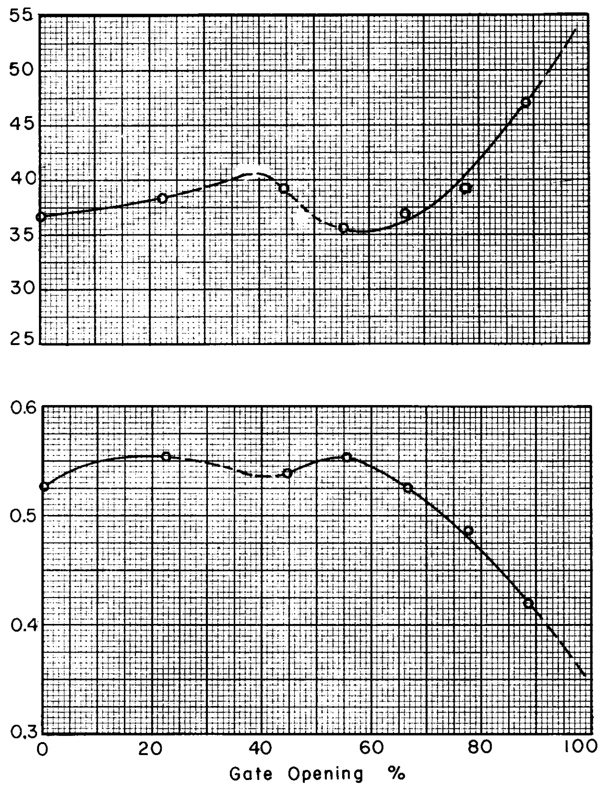

Figure 47. Variations of C_L and n with gate position

Contraction Coefficients

For an idealized one-dimensional flow under the service gate, using the variables indicated in Figure 44, an expression for the contraction coefficient can be determined from one-dimensional continuity and energy relationships. If the downstream flow is unsubmerged,

$$Q_G = Q_o - Q_L = C_c \, by \, V_c = bh_o \, V_1 - Q_L \, ,$$

where Q_G is flow under the gate,
Q_o is flow in the passage, and
C_c is the contraction coefficient.
The energy equation for the flow, considering an upstream section and the vena contracta may be written

$$\frac{V_1^2}{2g} + H_1 = \frac{V_c^2}{2g} + H_2 + H_L' = \frac{V_c^2}{2g} + C_c y + H_L'$$

where H_L' is the loss across the gate and includes the losses brought about by the cascading water stream from top seal gap. If Q_L is considered small in relationship to Q_o or Q_G, and H_L' is ignored, then

$$Q_o = C_c \, by \sqrt{2g(\Delta H + \frac{V_1^2}{2g})}$$

where $\Delta H = H_1 - H_2 = H_1 - C_c y$.
When the gate is submerged, and again ignoring H_L' the energy equation can be written

$$\frac{V_1^2}{2g} + H_1 = \frac{V_c^2}{2g} + H_2$$

where H_2 now includes the depth of the contracted flow and a pressure head on the submerged jet or,

$$H_2 = \frac{P_2}{\gamma} + C_c y \, .$$

By combining with the continuity equation,

$$Q_o = C_c \, by \sqrt{2g(\Delta H + \frac{V_1^2}{2g})}$$

which is precisely the same as for the unsubmerged flow.

The contraction coefficients for submerged and unsubmerged jets are reported in published literature to be the same. However, some difference should be noticeable because the difference in drag at the upper surface of the jet will differ for the two cases. In one case the upper surface is air, and in the other it is water.

The test results obtained from the model are shown in Figure 48 for both submerged and unsubmerged flows. The scatter of data for the "free stream" tests is greater than for the submerged condition because of the difficulty in observing the free surface for the former tests. Although it could be argued that the two curves are essentially the same, a least-square best fit curve was used for the separate sets of data in analyzing test results.

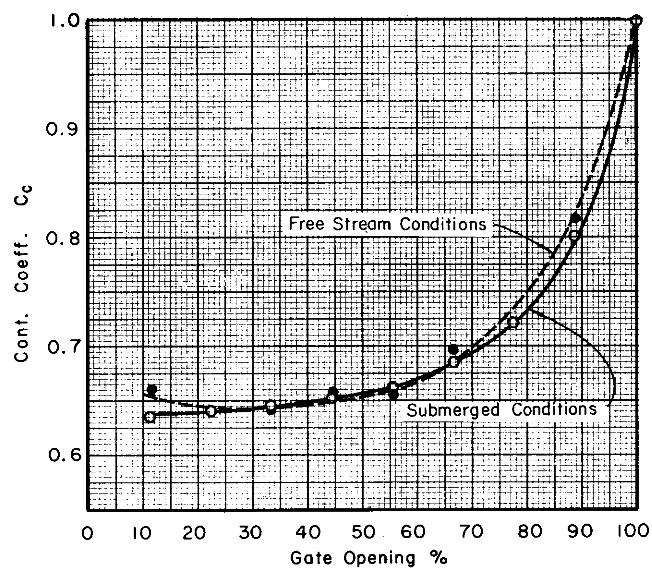

Figure 48. Contraction coefficients for service gate

Downpull Forces and Pressures: Steady State Condition

Steady state refers to a condition of the experiment during which the gates were held at a fixed position and discharge was held constant at fixed head. With such conditions the time-mean values of the hydraulic grade lines, piezometric heads on the walls of the gate structure and piezometric heads on the gates could be measured. From these measurements the dimensionless parameters discussed in a previous section could be calculated and used to determine downpull forces on the prototype gates.

There were three groups of steady state tests made. Most of the measurements involved only the left passage and the left gate. The three groups involved the following conditions: (1) the gate being completely submerged below the water level in the service gate well, (2) the gate partially submerged where the water level in the downstream transition was higher than the level of the bottom gate seal, and (3) no submergence where the water surface of the contracted jet was clearly identified to be below the level of the bottom seal. This condition (3) is also referred as "free flow" or "free surface flow." These three conditions were identified in the small model as being possible hydraulic conditions for various reservoir levels and radial gate openings. The test procedures for all three groups were essentially the same as described below.

Test procedure - All 164 piezometer lines were purged of entrapped air at the beginning of testing each day and also whenever air bubbles were observed in the lines during a test. The "bleeding" was accomplished by back-flushing the lines using water and the pressure from the potable "city" supply. The transducers were calibrated using appropriately the open tube 22-ft long water manometer or the differential manometers. The model was then filled, using the 2-in. bypass line, until the water level in the service gate well was above the tops of the gates. With the gates thus submerged, the LVDT force indicators were zeroed. Corrections were thus necessary to the LVDT measurements because the hydrodynamic downpull must include the hydrostatic (buoyant) force. These corrections will be discussed in the appropriate sections.

The gates were positioned to predetermined openings. The flow was then initiated through the model by simultaneously adjusting the flow control valves in the line until the desired water levels in the bulkhead and service gate wells were established. When steady state conditions were achieved, the piezometer and force measurements were recorded on the FM tape recorder. Whenever possible or appropriate the measurements were monitored, and the monitored readings indicated by the digital voltmeter, strip chart or oscilloscope were recorded manually on data sheets.

The tests were identified by a five or six digit number, as for instance, 100203. The first pair of digits 10 represents the month, the next pair 02 identifies the day of the month, and the final pair 03 indicates the test run on that day. These identification numbers facilitated the clerical bookkeeping involved in handling the data during reduction and analysis processes.

Data reduction - The bulk of data reduction was performed with the computer. The analog tape records were first converted to discrete digital form on digital magnetic tape using an analog-to-digital (A/D) converter. The analog data were filtered at 100 Hz before digitizing, and the digitizing rate was at 200 samples per second per channel. The converted digital records were then processed. The simplified flow chart which describes the data processing and reduction procedure is shown in Figure 49. A typical output of the computer analyzed data is included in Appendix B.

The computer output provided the following measured information for each test:

1. The position of the gate.
2. The force indicated by the LVDT without corrections.
3. The discharge measured at the orifice.
4. The piezometric heads for each piezometer with prototype sea level as the datum.
5. The pressure head for each piezometer.
6. The average gate position, force and discharge.

From these measured values the following information were calculated:

1. Forces on each horizontal beam of the gate.
2. Forces on the seal clamp bars.
3. Sum of the individual forces.
4. Leakage around the gate.
5. Flow under the gate.
6. Total flow in the passage.
7. Velocity at the vena contracta.
8. Velocity head at the vena contracta.
9. A hypothetical reservoir elevation.
10. Velocity head in the upstream tunnel.

Results of Tests and Discussion

Hydraulics - submerged conditions - The hydraulic grade line along the entire model was plotted for each test run to calculate the values H_i , $i = 1, \ldots 5$, as given in the definition sketch. It was noted that anomalous values were often prevalent for the 5 piezometers in the 45-ft diameter approach tunnel. Using the value measured at piezometer number 1-5 (Figure 12) as a key value, a grade line was fitted to other measured piezometric heads. The water level in the bulkhead gate well was measured by piezometer 3-55. In plotting the hydraulic grade line this value was checked with the value at piezometers 1-10 and 3-36 (the right bulkhead gate well) for consistency. The water level in the service gate well was measured by piezometers 3-38 through 3-41, and depending upon the actual level, the reading from the highest positioned piezometer, but below the water surface, was used to determine the water level in the gate well. Piezometers along the centerline of the downstream transition and tunnel were used to establish the hydraulic grade line in the 36-ft diameter tunnel. For gate openings between 5 and 30 ft, the values of head near piezometer 1-27 were used to calculate H_5 . For gate openings less than 5 and greater than 30 ft, the level of the hydraulic grade line at the beginning of the 36-ft diameter tunnel was used. The calculated values of H_i are listed in Table C-1 of Appendix C.

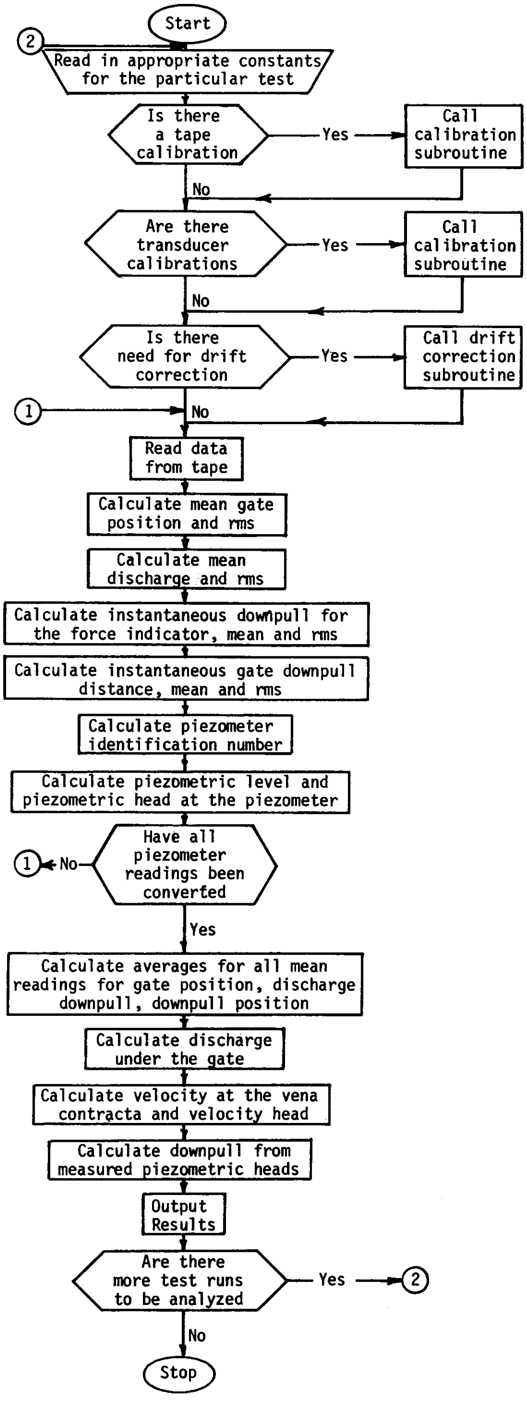

Figure 49. Flow chart for data processing

The loss of head between the beginning of the upstream transition and end of the downstream transition (or piezometer 1-27 for gate openings between 5 and 30 ft) may be expressed in the following manner.

The one-dimensional energy equation between the two cross-sections of concern may be written as

$$\frac{V_a^2}{2g} + H_a = \frac{V_b^2}{2g} + H_b + H_L$$

where V_a and V_b are the average cross-sectional velocities in the 45 and 36-ft diameter tunnels respectively,
H_a and H_b are piezometric heads referenced to sill level 1135.8, and
H_L is the loss in head between the two sections.

Using the continuity relationship for steady flow, the energy equation may be rewritten as

$$\frac{2gH_L}{V_b^2} = \frac{2gH_5}{V_b^2} - 0.59$$

where the values H_5 are given in Table C-1. The parameter $2gH_L/V_b^2$, which is one form for the head loss coefficient, is calculable directly upon determination of V_b from the discharge through the tunnel. The head loss coefficient is shown on Figure 50 as a function of gate opening and the calculated values are tabulated in Table C-2 of Appendix C. As can be seen, the coefficient becomes very large for small gate opening and this particular form for a coefficient is somewhat objectionable from this point of view. Also, for gate opening larger than about 50 percent, the coefficient is less sensitive to gate opening.

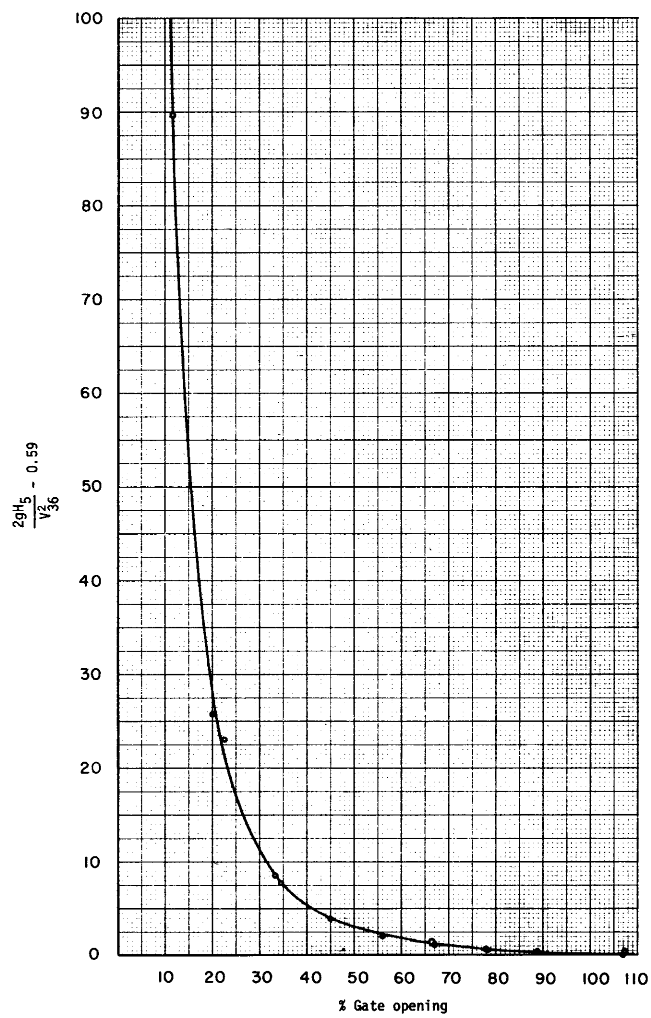

Figure 50. Head loss coefficients.

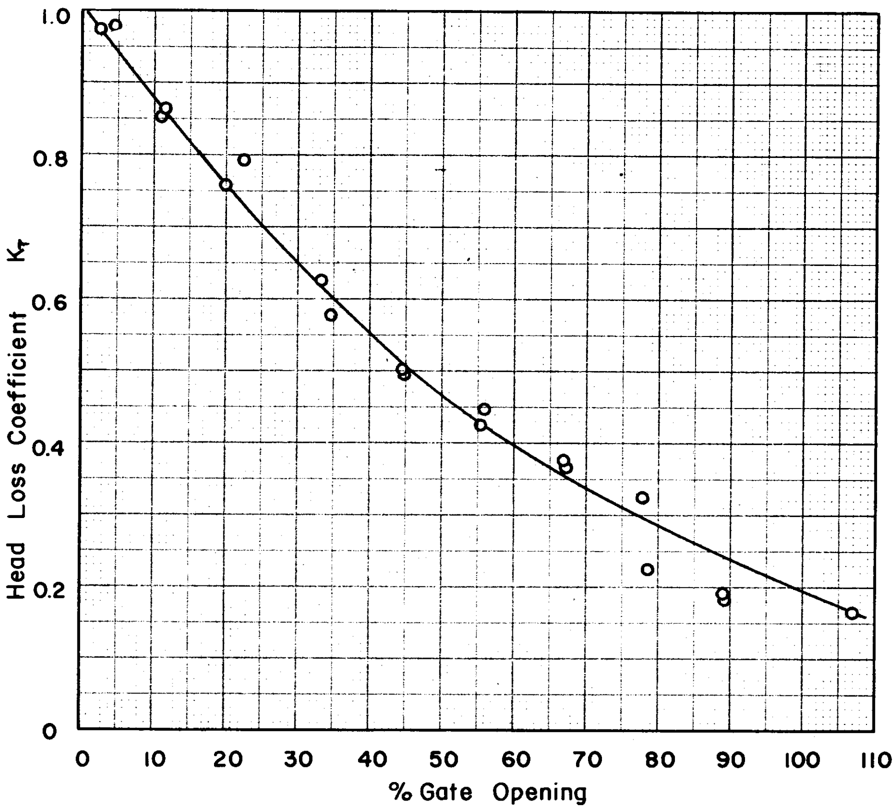

Figure 51. Head loss coefficient, K_T

The head loss can be nondimensionalized with velocity head at the vena contracta of the flow beneath the gate, resulting in a head loss coefficient expressed as

$$K_T = \frac{2gH_L}{V_c^2} .$$

The variation of K_T with gate opening is shown on Figure 51. The curve drawn on the figure was fitted by eye. Calculated values are tabulated in Table C-2.

The water level in the service gate shaft is a function of the service gate opening, discharge, and control offered by the radial gates at the outlet end of the tunnels. The parameter

$$K = \frac{2gH_4}{V_c^2}$$

is shown in Figure 52 as a function of gate opening. H_4 is the difference in water levels in the bulkhead and service gate wells (see Figure 44). A curve designated "free surface" is also included in the figure and will be discussed later. It is seen that the differential head H_4 is dependent principally upon V_c and gate position. The curve shown thus enables calculation of H_2 with H_1 known.

It should be noted that values obtained for a gate position of 48 ft have been plotted at the 100 percent gate position because beyond full gate opening the service gate cannot have an effect on H_4 or $V_c^2/2g$. Also, the measured head H_2 was greater than H_1 at gate positions greater than 100 percent, due undoubtedly to the dynamic effect caused by the wider opening of the service gate shaft at the top of the passage with the added influence of the downstream transition. The data for Figure 52 are tabulated in Table C-2.

Forces on the gate - submerged conditions - The one-dimensional characterization of the flow was discussed in the foregoing sections. With these parameters, now determinable for all flows in the tunnel, it is desirable to express the downpull on the service gate in terms of the hydraulic parameters. As discussed earlier in this chapter, the downpull force is more conveniently divided into its separate parts. Although the coefficients which follow in this discussion are not expressed in terms of force, they are interpretable as forces because the "effective head" acting on a relevant portion of the gate $(H_i - Z_i)$ may be expressed as

$$H_i - Z_i = \frac{F_i}{\gamma A_i}$$

where H_i, i = 1, 2, . . . are piezometric heads above sill level,
F_i, i = 1, 2, . . . are the forces as shown on the definition sketch of Figure 44,
A_i, i = 1, 2, . . . are the appropriate horizontal areas,
Z_i, i = 1, 2, . . . are elevations of the particular piezometer above sill level, and
γ = specific weight of water.

To express the heads, H_i , nondimensionally, they are combined with the significant flow parameters to form a pressure head coefficient, called pressure coefficient herein for brevity.

(a) Forces on the top seal - The force referred to in this section as the top seal force, F_1 , is only the upward force on the top seal clamp bar. The downward force on the top seal clamp bar is included as part of the downward force on the top beam (beam 18). This separation of forces is reasonable since the pressures on the top sides of the top seal clamp bars are responsive to different hydraulic parameters of the flow.

The pressure head, hence the force, on the lower face of the top seal clamp bar is a function of the ambient pressure head expressed by H_1 and the velocity of flow V_s through the gap (discussed earlier). This velocity is in turn dependent upon the differential head H_4 , thus the relevant flow variables are H_1 and H_4 . The pressure head acting on the clamp bar is assumed to be measured by piezometer 3-32 (see Figure 31) which was located on the face plate of the gate but in the corner formed by the clamp bar where stagnation can be assumed reasonably to exist. A pressure coefficient C_{TS} is defined by

$$C_{TS} = \frac{H_1 - H_{32}}{H_4}$$

where H_{32} is the pressure head on the bar measured at piezometer 3-32, referenced to the sill level. The coefficient C_{TS} as a function of gate position is shown on Figure 53. A curve labeled C_{TF} , C_{TP} is also shown on this figure and will be discussed later.

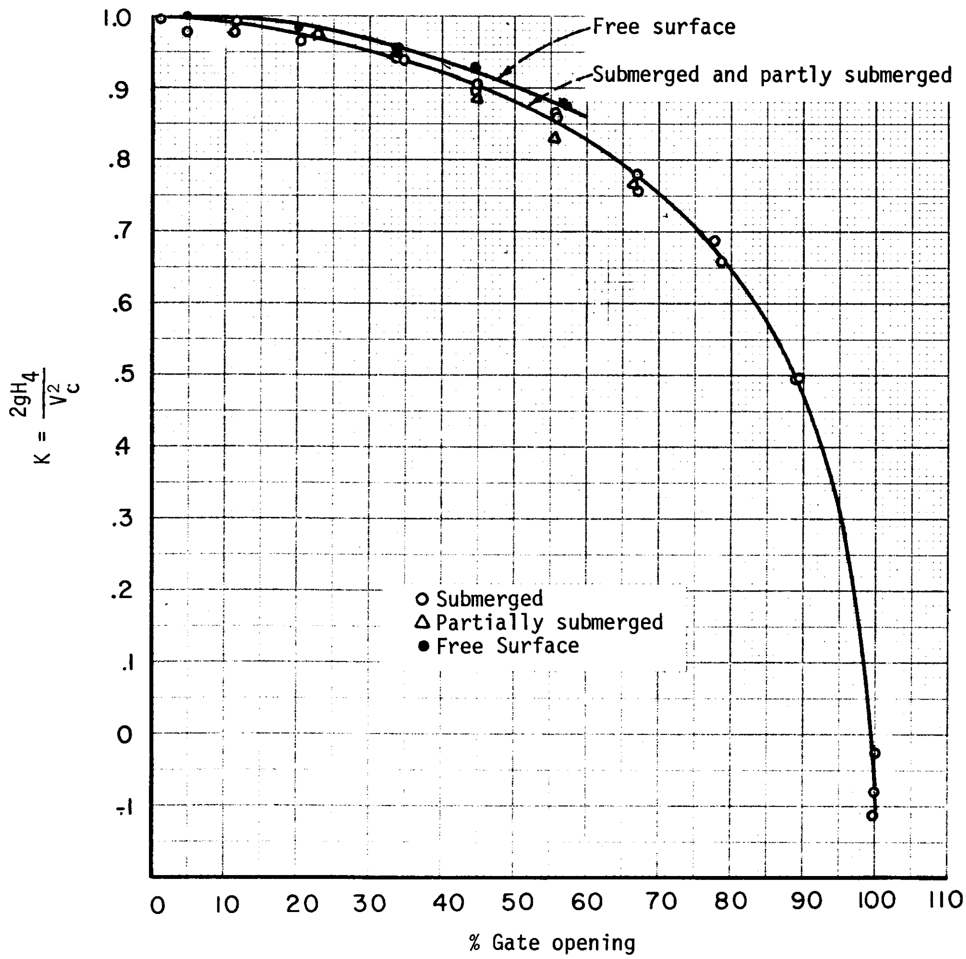

Figure 52. Variation of K with gate position

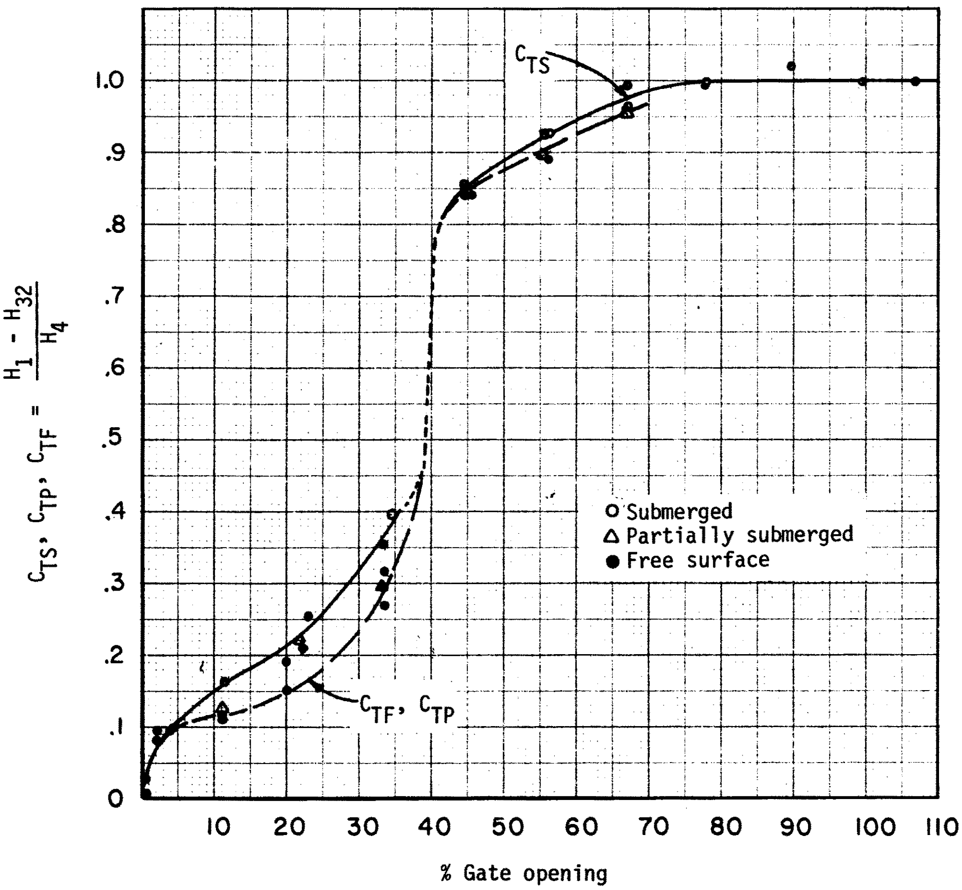

Figure 53. Variation of pressure heads on the top seal clamp bar.

There is a discontinuity of C_{TS} at about 40 percent gate opening. This is the gate position (about 17 ft gate opening) where the change in geometry of the shaft wall affects the pressure at the top seal quite significantly. Where, for gate openings less than 40 percent the control of flow along the wall of the gate shaft is effected by the top seal and clamp bars, beyond 40 percent gate opening the control changes to the gap between the seal surface at the top of the passage and the face of the gate. The ambient pressure H_1 then has less effect on H_{32} and is reflected in a "discontinuity" of the curve. When the gate is beyond 75 percent open, the head H_{32} is essentially the head H_2 so that C_{TS} is equal to unity. Only a hydrostatic pressure difference, or buoyant force, is then effective, and neither H_1 nor the dynamic effect of the velocity through the gap has influence on the upward force on the top seal clamp bar. The data for Figure 53 are included in Table C-2.

(b) Forces on the bottom seal plate - The force F_2 is the downward force acting on the top edge of the plate backing the bottom seal. This plate extends 3 feet above the bottom seal along the gate face. The pressure head along this top edge is assumed to be measured by piezometer 3-30 (see Figure 31) located as with piezometer 3-32 in the corner formed by the face plate and the backing plate.

Because the pressure is strongly influenced by the flow pattern near the bottom of the gate, $V_c^2/2g$ is used to nondimensionalize the pressure head H_{30} which is the piezometric head measured by piezometer 3-30 and referenced to sill level. The pressure head H_1 in the passage will obviously influence the magnitude of H_{30} and must be included. The pressure coefficient may be written as

$$C_{BS} = \frac{2g(H_1 - H_{30})}{V_c^2} .$$

The variation of C_{BS} with gate position is shown in Figure 54. If the top of plate is above the top of the passage (i.e. above gate opening of 92 percent) the expression for C_{BS} above is no longer a reasonable parameter for H_{30} . A parametric expression

$$C'_{BS} = \frac{H_1 - H_{30}}{H_4}$$

similar to C_{TS} might better express the coefficient for H_{30} . However, there was insufficient data in the range of gate openings from 92 to 100 percent to develop a graphical representation of C'_{BS} . Thus, the curve for C_{BS} is terminated at gate opening of 92 percent and a dashed vertical line is shown to accentuate the discontinuity with the isolated points plotted near 100 percent gate opening. A dashed horizontal line at $C_{BS} = -0.05$ is drawn to suggest a value which may be used to estimate H_{30} for gate openings greater than 92 percent. Beyond 100 percent, H_{30} should be identical with H_2 , thus $C'_{BS} = 1.0$. The data are included in Table C-2.

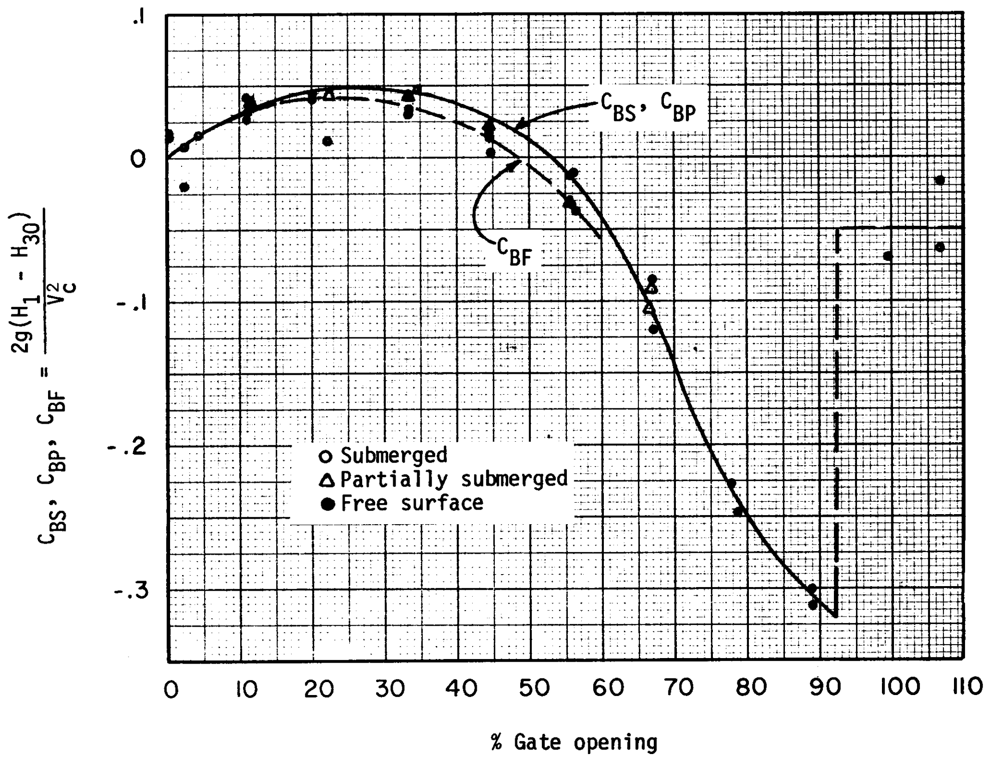

Figure 54. Variation of pressure heads on the bottom seal plate.

(c) Forces on the bottom beam (beam 1) - The measured pressure heads at all piezometers on the horizontal beams of the left gate (piezometers 3-1 through 3-29) are shown in Figures 55(a) and (b) for the submerged steady state tests. From these pressure head profiles it was observed that:

1. The pressures are always approximately hydrostatic above beam 6.

2. Although the pressures are less than hydrostatic below beam 6, the difference between top and bottom pressures at beams 2, 3 and 4 are not substantial and may be assumed zero.

3. Variations in pressure heads occur between the top and bottom sides of beams 1 and 18. This is a consequence of the high velocity of the jet through the gate opening which affects the pressures on the bottom side of beam 1 more than the top side, and also the probable variation of velocity across the passage width. The pressures at beam 18 are affected in most cases by the sudden change in area which the flow down the service gate shaft encounters.

4. The pressures acting on the bottom of beam 1 are significantly less than the pressures at the top of that beam.

5. The pressure differences at beams 1 and 18 contribute most significantly to the hydrodynamic downpull.

The variations in head at the top and bottom of beam 1 are replotted in Figure 56. Also indicated on each plot are area weighted average pressure heads (shown as horizontal dashed lines) for the top and bottom of the beam. The weighted average was calculated using the assumption that pressure measured at a given piezometer was effective over an area as indicated on Figure 57.

As a consequence of observation 3 stated above, the pressure coefficients for beam 1 are expressed separately for the top and bottom. The pertinent nondimensionalizing parameters are $V_c^2/2g$ and reference head H_1 for the pressure coefficient for the bottom side of the beam. Because the top side of beam 1 is also in the same region of the flow field, it would be expected that these same variables (H_1 and $V_c^2/2g$) would be relevant nondimensionalizing parameters also.

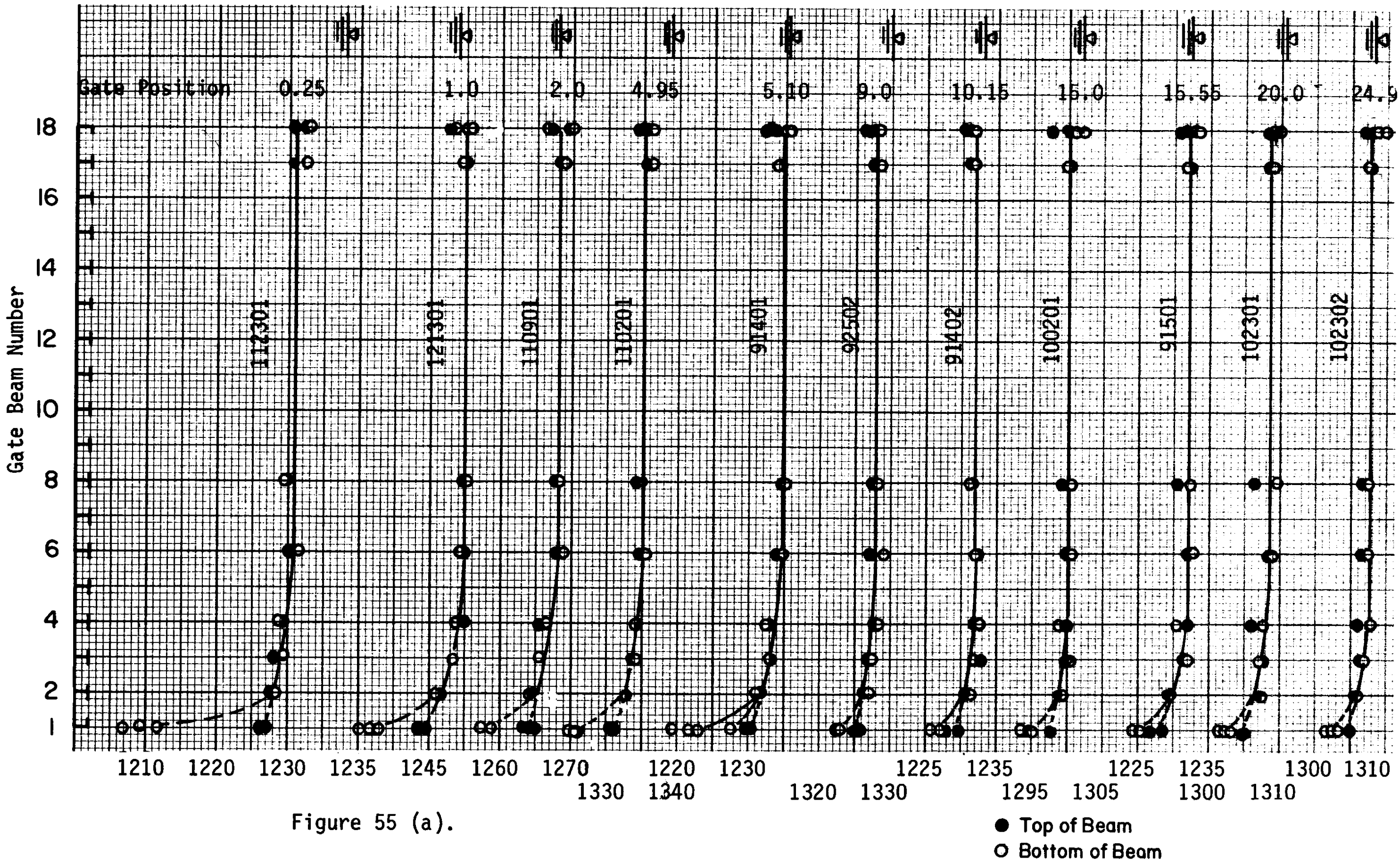

Figure 55 (a).

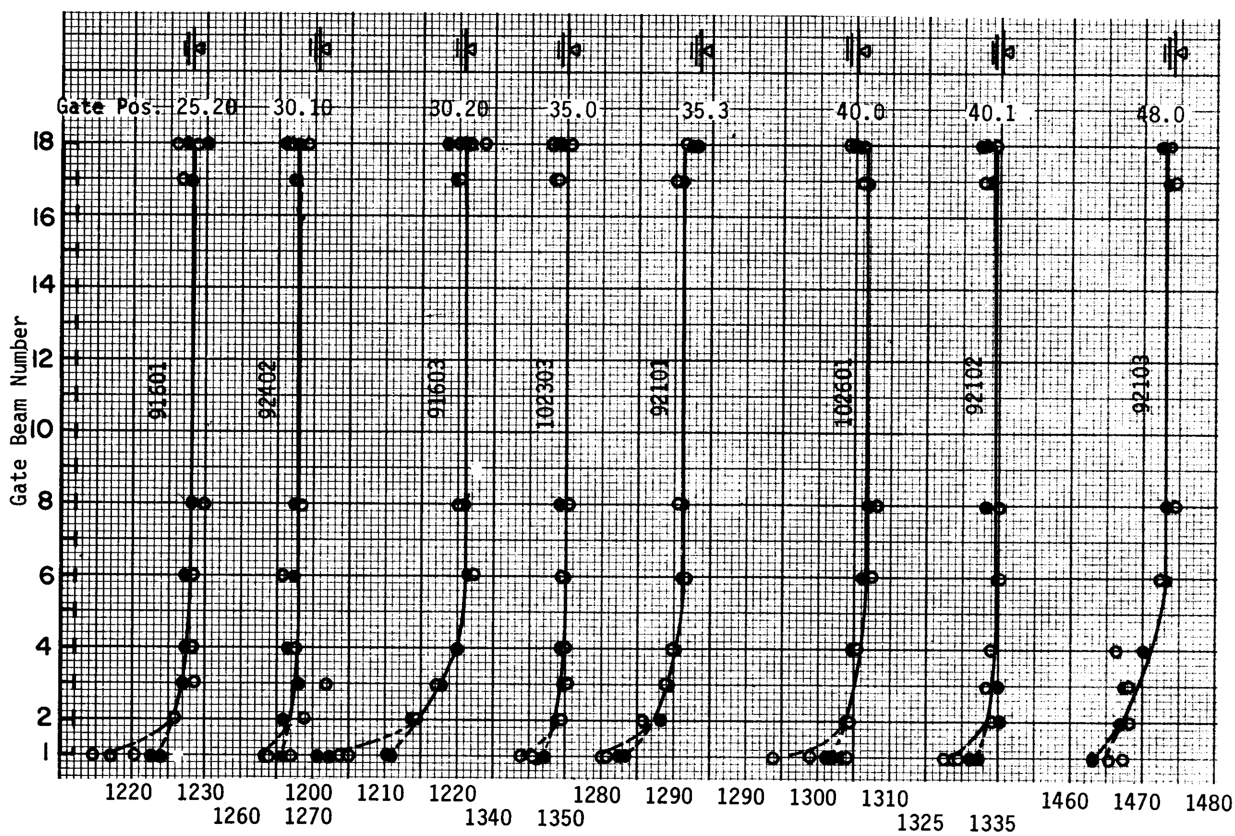

Figure 55 (b).

Figure 55. Piezometric head profiles along gate beams.

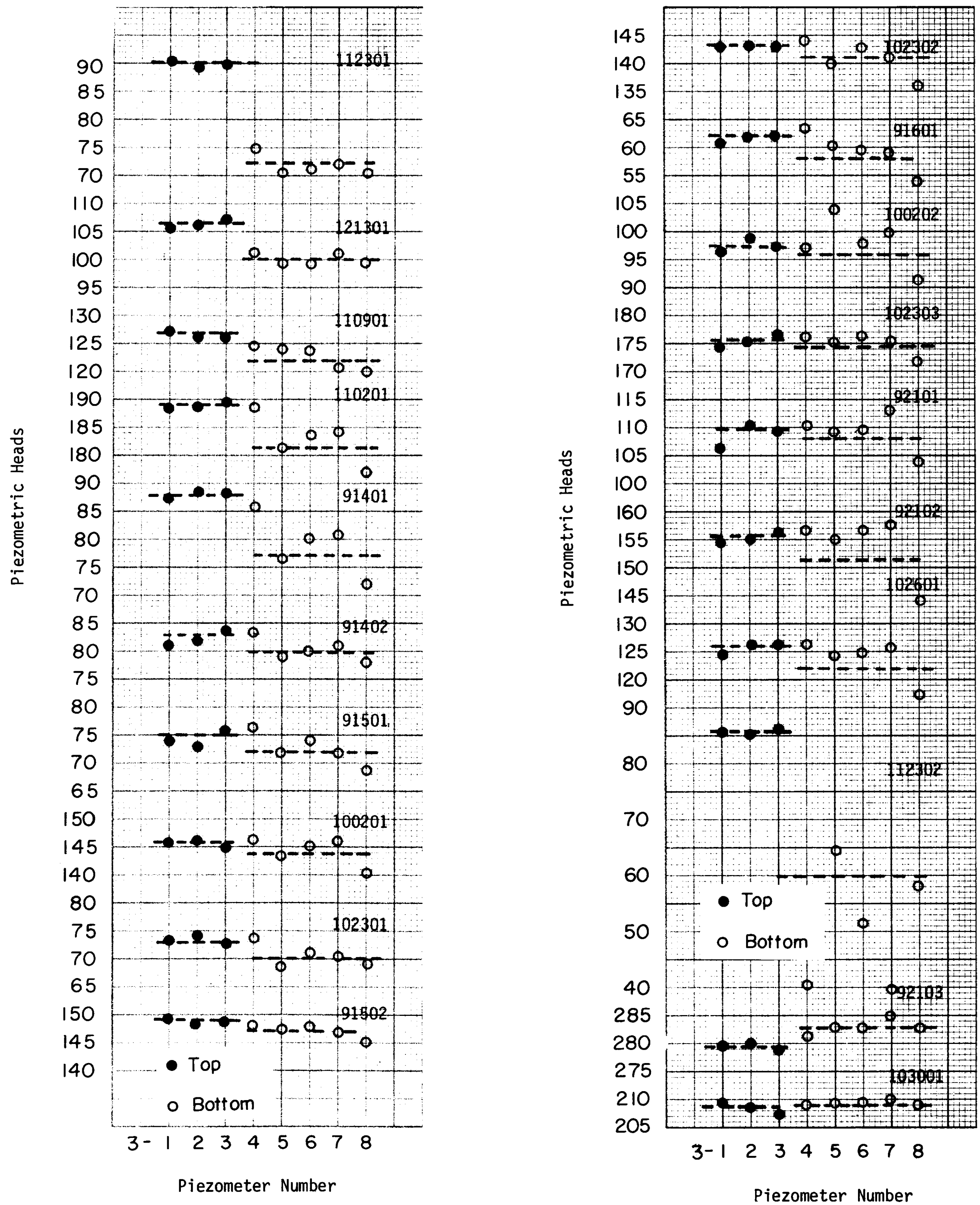

Figure 56. Distribtuion of heads on beam 1.

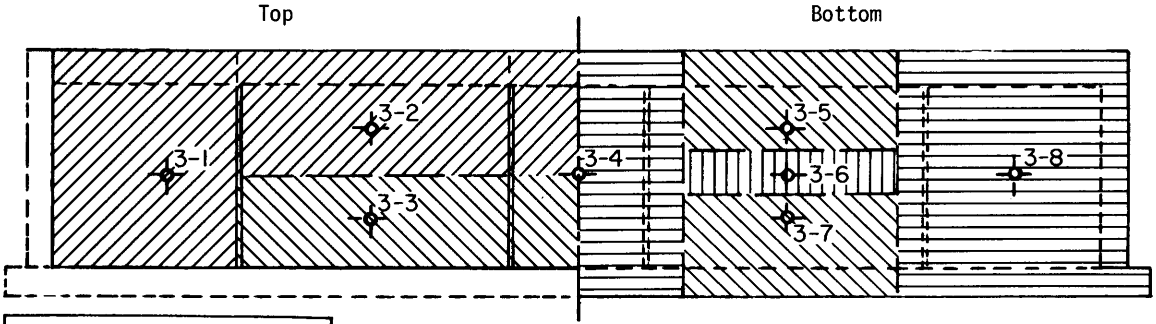

Effective Areas	
Piezometer No.	Area Ft^2
3-1	7.09
3-2	8.30
3-3	6.03
3-4	5.08
3-5	4.12
3-6	1.83
3-7	4.11
3-8	11.79

Figure 57. Effective areas on beam 1.

Thus pressure coefficients for the bottom of beam 1 are defined as

$$C_{b1s} = \frac{2g(H_1 - H_{b1})}{V_c^2}$$

and for the top, the coefficient is expressed as

$$C_{t1s} = \frac{2g(H_1 - H_{t1})}{V_c^2} \quad .$$

The subscripts b and t refer to bottom and top side of the beam respectively; the second subscript, 1 , identifies the beam number (see Figure 31) and the third subscript, s , indicates the gate was submerged. H_{b1} and H_{t1} are the weighted pressure heads indicated on Figure 56 and listed in Table C-2 of Appendix C.

There is a unique relationship between $V_c^2/2g$ and H_4 for any gate position as was shown on Figure 52. Therefore, C_{b1s} and C_{t1s} may alternatively be expressed as

$$C'_{b1s} = \frac{(H_1 - H_{b1})}{H_4} = C_{b1s} \cdot \frac{1}{K}$$

$$C'_{t1s} = \frac{(H_1 - H_{t1})}{H_4} = C_{t1s} \cdot \frac{1}{K} \; .$$

These coefficients, C_{b1s} , C'_{b1s} and C_{t1s} , C'_{t1s} are plotted on Figures 58 and 59 as functions of gate opening, with calculated values tabulated in Table C-2. The curves have been fitted by eye.

The pressure coefficient for greater than full gate opening is erratic, because $V_c^2/2g$ is not the appropriate nondimensionalizing parameter, nor for that matter is H_4 a better parameter (see data in Table C-2). Points for C'_{b1s} and C'_{t1s} near full gate opening have not been plotted on the figures for that reason. In utilizing these coefficients, the curves for C_{b1s} and C_{t1s} could be used near full gate (90 - 100 percent) openings.

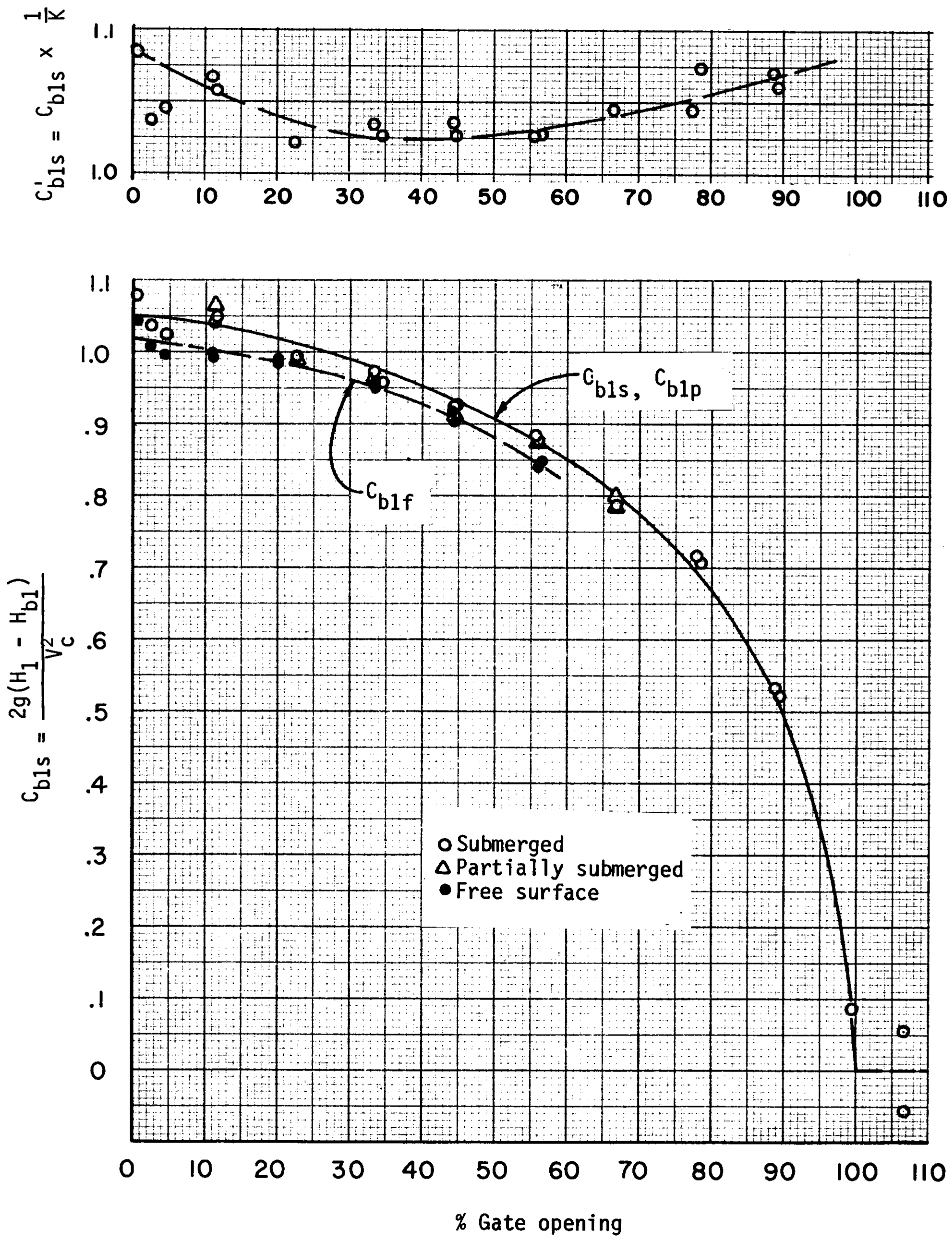

Figure 58. Pressure head coefficient for bottom side of beam 1.

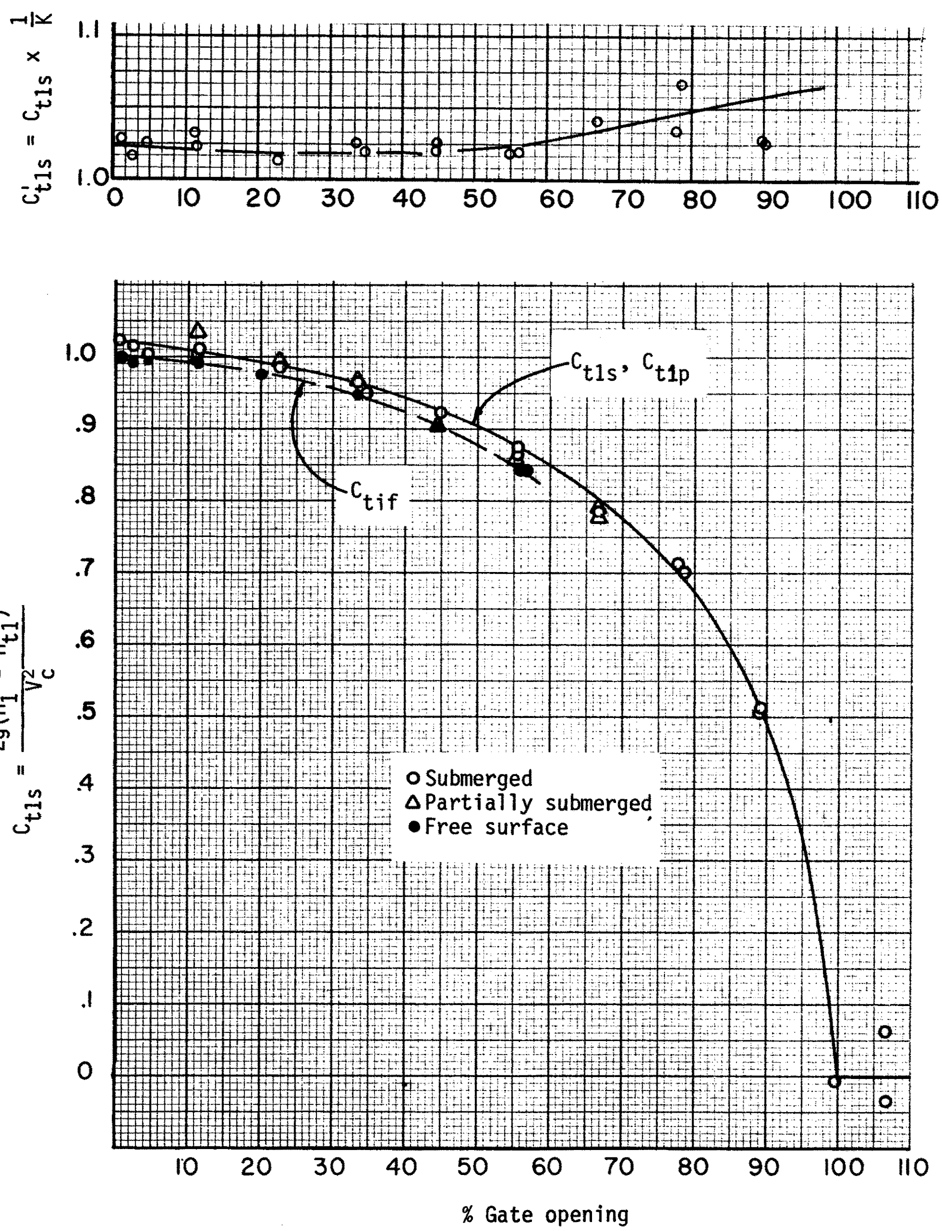

Figure 59. Pressure head coefficient for top side of beam 1.

(d) Forces on the top beam (beam 18) - The measured pressure heads at all piezometers (3-21 through 3-29) on the top beam (beam 18) are shown on Figure 60. The effective heads are substantially constant across the beam. Area weighted averages in accordance with the distribution of areas shown on Figure 61 were calculated for each test run and are shown as a dashed horizontal line on Figure 60. The values are tabulated in Table C-2.

The pressure coefficient for the bottom of beam 18 is defined as

$$C_{b18s} = \frac{H_1 - H_{b18}}{H_4}$$

and for the top the coefficient is

$$C_{t18s} = \frac{H_1 - H_{t18}}{H_4} .$$

H_4 was used as the nondimensionalizing parameter because V_c is not a directly relevant flow variable in relating the top beam forces. The values for H are referenced to the sill level, elevation 1135.8.

The values of the coefficients are included on Table C-2. The coefficient C_{b18s} is plotted as a function of gate position on Figure 62 and C_{t18s} is plotted on Figure 63. The data indicate that the pressure heads are slightly less than hydrostatic heads because there is flow along the back side of the gate downward through the shaft and the pressure coefficient is substantially a constant for all gate positions. It should also be noted that the magnitude of the difference in weighted heads across the top beam was not greater than 1.5 ft for any of the test runs as can be seen on Figure 60 (see also Table C-2).

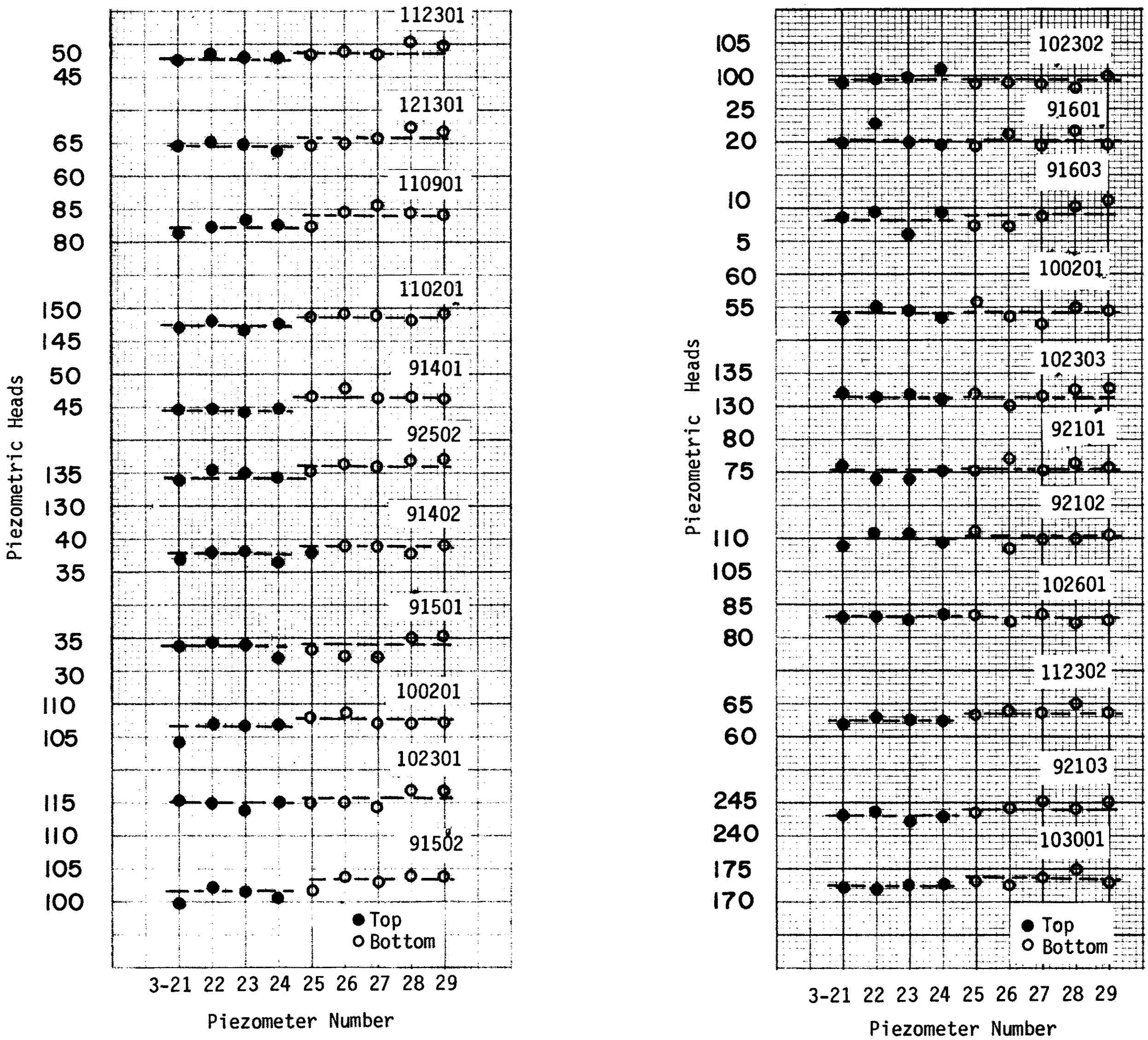

Figure 60. Piezometric head profiles on beam 18
for the submerged gate condition

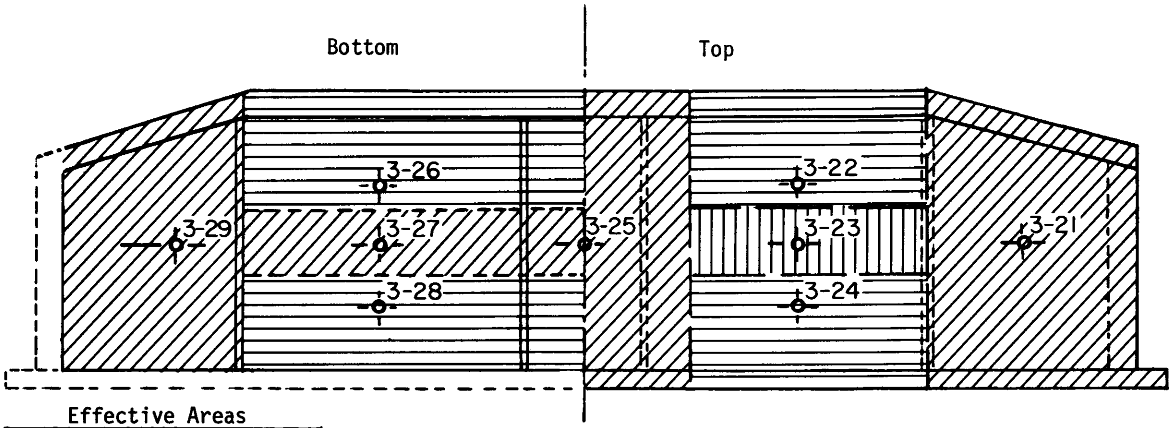

Effective Areas

Piezometer No.	Area Ft^2
3-21	12.82
3-22	4.19
3-23	2.47
3-24	5.31
3-25	6.03
3-26	6.93
3-27	4.08
3-28	6.33
3-29	7.50

Figure 61. Effective areas on beam 18.

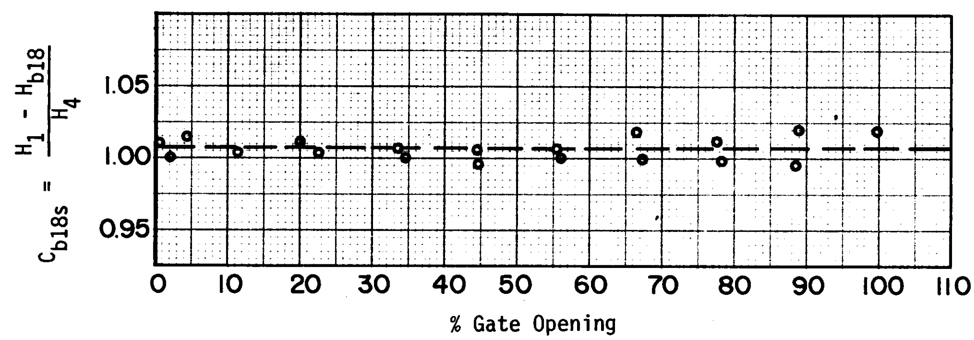

Figure 62. Pressure head coefficients for the bottom side of beam 18

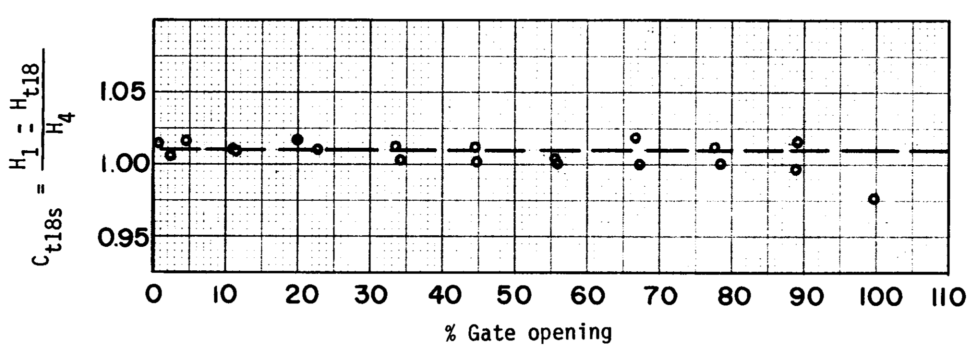

Figure 63. Pressure head coefficients for the top side of beam 18

(e) Force indicator measurements - The zeroing of the output from the force indicator (LVDT) was made with the gate submerged (see section on test procedure). Thus, the measurements of the force with the LVDT were referenced to the buoyant weight of the gate. The hydrodynamic downpull is the vertical component of the integrated pressure acting over all the exposed surfaces of the gate. This includes not only the seal clamp bars and beams as discussed in previous sections, but also the wheels of the gate. Because the buoyant force, which is the integrated hydrostatic pressure acting over the gate surfaces, is a part of the total hydrodynamic force, a correction needs to be made to the measurements to include the buoyant force which was initially eliminated by the zeroing of the instrument output.

The buoyant force of the left gate was approximately 3.2 lbs or 44.3 kips prototype. The net hydrodynamic force therefore is the output from the instrument (converted to force) less 44.3 kips. The corrected force cell measurements F_m are tabulated in Table C-2 along with the net calcualted forces F_c using the coefficients for forces on various components of the gate given in Figures 53, 54, 58, 59, 62 and 63. The calculations included a buoyant force of 10.5 kips (for the model gate) which act on beams 6 through 17 inclusively and a buoyant force of 8.3 kips for the gate wheels (for model size see page 16). The net force on beams 2 through 5 is assumed to be zero in accordance with observation 2 listed on page 35.

Hydraulics - Partially submerged conditions - For partially submerged flows, the definitions of flow parameters in Figure 44 require clarification. The head H_2 is the depth of water immediately downstream of the gate, where the head was measured by the piezometers on the gate beams. H_3 will be less than zero and is significant only to indicate the percent submergence of the gate. H_5 was not determined in the tests, thus the loss of head between upstream and downstream transitions was not determined. The hydraulic condition in the downstream tunnel is determinable from knowledge of discharge, velocity in the vena contracta and radial gate openings. Because these calculations were not material to the study at hand, they are not included herein. The data and calculations are tabulated in Table C-3 of Appendix C.

The hydraulic conditions upstream of the gate were the same as for the submerged gate. The curve of $2gH_4/V_c^2$ is plotted on Figure 52 (data points are triangles) and it is noted that within experimental accuracy the curve is the same as the curve for the submerged gate.

Forces on the gate - partially submerged conditions

(a) Forces on the top seal - The coefficient for piezometric head acting on the bottom of the top seal clamp bar for the submerged gate was defined as

$$C_{TS} = \frac{H_1 - H_{32}}{H_4} \; .$$

The value H_4 for inclusion in computations of coefficients for the partially submerged gate must be corrected to be the differential head effective for driving the flow through the seal gap, which can be characterized by

$$H_4' = H_1 - \text{elevation of piezometer 3-32} \; .$$

The values for

$$C_{TP} = \frac{H_1 - H_{32}}{H_4'}$$

are plotted on Figure 53, where the subscript P identifies partially submerged gate. The curve through the data points (fitted by eye) is seen to be slightly lower than the curve for C_{TS}. The curve terminates at about 70 percent gate opening for two reasons: (1) data were not available for larger gate openings because partial submergence was a sensitive condition to achieve in the model for those gate openings, and (2) the jet of water from the top seal gap has little effect on the seal clamp bar for openings larger than 70 percent. That is, the pressure in the jet is essentially atmospheric at that level.

(b) Forces on the bottom seal - The coefficient for head for piezometer 3-30 is defined as

$$C_{BP} = \frac{2g(H_1 - H_{30})}{V_c^2}$$

and is plotted on Figure 54 on which the data points are identified by triangles. The curve essentially follows that for the submerged gate.

(c) Forces on the bottom beam - The coefficients for effective heads acting on the bottom and top of beam 1 may be expressed as

$$C_{b1p} = \frac{2g(H_1 - H_{b1})}{V_c^2}$$

and

$$C_{t1p} = \frac{2g(H_1 - H_{t1})}{V_c^2}$$

respectively. As for the submerged gate condition, alternative pressure coefficients C_{b1p}' and C_{t1p}' can be formulated because of the relationship between H_4 and $V_c^2/2g$ as

$$C_{b1p}' = \frac{H_1 - H_{b1}}{H_4} = C_{b1p} \cdot \frac{1}{K}$$

and

$$C_{t1p}' = \frac{H_1 - H_{t1}}{H_4} = C_{t1p} \cdot \frac{1}{K} \; .$$

From the discussion above, it is easy to see that C_{b1p}' and C_{t1p}' are indistinguishable from the data for C_{b1s}' and C_{t1s}' in Figures 58 and 59.

The distributions of pressures measured on the beam are shown in Figure 64 along with the area weighted effective heads which are indicated by horizontal lines. As expected, the coefficients plot around the curves shown on Figures 58 and 59 for the submerged gate.

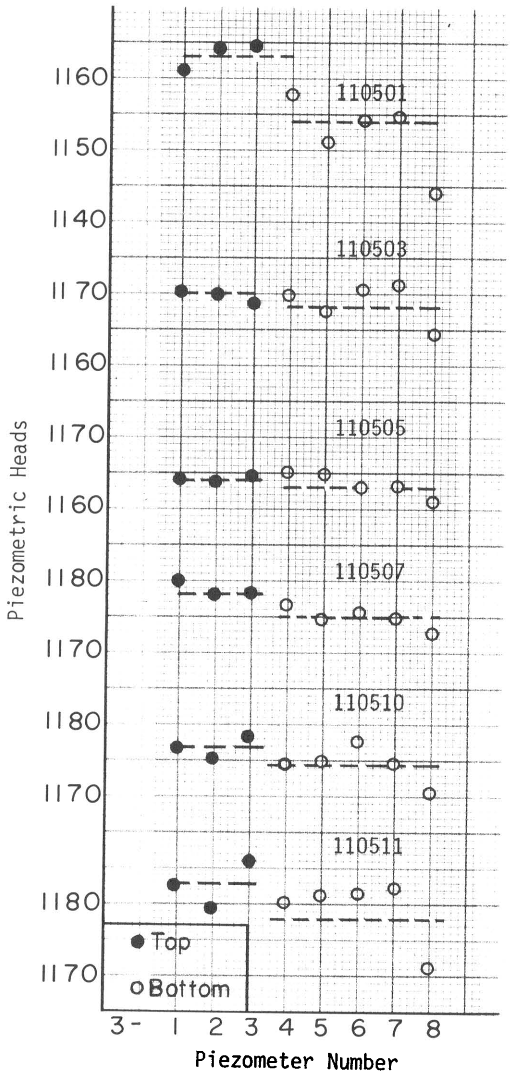

Figure 64. Piezometric head profiles for beam 1, partially submerged gate.

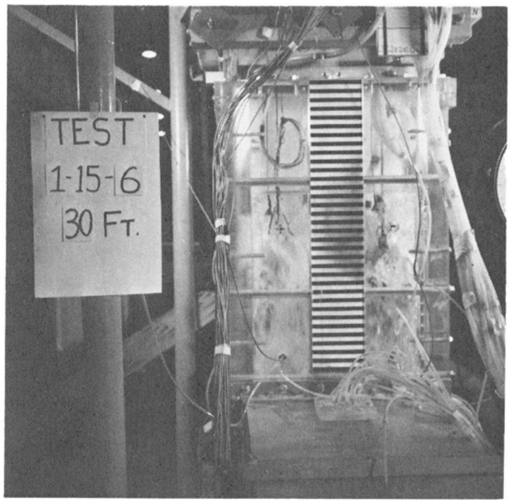

Figure 65. Gates partially submerged. Note the cascade of flow on the gates.

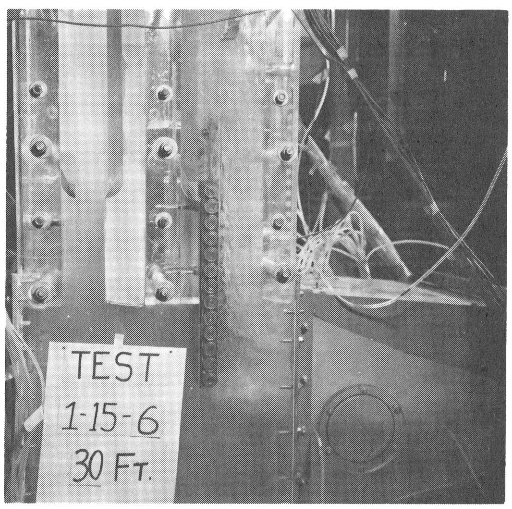

Figure 66. Gates partially submerged.

(d) Forces on the top beam - The heads on the top beam were measurably small, because with the downstream water level considerably below the top of the gate, the force on the top beam was effectively that of the flow cascading down on top of the gate. This effect can be better visualized in the photographs of Figures 65 and 66. The effective heads could not be determined by measurement. The major effect of the cascading flow was to partly fill the region between the beams with water, which adds to the downpull. An estimated weight of water trapped above each exposed beam is about 1.5 kips.

(e) Force indicator measurements - The corrected force indicator outputs in terms of downpull in kips, F_m , are tabulated in Table C-3 along with calculated forces F_c on the beams and seal clamp bars. The values of F_c were calculated using the curves for the coefficients given in the preceding figures. The values of F_c include the weight of water trapped on the beams which were not submerged and the buoyant forces acting on the gate wheels which were submerged.

Hydraulics - unsubmerged conditions - The flow upstream of the gates was reasonably unaffected by conditions downstream of the gate. The magnitude of H_2 was considered to be the depth of flow at the vena contracta. The coefficient $2gH_4/V_c^2$ are plotted on Figure 52 and labelled "free surface." The data and calculations for the unsubmerged tests are tabulated in Table C-4 of the Appendix. The values of K for the free surface curve is slightly greater than for the submerged and partly submerged gate conditions. The curve is terminated at a gate opening of 60 percent, because for larger openings (with both left and right gates open an equal amount) the gate becomes partially submerged as the tunnel fills downstream.

Forces on the gate - unsubmerged conditions -

(a) Forces on the top seal - As with the case of partially submerged gates, the differential head H_4 requires correction for it to be useful in defining the pressure head coefficient for the top seal. The coefficient for piezometric head on the top seal is defined as

$$C_{TF} = \frac{H_1 - H_{32}}{H_4'}$$

where H_4' is the corrected differential head relative to the elevation of piezometer 3-32.
The dashed curve drawn through the data on Figure 53 for both the free surface and partly submerged conditions is labelled C_{TF}, C_{TP}. The data for the free surface are plotted as full circles.

(b) Forces on the bottom seal plate - The pressure head coefficient for piezometer 3-30 is defined as

$$C_{BF} = \frac{2g(H_1 - H_{30})}{V_c^2}$$

and are plotted on Figure 54 as a dashed curve. The streamline in the vicinity of the bottom of the gate are evidently altered sufficiently by the free jet flow beneath the gate to cause an identifiable difference between the submerged and unsubmerged or partly submerged curves. The curve is terminated near gate opening of 60 percent because the gate becomes partially submerged for larger gate openings.

(c) Forces on the bottom beam - The measured pressure heads on piezometers 3-1 through 3-8 are shown on Figure 67. It will be noted that the pressure head acting on the top of the beam (referenced to the beam level) is small, fluctuating about zero. For small gate openings, the pressure head on the bottom of the beam is less than atmospheric, and in the case of test run 112303, for y = 0.25 ft, piezometer 3-8 indicates a subatmospheric pressure which approaches vapor pressure. The subatmospheric pressures become less with increasing gate opening until the pressures are essentially atmospheric. The data indicate that for openings greater than 1 ft (2.2 percent) the measured heads were essentially atmospheric. The area weighted average heads are nevertheless computed from the data and pressure head coefficients

$$C_{b1f} = \frac{2g(H_1 - H_{b1})}{V_c^2}$$

$$C_{t1f} = \frac{2g(H_1 - H_{t1})}{V_c^2}$$

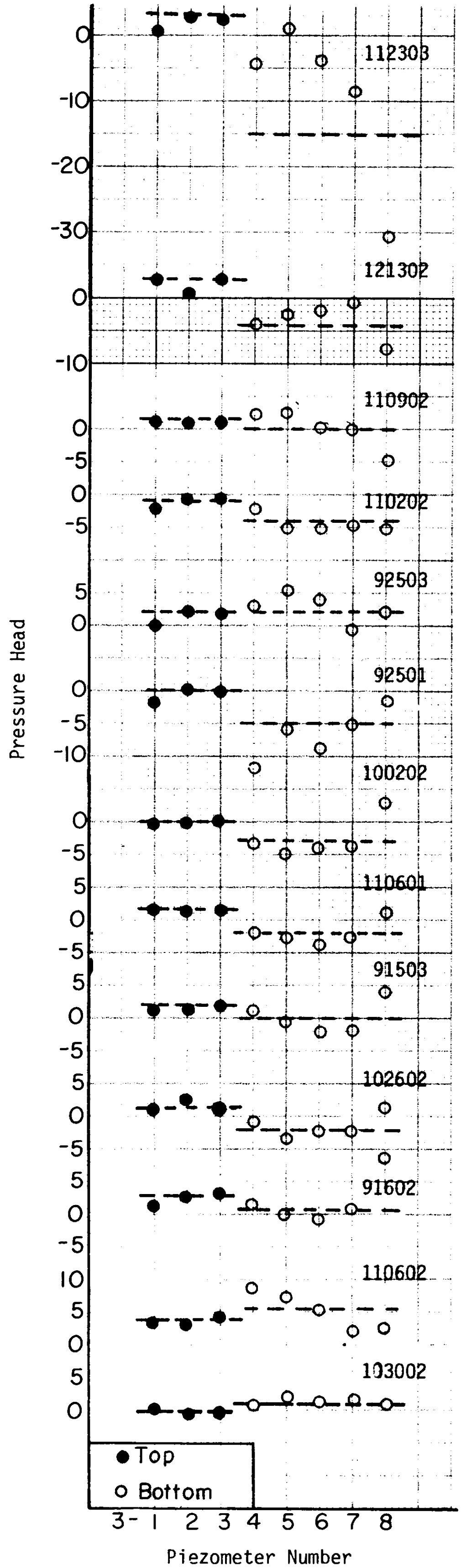

Figure 67. Pressure head profiles for beam 1, gate not submerged.

and are shown on Figures 58 and 59, respectively. The subscript f is to identify free surface condition.

(d) Forces on the top beam - For the reasons given before in the discussion on the partly submerged gate tests, the effective pressure head on the top beam was measurably small for the unsubmerged gate. The weight of water contained between the beams because of the water cascading from the flow through the seal gap may be included as part of the downpull. An estimate of that weight is about 26 kips for the 17 exposed beams of the gate.

(e) Force indicator measurements - The forces measured by the force indicator F_m are tabulated in Table C-4. Corrections because of the instrument zeroing procedure have been applied. The calculated values, also listed, included the weight of water trapped on the beams.

Gate oscillations - Oscillations of the gate were observed during the tests. It should be recalled that the wheels of the model gate were purposely set so that the side seals would not be in contact with the sealing surface. This was to avoid frictional forces along the seals which would add unresolvable complication to the force indicator measurements. With this "free-wheeling" condition, oscillations of the gate were observed during tests with the gate submerged. Using the displacement of the LVDT to measure the oscillations, analysis of the data showed that oscillations were less than 0.1 inch prototype. Visual observations indicated oscillations to be less than 1/32 in., model, which is 0.75 in. prototype. The visual observations were approximate, and were subject to considerable error due to refraction of light through the 3-in. thick plastic wall.

To establish a more realistic test condition with respect to the prototype, a threaded bolt was installed horizontally in the downstream wall of the service gate well. By turning the bolt (by hand) the gate seal could be pressed forward against the seal surface. Only a very "small amount" of friction along the gate seal was needed to suppress the oscillations completely.

Although these latter tests were completely qualitative, it was thought that there would be sufficient friction from the side seals for the prototype gates to suppress the oscillations. The prototype gates will always have side seal contact for partial gate openings.

The partially submerged flows caused some oscillations, associated principally with the surging of the water level in the turbulent flow downstream of the gate. These oscillations were small. For free surface conditions, the oscillations ceased altogether even without the frictional forces along the gate seal.

Water level fluctuations - Fluctuations of the water level in the service gate wells were observed during tests with the gates submerged. These fluctuations occurred for all gate openings less than 100 percent, and were observed to be negatively correlated between the two service gate wells. That is, fall of water level in one well was associated with a rise in the other. These fluctuations did not occur for the water levels in the bulkhead gate wells. The fluctuations must be associated with a downstream condition and at such location that an interaction is created between fluctuations in the left and right passages. A logical source of these oscillations is then the instability of the flow downstream from the end of the divider wall in the downstream transition where the flows from the two gate passages recombine. Another source might be vortex shedding at the gate bottom.

The fluctuations seemed random, and because of the large masses of water in the gate shafts, large amplitude fluctuations were associated with low frequency of oscillation. The significance of these oscillations is that upward and downward forces can be developed on the gate as the water surges in and out respectively from the service gate well. The larger forces would be associated with larger amplitudes.

To determine the amplitudes and frequencies of these oscillations for several gate openings, motion pictures were taken. Analysis of these pictures resulted in the following observations:

1. The maxima of the amplitudes of oscillations were large, about 25 feet (prototype).
2. The frequency of these large oscillations was about 0.5 Hz in the model, equivalent to about 0.1 Hz prototype ($T_r = L_r^{1/2}$).
3. The amplitudes and frequencies were not dependent upon gate position.
4. With unequal gate openings (one partially open and the other in the stored position) the oscillations were small, of order 1 to 2 ft in amplitude.
5. With gates above full opening, oscillations were not observed.

The effect of these oscillations on the gate may be estimated from the momentum equation in the vertical direction within the gate shaft. The analysis follows.

Referring to Figure 68, and the control volume ABCD, the momentum equation can be written

$$\sum\vec{F} = \frac{\partial}{\partial t}\int_{cv} \rho\vec{V}d\forall + \int_{cs} \rho\vec{V}(\vec{V}\cdot d\vec{A})$$

where $\sum\vec{F}$ is the unbalanced force on the control volume including body and surface forces and the control volume extends laterally to the width of the gate shaft,
cv is the control volume, and
cs is the surface of the control volume.

The body force and integration of the surface hydrostatic force on the control volume will balance approximately because water fills the region between the gate beams. Let the frictional force along the walls of the gate shaft be assumed small in comparison to the force on the gate F_z, and the flow through AE is assumed to be negligible. Thus in the notation of Figure 68, with vertical force downward designated positive, the one-dimensional form of the momentum equation reduces to

$$\vec{F}_z = \rho A_2 V_2(\vec{V}_2) - \rho A_1 V_1(\vec{V}_1) + \rho\int_{cv} \frac{\partial\vec{V}}{\partial t}\, d\forall$$

where the momentum correction factor β is assumed equal to unity and F_o is the force of the gate on the control volume. The force on the gate is of course oppositely directed.

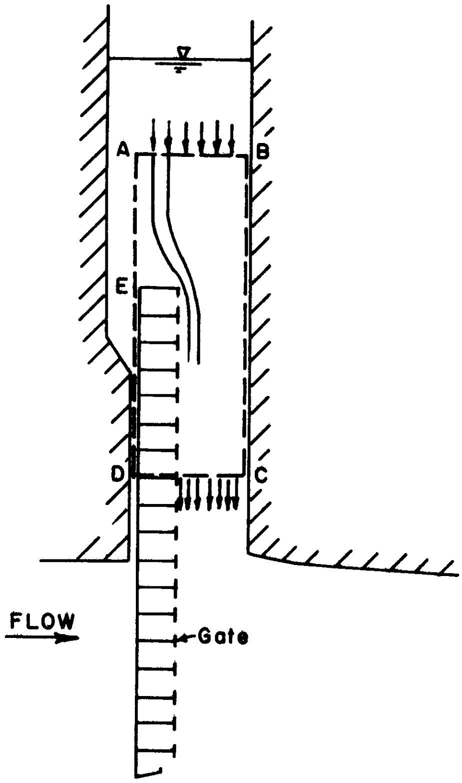

Figure 68. Definition sketch.

In particular, the concern is with maximum downpull force caused by the oscillating flow, which occurs when V is a maximum, i.e. $\partial V/\partial t = 0$. Thus, the momentum equation reduces to

$$-F_z = \rho A_1 V_1^2 - \rho A_2 V_2^2 \quad .$$

Because the fluid is incompressible, the continuity equation is

$$A_1 V_1 = A_2 V_2$$

and substituting this into the momentum equation,

$$-F_z = \rho A_1 V_1^2 \left(1 - \frac{A_1}{A_2}\right) \quad .$$

As an approximation, assume the oscillation of the water level to be a simple harmonic motion described by

$$\eta = a_o \sin 2\pi nt$$

where η is the displacement above mean level,
a_o is the amplitude observed from measurements,
n is the frequency in hertz observed for amplitudes a_o , and
t is time.

Then

$$V_1 = \frac{d\eta}{dt} = a_o 2\pi n \cos 2\pi nt$$

is the one-dimensional velocity as a function of time. At maximum velocity,

$$\frac{dV_1}{dt} = 0 = -a_o(2\pi n)^2 \sin 2\pi nt$$

hence,

$$2\pi nt = 0, \ \pi, \ 2\pi, \ \text{etc.}$$

and

$$V_1 = \pm a_o 2\pi n \quad .$$

The following measurements are pertinent to the control volume which yields the maximum calculated force.

Horizontal projected area of gate and wheels = 68.1 ft^2.

Area at AB (see Figure 68), $A_1 = 160.1$ ft^2.

Area at DC (160.1 - 68.1), $A_2 = 92.0$ ft^2.

a_o (one half of peak to peak water level change at 30-ft gate opening) = 15 ft.

Frequency of oscillation n for a_o above = 0.090 Hz.

$A_1/A_2 = 1.740$.

The estimated force F_z due to maximum oscillating levels is thus approximately

$$F_z = 229.2(V_1^2) \; ,$$

and for the conditions listed above, $F_z = 16.5$ kips. This force represents a maximum for the observed oscillations. The observed oscillations and calculated forces are given in Table C-5 of Appendix C.

Coefficients of flow along the gate - There are forces on the gate upward and downward due to filling and emptying of the service gate well when the gate is opening and closing respectively. These forces may be estimated from the head losses of the flow. The head losses may be estimated from the steady-state one-dimensional energy equation for sections 1 and 2 in the definition sketch of Figure 69, which is written as

$$\frac{V_1^2}{2g} + h_1 = \frac{V_2^2}{2g} + h_2 + K_G \frac{V_2^2}{2g}$$

where the kinetic energy coefficients are assumed unity,
h_1 and h_2 are piezometric heads,
K_G is a head loss coefficient, and
V_1 and V_2 are average velocities at points 1 and 2 respectively.

For incompressible flow, the discharge along the back side of the gate may be written as

$$Q = A_1 V_1 = A_2 V_2$$

where A_1 and A_2 are effective flow areas normal to the axis of the shaft.

The coefficient K_G is due largely to form drag and may be expressed as

$$K_G = \left(\frac{1}{C_D}\right)^2 + \left(\frac{A_2}{A_1}\right)^2 - 1$$

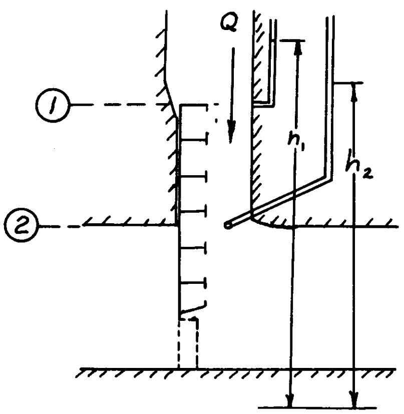

Figure 69. Definition sketch.

where C_D is the coefficient of discharge expressed as

$$C_D = \frac{Q}{A_2\sqrt{2g\Delta h}}$$

$$\left(\frac{A_2}{A_1}\right)^2 = 0.202 \quad \text{for gate openings greater than 40\%}$$

and

$$\left(\frac{A_2}{A_1}\right)^2 = 0.336 \quad \text{for gate openings less than 40\%.}$$

The head loss

$$H_L = K_G \frac{V_2^2}{2g}$$

may be used to estimate the force on the gate from

$$F_G = H_L \gamma A = K_G \frac{V_2^2}{2g} \gamma A$$

where γ is the unit weight of water and
A is the horizontal projected area of the gate and wheels.
K_G can be estimated if C_D is known.

The coefficients C_D were determined using the small model in the following manner. One flow passage was completely blocked, the gate in the other passage was raised to various openings and the opening under the gate was blocked to passage of flow. In performing the tests, water from the upstream tunnel rose upward through the bulkhead gate wells, into the service chamber and down through the service gate shaft. One service gate shaft was blocked at the top, thus all the water flowed downward through the other service gate shaft and into the tunnel downstream. The flow was regulated by a valve in the downstream tunnel, and the discharge was measured gravimetrically. Piezometers along the downstream wall of the service gate shaft were used to measure the piezometric heads. Several different rates of discharge giving different magnitudes of losses were measured for a given gate opening, and an average value of C_D was determined from these measurements.

To determine the coefficients K_G for upward flow, that is, flow up along the back side of the gate, the model gate shaft was disconnected, rotated 180 degrees about the vertical axis, and reconnected so that flow was upward through the service gate shaft and downward through the bulkhead gate shaft. The cross-sectional area at section 1 in Figure 69 in this case is the same as at section 2. Thus,

$$\frac{A_2}{A_1} = 1$$

and

$$K_G = \frac{2gH_L A_2^2}{Q^2}$$

where H_L is the head loss between the top of the flow passage and the top of the gate.

Curves of C_D and K_G are shown in Figure 70 for both upward and downward flows. The data and calculations are tabulated in Table C-6 of Appendix C.

Pressures on Passage Walls

Submerged conditions - The pressures on the walls of the left passage were measured at a variety of locations as indicated on Figures 17, 23 and 24. The only location where subatmospheric pressures were measured was at the top seal surface along the upstream wall of the service gate shaft. The piezometers which registered the subatmospheric pressures were 3-46 and 3-47. The magnitudes of the pressure heads are tabulated in Table C-7. Pressure heads along the transition fillets, and passage walls including those within the gate grooves were positive.

Unsubmerged conditions - There were three regions of subatmospheric pressure heads measured for the unsubmerged conditions: (1) the wall of the passage just downstream of the gate groove for the service gate as measured by piezometers 1-46, 1-47 and 1-15, (2) the divider wall within the downstream transition near the floor and on the floor as measured by piezometers 2-29, 2-27, 2-28, 2-35, 2-36, 2-38 and 2-45, and (3) the top seal surface on the upstream wall of the service gate shaft as measured by piezometers 3-46 and 3-47.

One test which involved the left gate fully open and the right gate completely closed also indicated flow separation and subatmospheric pressures just downstream from the nose of the upstream divide wall at piezometers 2-12 and 2-13 (Run 103002). The pressure heads are tabulated in Table C-7.

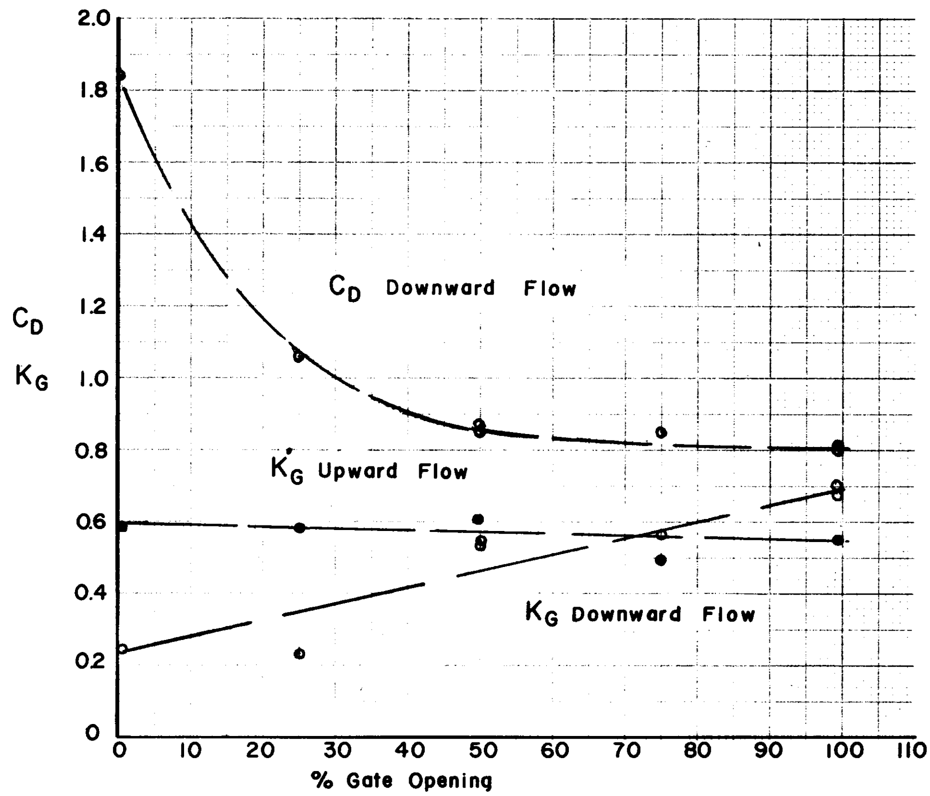

Figure 70. Coefficients for water level fluctuations in service gate shaft.

Downpull Forces and Pressures: Unsteady State Condition

Test procedure - Unsteady state tests refer to experiments that involved both gates in motion. As closely as possible the gates were moved at equal speeds and at rates comparable to the prototype gate speeds. The latter was very difficult to achieve because the hydraulic system of the model was regulated by relatively large valves and with the vibration of the pumps transmitted through the fluid, the valves tended to open or close minute amounts which affected the rate of gate motion. Approximate speeds of about 2 feet per minute were sought.

As explained in the discussion which described the model, the flow controllers of the model system had interactive effects on heads and discharge. Ideally, the unsteady tests should provide for continuous gate motion from closed to fully open gate positions and also for the reverse to represent continuous gate closure. For the model system it was not possible to provide this continuous motion because for any given upstream valve setting the range of discharges achievable was limited. For instance, consider the case of both gates opening. As the service gates rise, the discharge increases, the hydraulic grade line lowers upstream and rises downstream. The differential head across the gate reduces, hence the discharge reduces, and for the higher position of the gate, the head and discharge no longer represents the initial reservoir level and downstream radial gate openings. This effect was offset somewhat by limiting the gate motion to small increments, and by readjusting the flow control valves for successive increments.

Gate range zero to 5 feet - The results of gate motion from zero to 5 feet and for closure from 5 feet to zero are shown in Figures 71 and 72 for the submerged condition. As the gate began to rise (see Figure 71), the force indicator registered a sharp rise in downpull force for approximately the first 0.25-ft rise, and rapid decrease of downpull followed for the next 1.5-ft rise. The largest force measured was about 160 kips which includes friction, but excludes the dead (unsubmerged) weight of the gate. The hydrodynamic downpull combined with friction was essentially zero between 2.5 and 5 feet, and it is noted that there were fluctuations of the force registered in that range, due in part possibly by the fluctuation of the water level in the gate well.

The pressure measured by transducer number 1 (bottom beam, see Figure 32) shows a drop of pressure coincidentally as the force increased. It will be recalled in the steady state tests, the reduced pressure on the bottom side of beam 1 added materially to the downpull. Transducer number 2 was essentially constant head, which corresponded to the 5-ft rise in water level in the service gate shaft recorded by transducer 7 (from 1240 to about 1245) as the gate was lifted 5 feet. Transducer 7 was located in the downstream wall of the service gate shaft slightly above piezometer 3-37. There was a surge of water (approximately 15 feet) when the gate was about 1-ft open, as registered by transducers 3, 4, 5 and 7. The effect on the downpull is not discernable however, although the rate of force decrease changed at about the same gate position (correspondingly the same time).

The piezometric level at the bulkhead gate shaft reduced by about 220 feet during the tests, and the level in the service gate shaft rose by 5 feet. The significant points to note in this test were:

1. An increase in downpull force was measured for gate position at about 0.25 ft.
2. No significant hydrodynamic uplift occurred.

The results of gate closure from 5 feet to zero are shown on Figure 72. As the gate began to close, a negative force was measured by the force indicator. Some of this force was obviously necessary to overcome the friction forces of the wheels.

Just before closure, at about 0.25 ft, there was again a sharp rise in hydrodynamic downpull and transducer 1 coincidentally registered a sharp decrease in pressure head. The fluctuations of transducers 2, 3, 4 and 5 correspond with the fluctuation of the water level in the gate shaft.

The closure rate was faster than intended, arising from the problem with valve settings of the hydraulic system discussed earlier. The closure rate was 5.15 ft/min in terms of the prototype gate.

The experiments were repeated for the gates unsubmerged. The results are shown on Figures 73 and 74. The maximum downpull registered was about 180 kips (gate opening) again for gate position at 0.25 ft. The pressure head at transducer 1 was less than vapor pressure of the prototype, which gives rise to an exaggerated downpull force. When corrected to realizable pressures of the prototype (32 ft instead of 40 ft registered) the downpull force corrects to about 144 kips. Transducers 2 through 5 and 7 were essentially zero because of the free surface condition. Also, because of the free surface condition, pressure heads are shown as the ordinate rather than piezometric heads for the submerged conditions. The isolated increase in head at transducer 3 (at about 1 minute time on Figure 73) could have been due to water being trapped in between the beams. The opening rate for the gate was 1.71 ft/min, slightly lower than intended.

The gate closure results on Figure 74 again indicates the increase in downpull just prior to gate being completely closed, with corresponding decrease in pressure head for transducer 1. When corrected for a realizable -32 ft head, the downpull reduces from 75 kips measured to 60 kips. The rate of closure was 5.8 ft/min, and it is seen that a surge was set up in the upstream tunnel (see transducer 6).

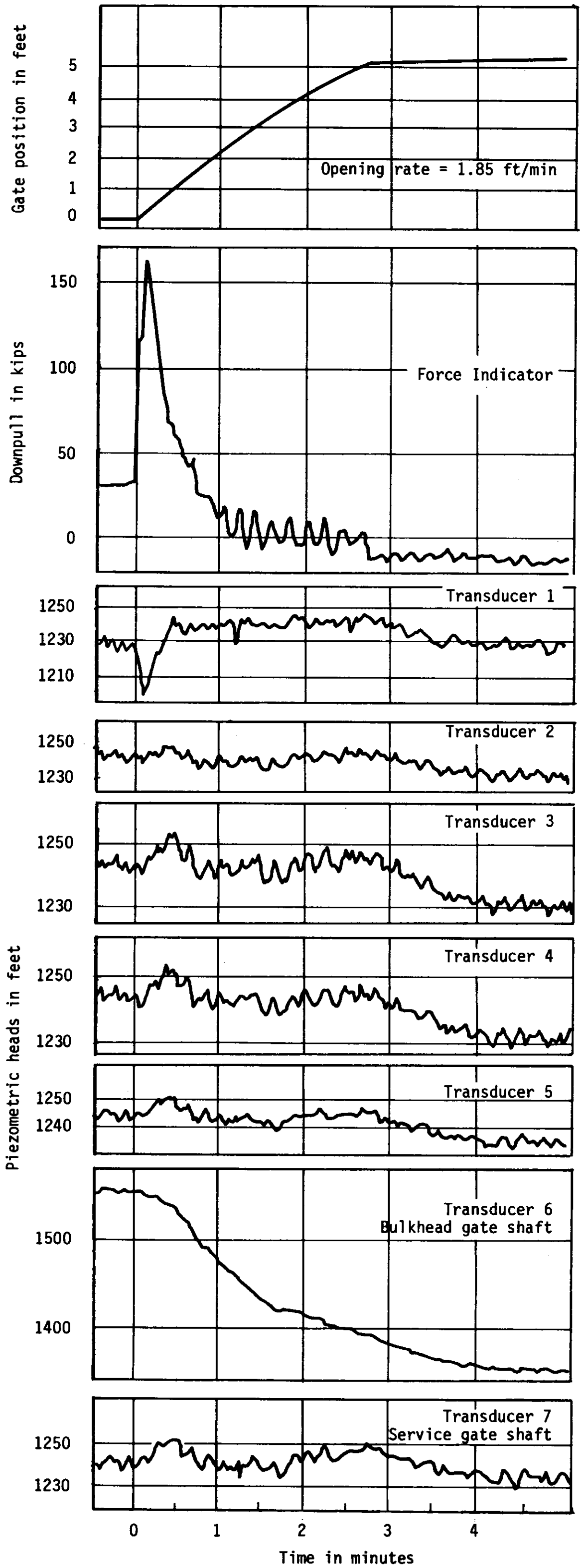

Figure 71. Gate opening - Range 0-5 feet Submerged

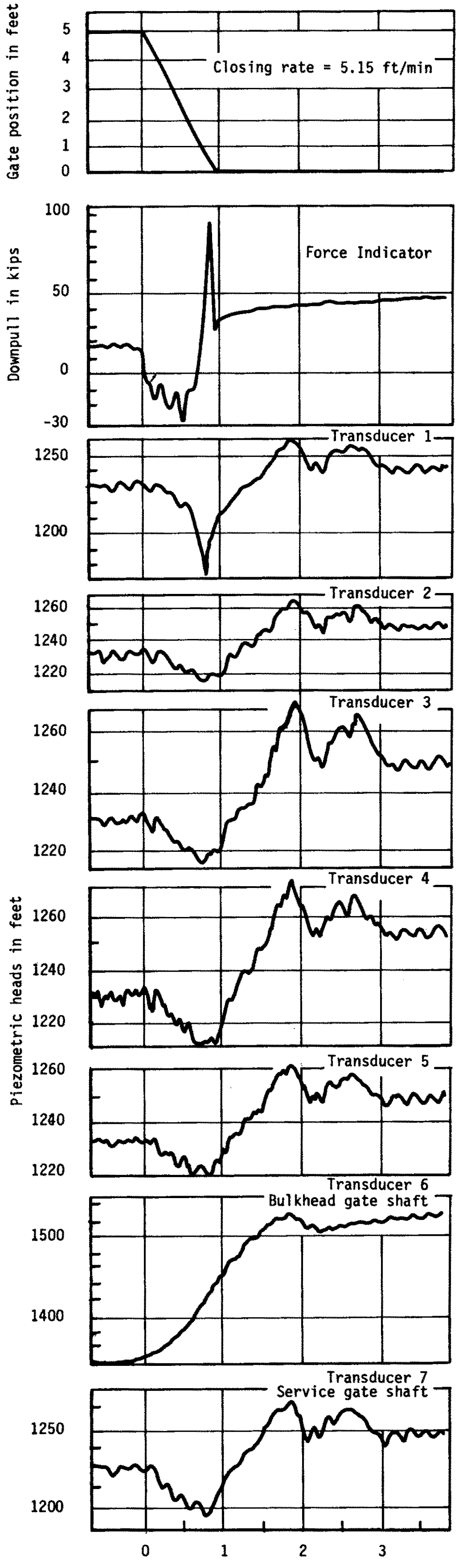

Figure 72. Gate closing - Range 0-5 feet
Submerged

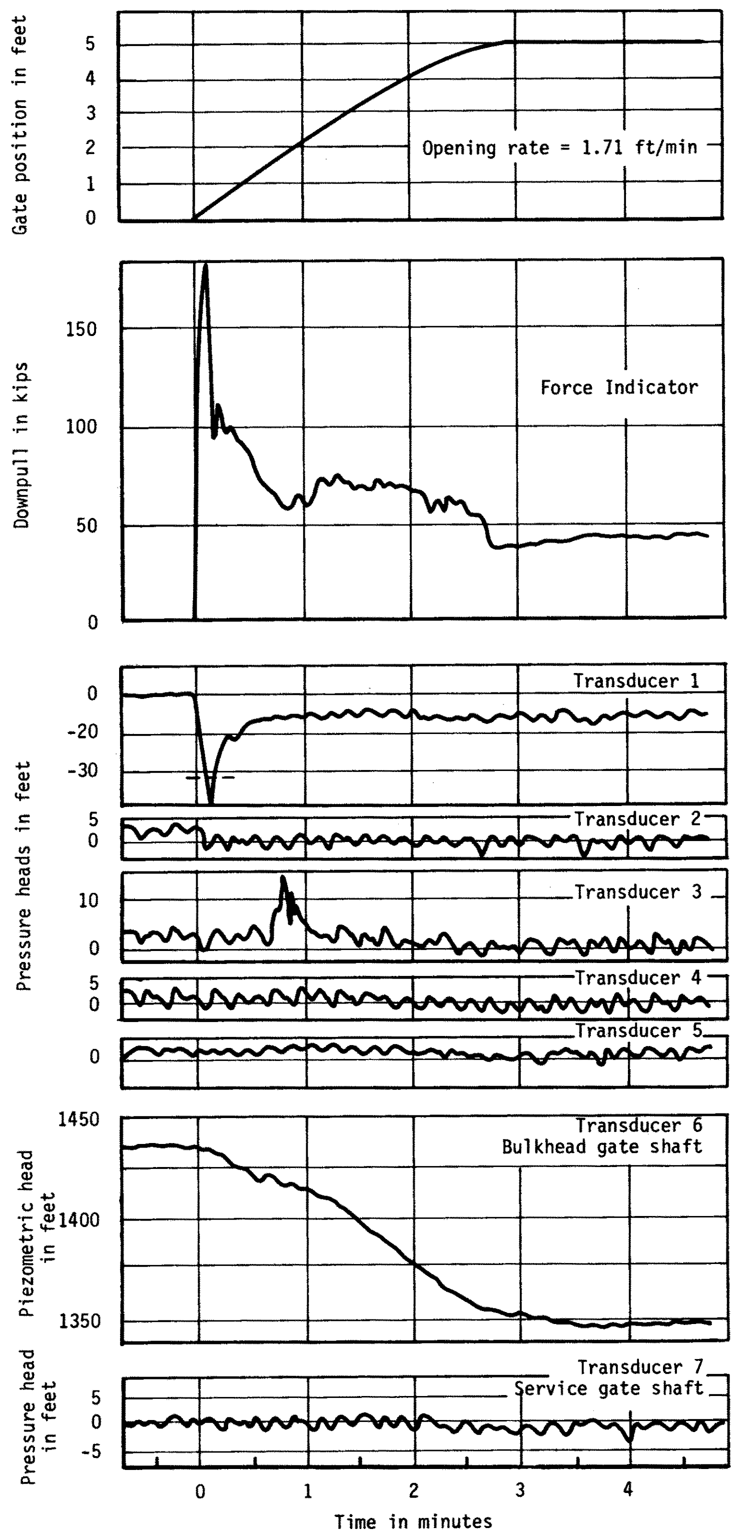

Figure 73. Gate opening - Range 0-5 feet
Free surface

Gate range 20 to 35 feet, submerged conditions - The results of tests for gate opening in the range from 20 to 35 feet are shown in Figures 75 and 76. There were no indicated forces or pressure changes of concern. A negative downpull of about 30 kips was measured by the force indicator which corresponds with the buoyant force on the gate and the fluctuations registered on the force indicator were about ±20 kips, caused probably by the water level fluctuations in the gate shaft. The gate opening rate was 1.81 ft/min and the closure rate was 1.53 ft/min.

Gate range 20 to 28.6 feet, unsubmerged conditions - The gate motion was terminated at 28.6 feet opening because for the particular valve settings the gate became submerged for larger gate openings. The results are shown on Figures 77 and 78 for opening and closing respectively.

On Figure 77 it will be noted that there was an increase in downpull from about 60 kips to about 80 kips (gate openings between 21.5 and 25.5 ft). There were no corresponding increases in pressure heads measured at any of the transducers. Part of this increase could have been due to the reduction of force on the top seal clamp bar as the gate rose above the level where the jet through the top seal gap no longer affects the force on the clamp bar, and part to wheel friction. It will be noted on Figure 78 that a corresponding effect during gate closure was not indicated. The sudden reduction of force on Figure 78 occurred after gate motion ceased and was not a result of a hydraulic condition.

Gate range 30 to 48 feet, submerged conditions - The results of gate motion in the range from 30 to 48 feet are shown on Figures 79 and 80. Fluctuations of the force indicator of about ±20 kips are noted for gate positions between 30 and 36 feet. The fluctuations subside for larger openings as do the oscillations of the water level in the gate shaft. When the bottom seal of the gate is just below the top of the passage, an increase in downpull was recorded. This phenomenon was discussed earlier for the steady state tests. The increase in downpull was again noted for gate closure (Figure 80), as were the fluctuations of the forces and pressure heads.

The following observations are notable from these results:

1. Unexpected large uplift forces did not result because of gate motion.

2. A sharp increase in downpull force was recorded near gate closure at about 0.25-foot opening.

3. A small increase in downpull force was recorded near full open position of the gate.

4. Force fluctuations resulted in the range from 2 to 36 feet, probably as a consequence of water level fluctuations in the gate shaft.

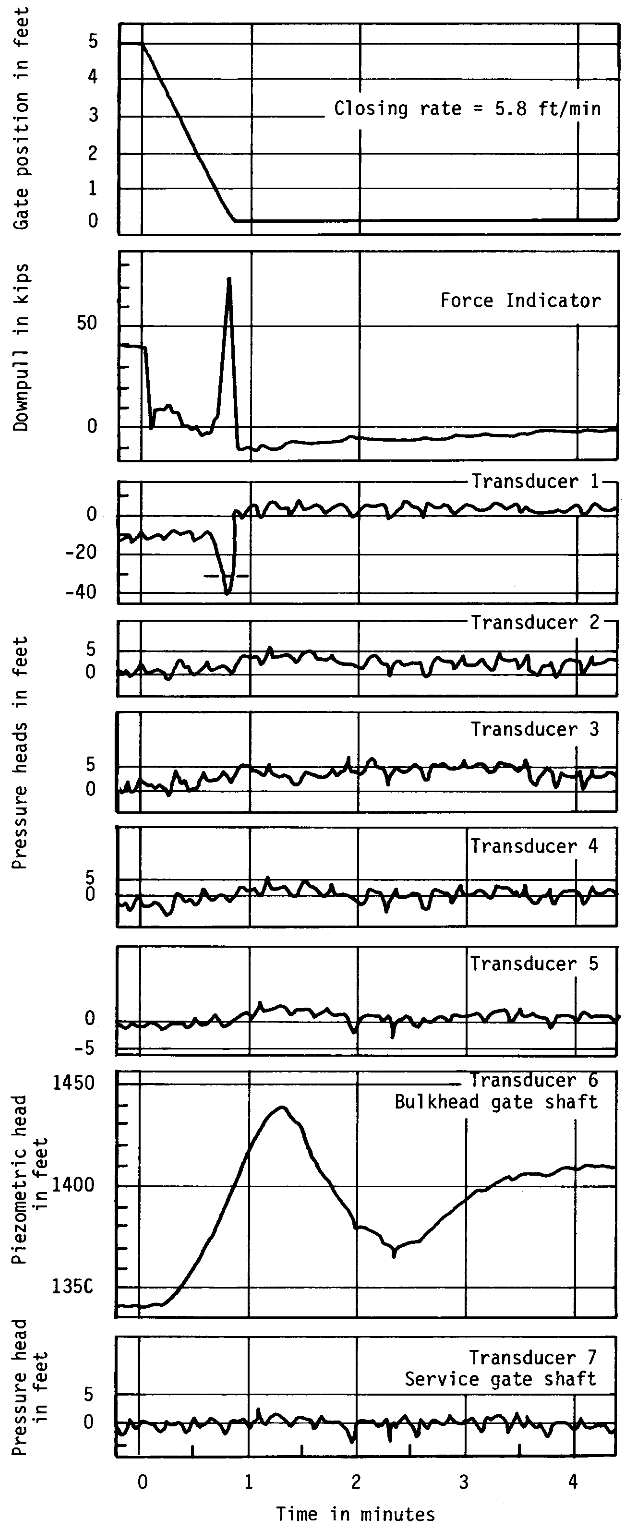

Figure 74. Gate closing - Range 0-5 feet
Free surface

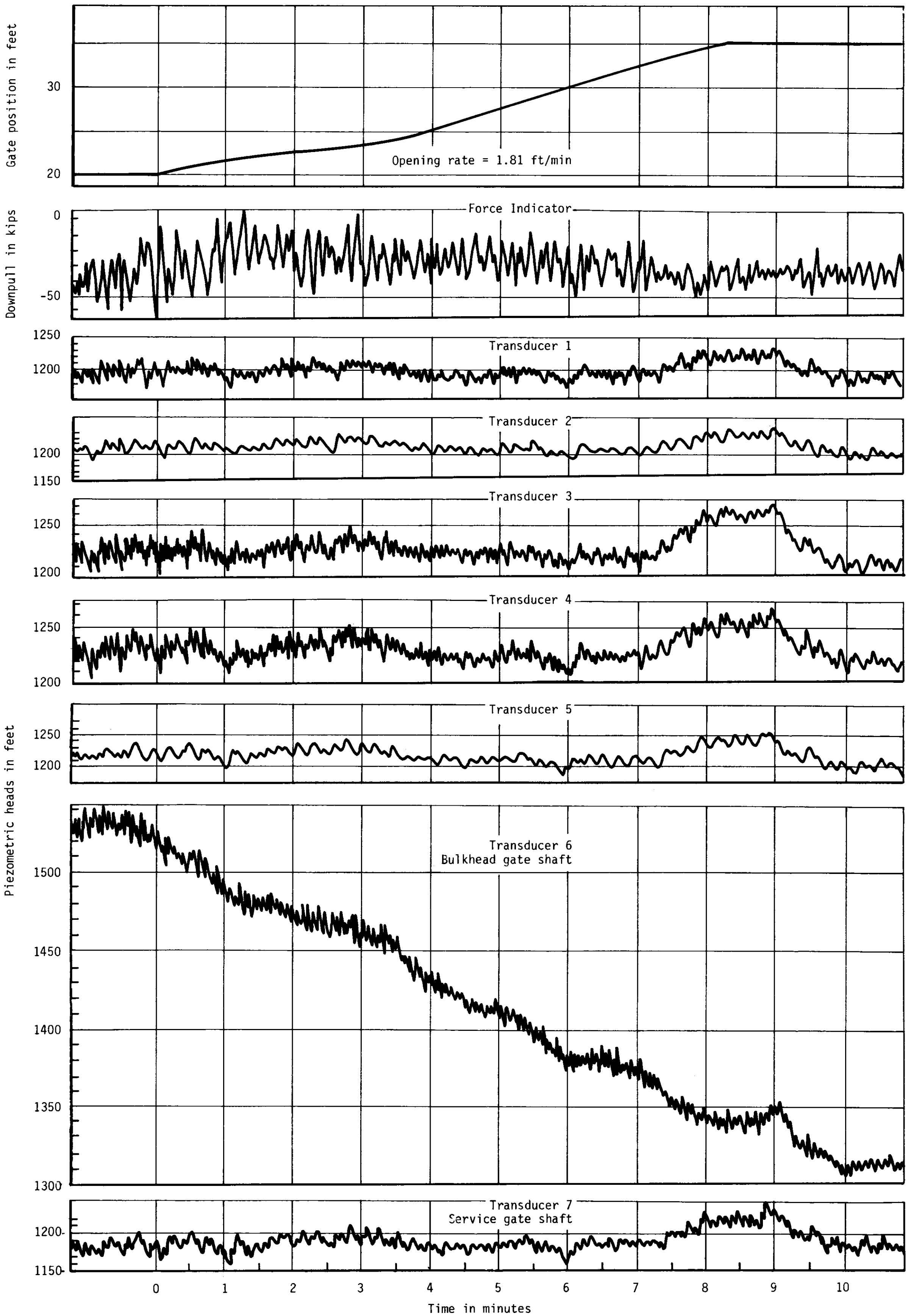

Figure 75. Gate opening - Range 20-35 feet
Submerged

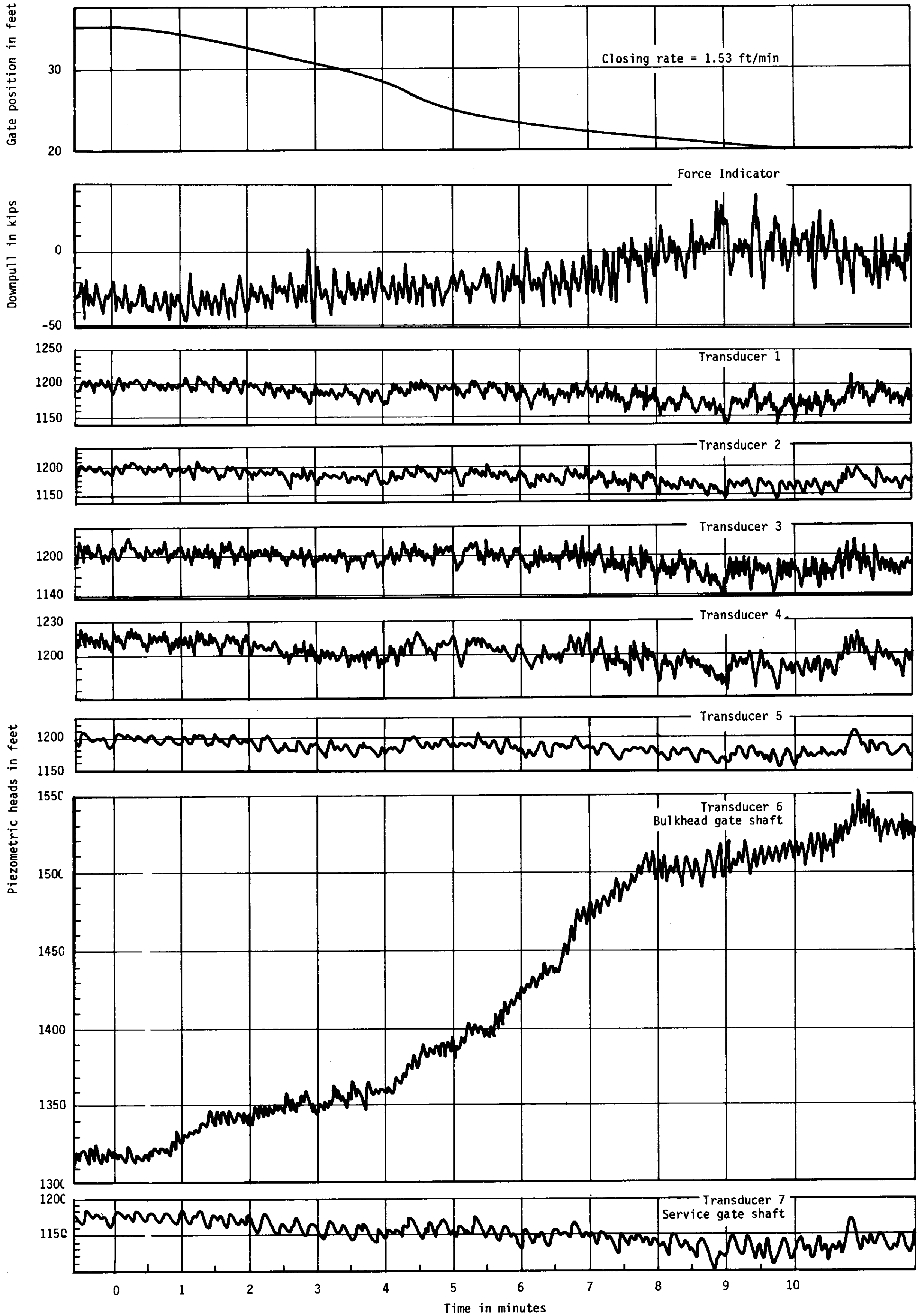

Figure 76. Gate closing - Range 20-35 feet
Submerged

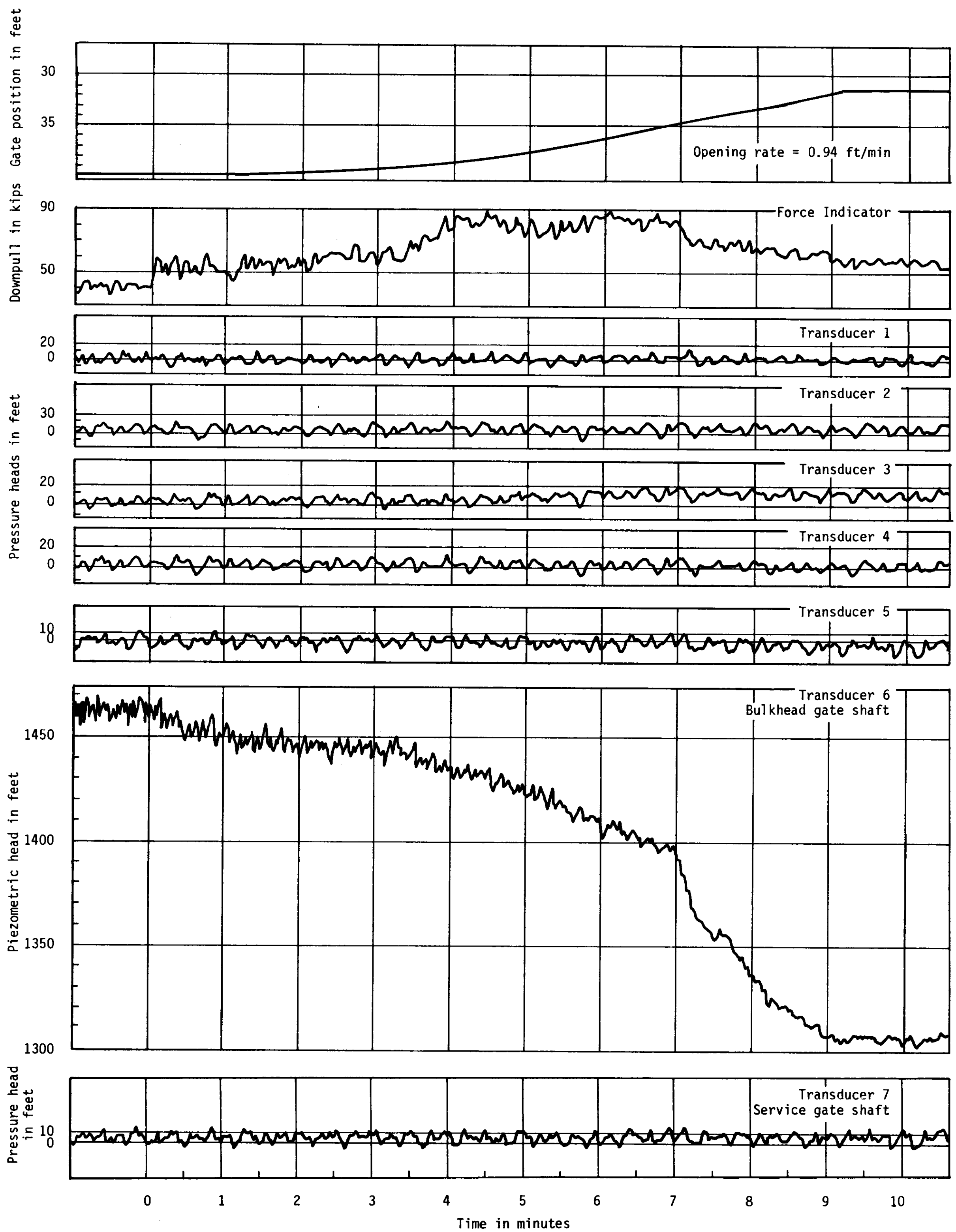

Figure 77. Gate opening - Range 20-28.6 feet
Free surface

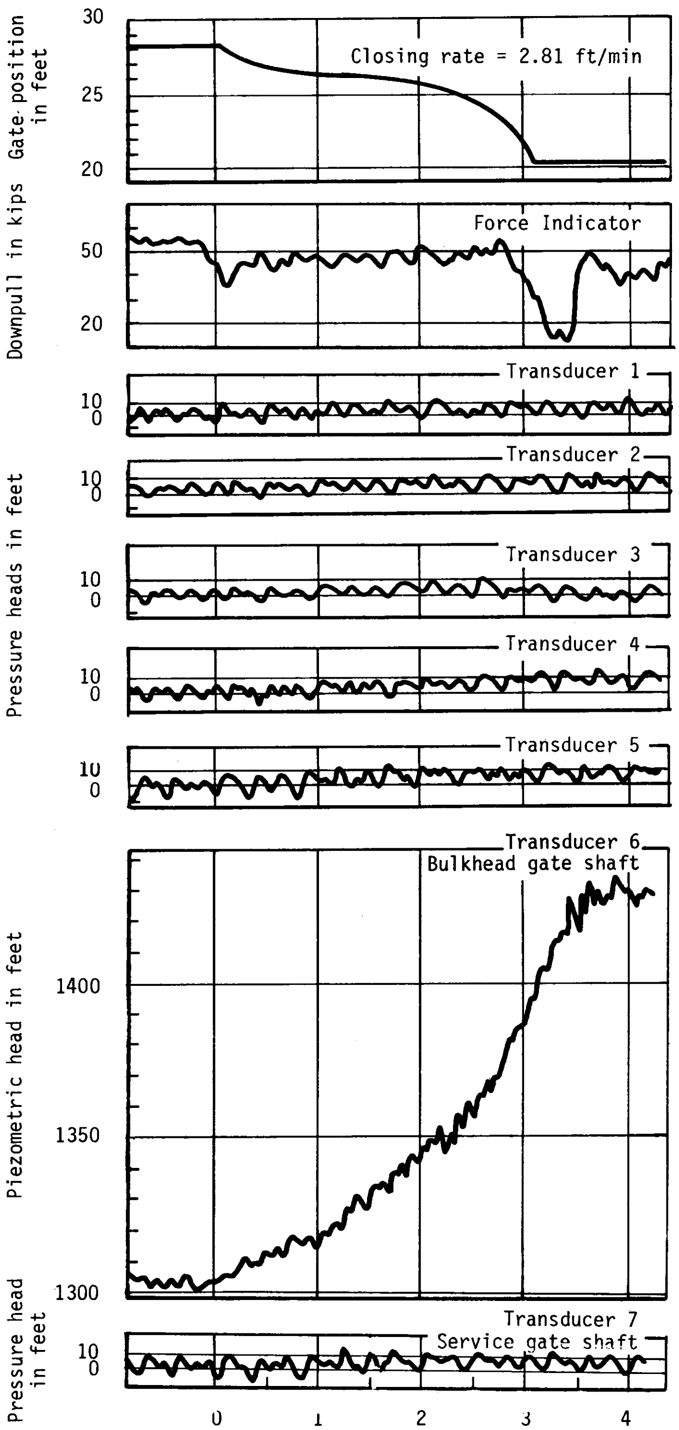

Figure 78. Gate closing - Range 20-28.6 feet
Free surface

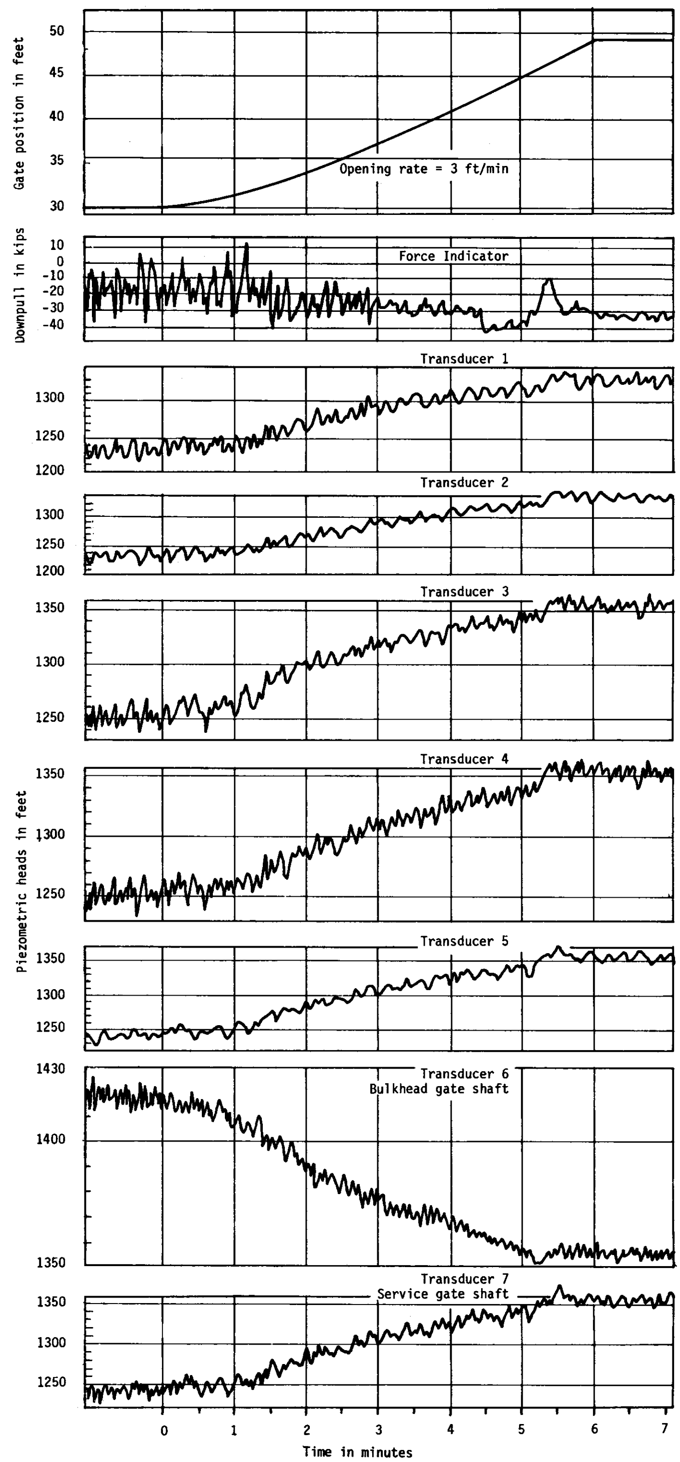

Figure 79. Gate opening - 30-48 feet
Submerged

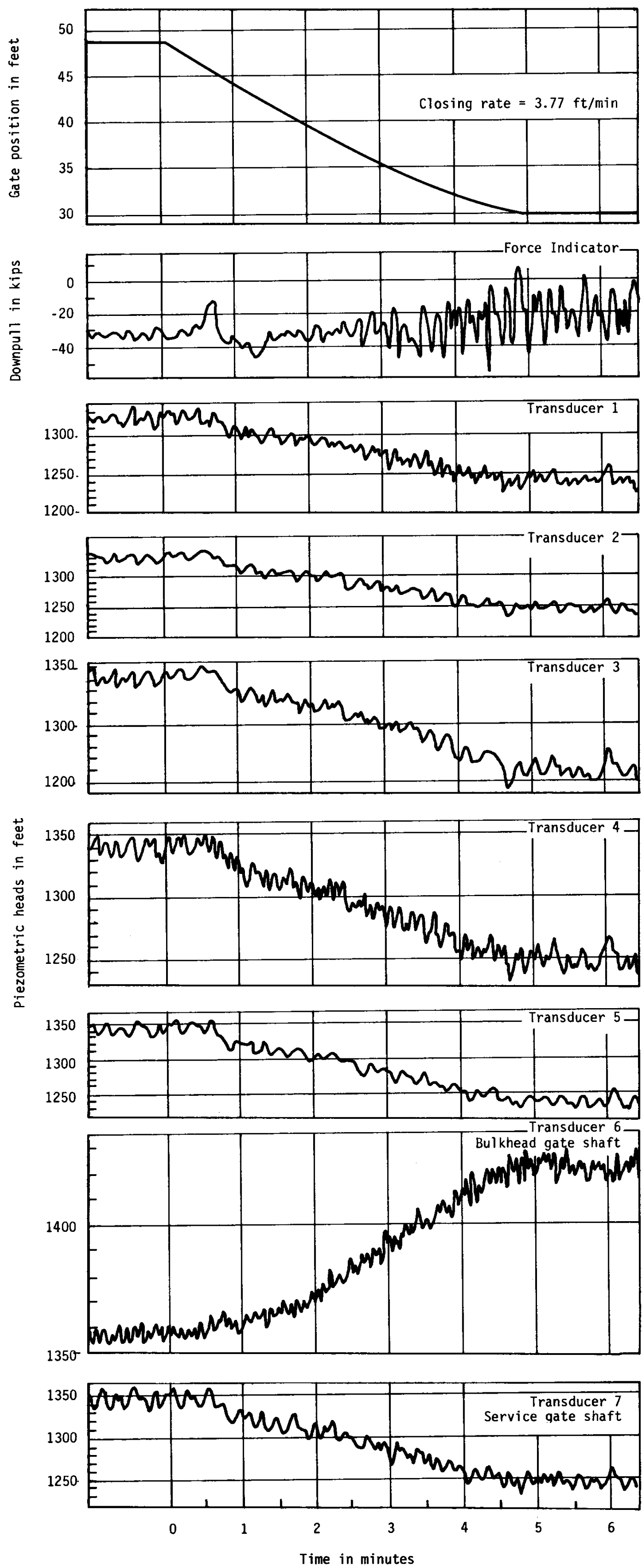

Figure 80. Gate closing - Range 30-48 feet
Submerged

CONCLUSIONS

The pertinent conclusions from the study are as follows:

1. The hydraulics of the flow through the tunnel and gate sections were described in one-dimensional form. The non-dimensional parameters are unique functions of gate positions. The head loss coefficient K_T for the head loss between the beginning of the upstream transition and end of the downstream transition is shown in Figure 51. The difference between the water levels in the bulkhead gate shaft and service gate shaft is shown in Figure 52. Thus, with H_1 known (from computations for given reservoir level and radial gate and service gate openings), H_4 and H_5 may be determined. Hence from H_1, H_4 and H_5, H_2 and H_3 (see definition sketch Figure 44) may be calculated.

2. The hydrodynamic downpull on the gate was expressed as pressure head coefficients, separately for (a) the top seal clamp bar (Figure 53), (b) the bottom seal plate (Figure 54), (c) the bottom beam (Figures 58 and 59) and (d) the top beam (Figures 62 and 63). By using the coefficients in these figures, the separate forces may be calculated as follows:

   (a) The pressure coefficient and H_4 (or $V_c^2/2g$) together with H_1 enables calculation of the average piezometric head on the particular part of the gate referenced to sill level

   $$H_i = (H_1 - C_i H_4) \ .$$

   (b) Subtract the pertinent elevation of the gate part above sill level, z, from the head and multiply by γA to obtain the force as in

   $$F_i = (H_i - z_i)\gamma A_i \ .$$

3. Gate oscillations were small and it was concluded that they would not occur for the prototype gate because of the restraint provided by the friction of the side seals.

4. Fluctuations in water level in the service gate shaft were noted. The fluctuations in the left and right shafts were negatively correlated. The magnitudes and frequency of the oscillations were measured and analysis indicated maximum downpull due to this cause would be about 16 kips.

5. Discharge coefficients for flow into and out of the service gate shaft along the back side of the gate were determined from the small model. The coefficients are shown on Figure 70.

6. Subatmospheric pressures occurred at the top seal surface along the upstream wall of the service gate shaft because of the large velocities of flow through the gap and the sharp corner at the junction of the passage roof and the upstream wall of the gate shaft. Appropriate protective measure against possible cavitation should be provided. Low pressure areas were identified along the junction of the divider wall and floor in the downstream transition for flows with free surface in the downstream tunnel. If possible such flow conditions should be avoided.

7. The unsteady state tests indicated no unusual condition arising because of the gates in motion. Although there were two regions of downpull increase near closed (0.25 to 1 ft) and fully open (about 44.7 to 44.9 ft) in no region of gate opening was any uplift encountered.

REFERENCES

Naudascher, M., Kobus, H.E., and Rao, R.P.R. Hydrodynamic analysis for high-head leaf gates. Journ. Hyd. Div. ASCE, Vol. 90 HY3, May, 1964. pp. 155-192.

Smith, P.M. Hydraulic downpull on Ice Harbor powerhouse gate. Journ. Hyd. Div. ASCE, Vol. 90, HY3, May 1964. pp. 193-213.

Karaki, S. and Ruff, J.F. Diversion, power and irrigation tunnels, Hydraulic model studies. Tarbela Dam Project, Indus River, West Pakistan. Civil Eng. Dept. Colo. State Univ. Report No. CER65SSK-JFR6. Jan. 1965.

Murray, R.I. and Simmons Jr., W.P. Hydraulic downpull forces on large gates. USDI Bureau of Reclamation Research Report No. 4, U.S. Govt. Print. Office, Wash. D.C. 1966.

Karaki, S., Mercer, A.G., and Tullis, J.P. Outlet gates for tunnels 3 and 4, Hydraulic model study. Tarbela Dam Project, Indus River, West Pakistan. Civil Engng. Dept. Colo. State Univ. Report No. CER69-70SK28, April 1970.

Robertson, R.A., and Ball, J.W. Model Study of power intake gate of Mossyrock Dam. Journ. Hyd. Div. ASCE, Vol. 98, HY7, July, 1971. pp.889-906.

APPENDIX A

COEFFICIENT OF FRICTION FOR GATE WHEELS

Tests were made to determine the coefficients of friction for the stainless steel wheels rolling on the plastic runners of the model. These tests were conducted with the gate in the model structure. The 5-ft plastic length of the gate structure (see Figure 20) was placed horizontally and the runners were levelled using precision levels. Calibration weights (weights used for calibrating scales in the laboratory) were placed on the gate face plates to load the wheels. A towing string was attached to the top end of the gate and extended to the open end of the plastic section. There, a 2-in. diameter pully with a precision bearing was centered in the opening, so that the towing line was parallel with the runners. A platform for small weights was attached to the end of the string. By loading the platform with weights, the forces needed to initiate motion of the gate and forces needed to keep the gate moving at constant speed could be determined.

The friction of the pulley bearing was small in comparison to the friction of the gate wheels. This was determined by hanging equal weights (200 and 300 grams) on either side of the pulley and adding minute weights until the pulley was set in motion. It was found that 2 grams would start the pulley in motion and unloading by ½ gram would keep the pully in motion.

The motion of the gate for these friction tests was restricted by the weights placed on the face plate. Since the structure was already fabricated, the upstream wall of the gate shaft restricted movement of the gate to 6 inches of travel. The number of weights which could be placed conveniently on the gate was limited. The weights were 50 pounds lead and steel calibration weights measuring approximately 5 x 8 inches and 6 inches high with a handle on top. The weights were centered on the gate and stacked vertically. There were 4 wheels of the gate made to contact the plastic runners. In order to represent the water load which would be acting on the gate in the model, the total weight in these tests was limited to 250 pounds, and with the dead weight of the gate, the maximum load was 275.6 pounds.

Tests were made with bearings rolling on dry plastic. Also, tests were made with bearings rolling on wet plastic. This was done by sealing the open ends of the gate structure and putting in enough water to just submerge the runner. The results of these tests are shown in Tables A-1, A-2 and A-3. The coefficient of rolling friction is simply

$$C_{fr} = \frac{F_r}{L}$$

where C_{fr} is the coefficient of rolling friction,
F_r is the weight needed to keep the gate in motion, and
L is the total load on the wheels.

Starting friction was also measured, but in general it was difficult to distinguish between starting and rolling friction. In those tests,

$$C_{fs} = \frac{F_s}{L}$$

where C_{fs} is the starting friction coefficient and
F_s is the weight needed to start motion.

The results in Tables A-1, A-2 and A-3 were obtained from tests conducted before the entire system was assembled. It turned out later that these tests could be repeated after the model had been in operation for a short period of time. There was a time span of two months between the tests described above and the results given in Tables A-4 and A-5.

It will be noted that the coefficients for the left and right gates are different, but the coefficients determined from tests two months separated in time yielded approximately the same values as the first set of measurements. Also, wetting the runners had little effect on the coefficient of friction and there was little difference between starting and rolling friction coefficients.

TABLE A-1 TEST FOR DRY RUNNERS - LEFT GATE

L	F_r	C_{fr}	F_s	C_{fs}
75.6	.243	.0032	No distinguishable difference from F_r and C_{fr}	
125.6	.386	.0031		
175.6	.452	.0026		
225.6	.635	.0028		
275.6	.805	.0029		
Mean Value		.0029		

TABLE A-2 TEST FOR WET RUNNERS - LEFT GATE

L	F_r	C_{fr}	F_s	C_{fs}
75.6	.162	.0021	.212	.0028
125.6	.374	.0030	.357	.0028
175.6	.485	.0028	.558	.0032
225.6	.595	.0026	.690	.0031
275.6	.795	.0029	.809	.0029
Mean Values		.0027		.0030

TABLE A-3 TEST FOR WET RUNNERS - RIGHT GATE

L	F_r	C_{fr}	F_s	C_{fs}
69.7	.121	.0017	No distinguishable difference from F_r and C_{fr}	
119.7	.206	.0017		
169.7	.310	.0018		
219.7	.495	.0023		
269.7	.634	.0024		
Mean Value		.0020		

TABLE A-4 TEST FOR DRY RUNNERS - LEFT GATE

L	F_r	C_{fr}
83.83	.2308	.0028
123.85	.3455	.0028
173.85	.4623	.0027
223.85	.6056	.0027
273.85	.7709	.0028
Mean Value		.0028

TABLE A-5 TEST FOR DRY RUNNERS - RIGHT GATE

L	F_r	C_{fr}
73.8	.1420	.0019
123.8	.2639	.0021
173.8	.3741	.0022
223.8	.5174	.0023
273.8	.6607	.0024
Mean Value		.0022

```
 PRESSURE HEADS AND DOWNPULL COMPUTATIONS FOR RUN NO 110201
DATA TAPE NO Z0284
THE FOLLOWING PARAMETERS WERE USED.....
IHEADER=YES  NCHAN =  12 LENARR = 100 FRSTREC = OK
NFILE1=  20 ISTART =   1 ISKIP =   0 CALIBTP =YES  DEV =    .250
NHEDPTS =  7 NDIFPTS = 1  COEFQ10 =  8925.5 COEFQ12 = 16652.1      STSTATE =YES
CALDRIF =YES  WRITDAT =  0  WRITAPE = NO
RITEGTE = NO  SKIPREC =      CALPRES =YES  NPIEZ1 =  49 NPIEZ2 =  60 NPIEZ3 =  55
NRUNS =   4 GTFAREA =      52.72   AREATN =    1590.43 AREAPAS =     607.50 WIDTH = 13.50
A0(1,1) =   0.00000 A1(1,1) =  35.25000 A0(1,2) =   0.00000 A1(1,2) =-352.51200 A0(1,3) =   0.00000 A1(1,3) =   -.81000
DIFFCAL =YES  WORFSZE = 10 TOLER =  .05 LPACDAT = 240 KEYCHN =  3
```

THESE ARE ELEVATIONS FOR PIEZOMETERS IN MANIFOLD BANK 1

PIEZO NO	ELEVATION	PIEZO NO	ELEVATION	PIEZO NO	ELEVATION	PIEZO NO	ELEVATION	PIEZO NO	ELEVATION
1	1157.63	11	1158.32	21	1155.92	31	1151.95	41	1136.36
2	1157.51	12	1158.36	22	1155.00	32	1180.42	42	1136.36
3	1157.79	13	1158.36	23	1154.05	33	1180.36	43	1136.36
4	1158.01	14	1158.34	24	1154.14	34	1180.32	44	1136.38
5	1158.10	15	1158.36	25	1154.06	35	1180.28	45	1136.36
6	1158.32	16	1158.34	26	1153.91	36	1180.38	46	1136.40
7	1158.32	17	1158.36	27	1153.64	37	1180.38	47	1136.42
8	1158.32	18	1158.32	28	1153.07	38	1180.42	48	1136.48
9	1158.32	19	1158.14	29	1153.05	39	1180.42	49	1136.40
10	1158.36	20	1157.03	30	1152.81	40	1180.42	50	0.00

THE TRANSDUCER ELEVATION FOR THIS MANIFOLD IS 1150.15

THESE ARE ELEVATIONS FOR PIEZOMETERS IN MANIFOLD BANK 2

PIEZO NO	ELEVATION	PIEZO NO	ELEVATION	PIEZO NO	ELEVATION	PIEZO NO	ELEVATION	PIEZO NO	ELEVATION
1	1158.32	13	1180.32	25	1135.82	37	1176.07	49	1139.42
2	1158.32	14	1135.82	26	1135.82	38	1136.22	50	1133.09
3	1158.32	15	1136.32	27	1135.82	39	1175.92	51	1137.13
4	1158.32	16	1158.36	28	1135.82	40	1136.22	52	1136.24
5	1158.14	17	1180.32	29	1136.32	41	1158.32	53	1136.58
6	1158.03	18	1135.82	30	1158.32	42	1175.82	54	1137.22
7	1155.92	19	1136.34	31	1180.32	43	1135.82	55	1139.10
8	1155.00	20	1158.34	32	1136.32	44	1135.82	56	1138.84
9	1154.05	21	1180.32	33	1158.32	45	1135.82	57	1141.28
10	1135.82	22	1136.32	34	1178.46	46	1146.35	58	1141.20
11	1136.32	23	1158.34	35	1136.22	47	1141.55	59	1141.20
12	1158.38	24	1180.32	36	1158.32	48	1140.51	60	1141.20

THE TRANSDUCER ELEVATION FOR THIS MANIFOLD IS 1150.14

THESE ARE ELEVATIONS FOR PIEZOMETERS IN MANIFOLD BANK 3

PIEZO NO	ELEVATION	PIEZO NO	ELEVATION	PIEZO NO	ELEVATION	PIEZO NO	ELEVATION	PIEZO NO	ELEVATION
1	1136.39	12	1141.38	23	1182.40	34	1145.41	45	1181.02
2	1136.57	13	1144.20	24	1182.39	35	1180.97	46	1181.07
3	1136.43	14	1144.10	25	1182.42	36	1190.76	47	1182.15
4	1136.38	15	1149.63	26	1182.29	37	1189.13	48	1182.72
5	1136.49	16	1149.53	27	1182.31	38	1242.02	49	1183.32
6	1136.40	17	1155.07	28	1182.31	39	1212.57	50	1198.57
7	1136.30	18	1154.97	29	1182.27	40	1203.32	51	1198.82
8	1136.41	19	1179.65	30	1139.41	41	1194.07	52	1199.22
9	1138.78	20	1179.56	31	1145.41	42	1184.82	53	1203.56
10	1138.67	21	1182.40	32	1180.97	43	1182.02	54	1204.12
11	1141.48	22	1182.39	33	1139.41	44	1181.62	55	1189.26

THE TRANSDUCER ELEVATION FOR THIS MANIFOLD IS 1150.14

NOTE.. ELEVATIONS FOR PIEZO NOS. 1--32 ARE GIVEN FORLEFT GATE CLOSED
TRUE ELEVATIONS ARE GIVEN BY ADDING THE GATE OPENING

AREAS APPLICABLE FOR EACH PIEZO ON THE LEFT GATE ARE AS FOLLOWS...

PIEZO NO	AREA	PIEZO NO	AREA	PIEZO NO	AREA	PIEZO NO	AREA	PIEZO NO	AREA
1	7.09	8	11.79	15	49.25	22	4.19	29	7.50
2	8.30	9	49.25	16	49.25	23	2.47	30	3.62
3	6.03	10	49.25	17	49.25	24	5.31	31	3.62
4	5.08	11	49.25	18	49.25	25	6.03	32	3.76
5	4.12	12	49.25	19	49.25	26	6.93	33	3.62
6	1.83	13	49.25	20	49.25	27	4.08	34	3.62
7	4.11	14	49.25	21	12.82	28	6.33	35	3.76

DATA FOR CALIBRATION NO 1

REC	CHANNEL NO											
NO	1	2	3	4	5	6	7	8	9	10	11	12
1	-.001	.002	.004	-.001	-.003	.017	.002	.006	.002	-.002	.006	.003
2	-.001	.003	.004	-.001	-.003	.020	.002	.003	.008	-.002	.006	.010
3	.000	.003	.002	.001	-.002	.034	.003	.004	.002	-.001	.007	.003
4	-.000	.003	.003	.002	-.002	.018	.003	.004	.003	-.001	.007	.003
5	-.002	.002	.002	.001	-.003	.020	.002	.003	.001	-.002	.006	.002
6	-.001	.003	.004	.002	-.002	.018	.002	.004	.001	-.001	.007	.016
7	-.000	.003	.005	-.002	-.001	.018	.003	.004	.002	-.001	.008	.003
8	-.002	.002	.002	.000	-.002	.017	.002	.003	.000	-.002	.006	.002
9	-.002	.002	.003	-.000	-.013	.017	.002	.003	.000	-.002	.006	.002
RMS	.003	.002	.007	.010	.028	.030	.003	.003	.016	.002	.003	.028

DATA FOR CALIBRATION NO 2

REC	CHANNEL NO											
NO	1	2	3	4	5	6	7	8	9	10	11	12
1	.503	.507	.512	.503	.500	.523	.506	.510	.506	.503	.512	.508
2	.503	.507	.512	.503	.500	.523	.506	.510	.505	.503	.512	.508
3	.503	.507	.512	.503	.501	.523	.506	.510	.507	.503	.512	.508
4	.503	.507	.512	.504	.501	.524	.506	.510	.505	.503	.512	.508
5	.504	.508	.513	.504	.501	.524	.506	.511	.506	.504	.513	.509
6	.503	.507	.512	.503	.501	.524	.506	.510	.505	.503	.513	.508
7	.506	.507	.512	.503	.501	.523	.505	.510	.505	.503	.512	.508
8	.504	.507	.512	.503	.501	.524	.506	.510	.505	.504	.513	.508
9	.504	.508	.513	.504	.501	.524	.506	.510	.506	.504	.513	.509
RMS	.007	.003	.003	.003	.003	.003	.003	.003	.007	.003	.003	.003

DATA FOR CALIBRATION NO 3

REC	CHANNEL NO											
NO	1	2	3	4	5	6	7	8	9	10	11	12
1	-.507	-.502	-.502	-.504	-.502	-.486	-.500	-.499	-.502	-.505	-.497	-.504
2	-.506	-.501	-.502	-.504	-.502	-.486	-.499	-.499	-.502	-.505	-.497	-.503
3	-.507	-.502	-.503	-.504	-.502	-.487	-.500	-.500	-.502	-.506	-.497	-.504
4	-.506	-.501	-.502	-.504	-.501	-.486	-.499	-.499	-.501	-.505	-.496	-.503
5	-.505	-.503	-.502	-.503	-.501	-.485	-.498	-.499	-.501	-.504	-.496	-.502
6	-.506	-.501	-.502	-.503	-.501	-.486	-.499	-.499	-.501	-.505	-.496	-.503
7	-.506	-.501	-.502	-.504	-.501	-.486	-.499	-.500	-.501	-.505	-.496	-.503
8	-.506	-.501	-.502	-.504	-.501	-.487	-.499	-.500	-.501	-.505	-.496	-.503
9	-.506	-.500	-.502	-.503	-.501	-.486	-.498	-.499	-.501	-.504	-.496	-.502
10	-.506	-.500	-.502	-.503	-.501	-.486	-.499	-.499	-.501	-.504	-.496	-.502
RMS	.002	.008	.002	.002	.002	.002	.002	.002	.002	.002	.002	.002

DATA FOR CALIBRATION NO 4

REC	CHANNEL NO											
NO	1	2	3	4	5	6	7	8	9	10	11	12
1	1.004	1.010	1.019	1.005	1.002	1.026	1.009	1.016	1.009	1.006	1.016	1.012
2	1.004	1.010	1.019	1.005	1.002	1.026	1.009	1.016	1.009	1.006	1.016	1.011
3	1.004	1.010	1.019	1.005	1.002	1.026	1.009	1.016	1.009	1.006	1.016	1.011
4	1.005	1.011	1.020	1.005	1.003	1.027	1.009	1.017	1.010	1.007	1.017	1.012

5	1.005	1.011	1.018	1.005	1.003	1.027	1.009	1.017	1.009	1.006	1.016	1.012
6	1.004	1.010	1.019	1.005	1.002	1.026	1.009	1.016	1.009	1.006	1.016	1.012
7	1.005	1.010	1.019	1.005	1.003	1.027	1.009	1.017	1.008	1.006	1.016	1.012
8	1.004	1.010	1.019	1.005	1.003	1.026	1.009	1.016	1.008	1.006	1.016	1.012
9	1.004	1.010	1.019	1.005	1.002	1.026	1.009	1.016	1.008	1.006	1.016	1.012
10	1.004	1.009	1.018	1.004	1.002	1.026	1.008	1.016	1.007	1.005	1.016	1.011
RMS	.003	.003	.006	.003	.003	.003	.003	.003	.003	.003	.003	.003

AN END OF FILE WAS ENCOUNTERED. THERE WERE 10 RECORDS IN FILE 1

DATA FOR CALIBRATION NO 5

REC	CHANNEL NO											
NO	1	2	3	4	5	6	7	8	9	10	11	12
1	-1.008	-1.002	-1.003	-1.004	-.998	-.985	-.997	-.996	-1.000	-1.005	-.996	-1.005
2	-1.008	-1.002	-1.004	-1.004	-.998	-.987	-.997	-.997	-1.000	-1.006	-.997	-1.005
3	-1.009	-1.002	-1.005	-1.004	-.999	-.988	-.997	-.999	-1.000	-1.006	-.997	-1.006
4	-1.009	-1.002	-1.006	-1.004	-.999	-.988	-.997	-.999	-1.001	-1.007	-.997	-1.006
5	-1.009	-1.002	-1.006	-1.004	-.999	-.989	-.998	-.999	-1.001	-1.007	-.997	-1.006
6	-1.009	-1.002	-1.006	-1.004	-.999	-.989	-.998	-1.000	-1.001	-1.007	-.997	-1.006
7	-1.009	-1.002	-1.007	-1.005	-.999	-.989	-.998	-1.000	-1.001	-1.007	-.997	-1.006
8	-1.009	-1.002	-1.006	-1.004	-.999	-.989	-.997	-1.000	-1.000	-1.007	-.997	-1.006
9	-1.009	-1.002	-1.007	-1.004	-.999	-.989	-.998	-1.000	-1.001	-1.007	-.997	-1.006
10	-1.010	-1.003	-1.007	-1.005	-.999	-.989	-.998	-1.000	-1.001	-1.007	-.998	-1.006
RMS	.002	.002	.002	.002	.002	.002	.002	.002	.002	.002	.002	.002

CHANNEL NO	POINT NO	TRUE VALUE	TAPE VALUE	RMS TAPE	REGRESSION SLOPE	REGRESSION INTERCEPT
1	1	0.000	-.001	.003		
1	2	.500	.504	.007		
1	3	-.500	-.506	.002		
1	4	1.000	1.004	.003		
1	5	-1.000	-1.009	.002		
					.99281	.002
2	1	0.000	.003	.002		
2	2	.500	.507	.003		
2	3	-.500	-.501	.008		
2	4	1.000	1.010	.003		
2	5	-1.000	-1.002	.002		
					.99347	-.003
3	1	0.000	.003	.007		
3	2	.500	.512	.003		
3	3	-.500	-.502	.002		
3	4	1.000	1.019	.006		
3	5	-1.000	-1.006	.002		
					.98746	-.005
4	1	0.000	.000	.010		
4	2	.500	.503	.003		
4	3	-.500	-.504	.002		
4	4	1.000	1.005	.003		
4	5	-1.000	-1.004	.002		
					.99500	-.000
5	1	0.000	-.003	.028		
5	2	.500	.501	.003		
5	3	-.500	-.501	.002		
5	4	1.000	1.003	.003		
5	5	-1.000	-.999	.002		
					.99898	.000
6	1	0.000	.020	.030		
6	2	.500	.523	.003		
6	3	-.500	-.486	.002		
6	4	1.000	1.026	.003		
6	5	-1.000	-.988	.002		
					.99234	-.019
7	1	0.000	.002	.003		
7	2	.500	.506	.003		
7	3	-.500	-.499	.002		
7	4	1.000	1.009	.003		
7	5	-1.000	-.997	.002		
					.99657	-.004
8	1	0.000	.004	.003		
8	2	.500	.510	.003		
8	3	-.500	-.499	.002		
8	4	1.000	1.016	.003		
8	5	-1.000	-.999	.002		
					.99208	-.006
9	1	0.000	.002	.016		
9	2	.500	.506	.007		
9	3	-.500	-.501	.002		
9	4	1.000	1.009	.003		
9	5	-1.000	-1.001	.002		
					.99499	-.003
10	1	0.000	-.002	.002		
10	2	.500	.503	.003		
10	3	-.500	-.505	.002		
10	4	1.000	1.006	.003		
10	5	-1.000	-1.006	.002		
					.99342	.001
11	1	0.000	.007	.003		

11	2	.500	.513	.003		
11	3	-.500	-.496	.002		
11	4	1.000	1.016	.003		
11	5	-1.000	-.997	.002		
					.99299	-.008
12	1	0.000	.005	.028		
12	2	.500	.508	.003		
12	3	-.500	-.503	.002		
12	4	1.000	1.012	.003		
12	5	-1.000	-1.006	.002		
					.99088	-.003

THERE WERE 48 RECORDS USED FOR THE CALIBRATIONS

AN END OF FILE WAS ENCOUNTERED. THERE WERE 10 RECORDS IN FILE 2

CHANNEL NO	POINT NO	HEAD	TAPE VALUE	RMS TAPE	REGRESSION SLOPE	INTERCEPT
6	1	0.000	-.762	.002		
6	2	69.744	-.410	.002		
6	3	142.032	-.045	.002		
6	4	214.152	.323	.003		
6	5	296.592	.754	.003		
6	6	356.280	1.065	.003		
6	7	414.360	1.374	.003		
					194.11580	149.563
9	1	0.000	-.959	.002		
9	2	69.744	-.575	.002		
9	3	142.032	-.176	.003		
9	4	214.152	.224	.003		
9	5	296.592	.691	.003		
9	6	356.280	1.029	.004		
9	7	414.360	1.365	.004		
					178.41688	172.527
12	1	0.000	-.239	.002		
12	2	69.744	.029	.003		
12	3	142.032	.307	.003		
12	4	214.152	.584	.003		
12	5	296.592	.908	.003		
12	6	356.280	1.142	.003		
12	7	414.360	1.374	.003		
					257.06530	62.576

THERE WERE 7 RECORDS USED IN THIS CALIBRATION. EACH RECORD CONSISTS OF 100 DATA POINTS

PRESSURE TRANSDUCERS HAVE BEEN CALIBRATED FOR RUN NO.110201
THIS TAPE IS TAGGED BY A CSU LABEL Z0284

AN END OF FILE WAS ENCOUNTERED. THERE WERE 10 RECORDS IN FILE 3

CHANNEL NO	POINT NO	HEAD	TAPE VALUE	RMS TAPE	REGRESSION SLOPE	REGRESSION INTERCEPT
3	1	0.000	-.166	.003		
3	2	5.313	.020	.003		
3	3	9.985	.169	.003		
3	4	14.821	.323	.003		
3	5	20.021	.485	.003		
3	6	25.308	.654	.004		
3	7	30.169	.806	.004		
3	8	35.256	.963	.004		
3	9	40.117	1.114	.004		
3	10	44.802	1.260	.004		
					31.60760	4.794

THERE WERE 100RECORDS USED IN THIS CALIBRATION. EACH RECORD CONSISTS OF 100 DATA POINTS

PRESSURE TRANSDUCERS HAVE BEEN CALIBRATED FOR RUN NO.110201
THIS TAPE IS TAGGED BY A CSU LABEL Z0284

CHANNEL NO	POINT NO	TAPE VALUE	DIFF
6	1	-.295	
6	2	-.291	
			.004
9	1	-.452	
9	2	-.448	
			.004
12	1	.116	
12	2	.121	
			.005

CONVENTION.... DOWNPULL (FORCE) IS + DOWNWARD,...PULLDOWN (POSITION) AND OSCILLATIONS ARE + DOWNWARD

AN END OF FILE WAS ENCOUNTERED. THERE WERE 0 RECORDS IN FILE 4

REC NO	POSITION FT	RMS FT	DOWN PULL KIPS	RMS KIPS	PULL DOWN IN	RMS IN	LARGEST FORCE KIPS	SMALLEST FORCE KIPS	OSCILLATIONS LOWEST IN	OSCILLATIONS HIGHEST IN
1	4.88	.09	32.500	5.236	.07	.01	39.88	22.95	.02	-.02
2	4.86	.09	21.936	1.624	.05	.00	24.88	19.08	.01	-.01
3	4.87	.08	24.182	.953	.06	.00	26.09	22.22	.00	-.00
4	4.89	.08	25.989	1.123	.06	.00	28.75	23.92	.01	-.00
5	4.90	.08	23.144	1.393	.05	.00	26.33	20.04	.01	-.01
6	4.88	.10	22.328	1.349	.05	.00	24.64	19.56	.01	-.01
7	4.91	.08	22.459	.722	.05	.00	24.40	21.01	.00	-.00
8	4.89	.08	20.932	1.024	.05	.00	22.95	19.08	.00	-.00
9	4.89	.09	23.894	2.764	.05	.01	28.75	19.32	.01	-.01
10	4.90	.05	22.316	1.898	.05	.00	26.33	19.08	.01	-.01
AVERAGES	4.89		23.968	NREC =	10 NPOINTS =	1000				
11	4.89	.09	19.050	4.739	.04	.01	29.24	13.27	.02	-.01
12	4.90	.09	31.692	2.653	.07	.01	36.74	27.06	.01	-.01
13	4.91	.08	26.209	3.302	.06	.01	31.17	21.01	.01	-.01
14	4.90	.05	21.046	1.033	.05	.00	23.43	18.59	.01	-.01
15	4.91	.08	26.422	2.023	.06	.00	30.21	22.22	.01	-.01
16	4.92	.09	29.301	1.561	.07	.00	32.14	26.33	.01	-.01
17	4.92	.09	30.153	2.594	.07	.01	34.08	24.40	.01	-.01
18	4.91	.09	28.208	1.770	.06	.00	30.45	24.16	.01	-.01
19	4.92	.09	27.257	1.568	.06	.00	30.69	24.16	.01	-.01
20	4.91	.09	26.911	.818	.06	.00	28.51	25.37	.00	-.00
AVERAGES	4.91		26.625	NREC =	20 NPOINTS =	1000				
21	4.89	.10	28.904	.832	.07	.00	30.69	26.82	.00	-.00
22	4.89	.07	28.104	.983	.06	.00	30.69	26.33	.01	-.00
23	4.89	.10	32.401	.993	.07	.00	34.56	29.96	.00	-.01
24	4.90	.09	33.572	.856	.08	.00	35.53	31.66	.00	-.00
25	4.90	.09	31.300	1.166	.07	.00	33.59	28.75	.01	-.01
26	4.90	.09	29.408	.983	.07	.00	31.17	26.82	.00	-.01
27	4.90	.08	31.769	2.125	.07	.00	35.53	27.79	.01	-.01
28	4.89	.09	32.785	1.081	.08	.00	35.29	30.69	.01	-.00
29	4.89	.08	31.387	1.046	.07	.00	34.32	29.48	.01	-.00
30	4.91	.09	37.491	2.894	.09	.01	41.34	30.69	.01	-.02
AVERAGES	4.90		31.712	NREC =	30 NPOINTS =	1000				
31	4.87	.08	36.959	2.357	.08	.01	40.61	31.17	.01	-.01
32	4.87	.08	39.911	.768	.09	.00	41.58	37.46	.00	-.01
33	4.88	.10	36.485	1.176	.08	.00	39.40	33.84	.01	-.01
34	4.91	.08	36.729	1.860	.08	.00	40.37	33.59	.01	-.01
35	4.90	.08	33.472	1.530	.08	.00	36.50	30.21	.01	-.01
36	4.89	.08	30.683	1.168	.07	.00	33.11	28.27	.01	-.01
37	4.90	.09	32.998	1.535	.08	.00	35.77	29.24	.01	-.01
38	4.89	.07	30.509	1.338	.07	.00	33.84	26.33	.01	-.01
39	4.89	.06	24.702	1.642	.06	.00	28.75	21.98	.01	-.01
40	4.91	.08	31.704	1.841	.07	.00	34.80	27.30	.01	-.01
AVERAGES	4.89		33.415	NREC =	40 NPOINTS =	1000				

MEASURED VALUES.. RUN NO 110201 LEFT GATE (LOOKING DOWNSTREAM)

AVE POSIT FT	FORCE CELL KIPS	ORIFICE DISCH CFS	RMS Q CFS	PIEZ NO	PIEZO HEAD BANK 1	PIEZ NO	PIEZO HEAD BANK 2	PIEZ NO	PIEZO HEAD BANK 3	PRESSURE HEAD BANK 1	PRESSURE HEAD BANK 2	PRESSURE HEAD BANK 3
4.89	23.968	19796	4898	1	1549.77	1	1547.51	1	1330.05	391.14	389.19	188.71
4.91	26.625	19838	5337	2	1547.38	2	1546.97	2	1330.62	389.87	388.65	189.10
4.90	31.712	19780	5022	3	1547.70	3	1546.52	3	1331.32	389.91	388.20	189.94
4.89	33.415	19797	5063	4	1548.70	4	1546.81	4	1330.22	390.69	388.49	188.89
4.89	32.556	19829	5064	5	1549.00	5	1333.44	5	1322.67	390.90	175.30	181.23
4.92	24.157	19983	5142	6	1549.38	6	1332.63	6	1325.30	391.06	174.60	183.95
4.92	23.925	19956	5137	7	1548.75	7	1331.55	7	1325.96	390.43	175.63	184.71
4.90	21.476	19894	5296	8	1548.63	8	1333.55	8	1318.35	390.31	178.55	176.99
4.92	30.649	19969	8079	9	1549.19	9	1343.00	9	1332.83	390.87	188.95	189.10
4.91	31.229	19981	5016	10	1548.74	10	1547.74	10	1332.52	390.38	411.92	188.90
4.92	22.834	20053	5066	11	1548.79	11	1547.69	11	1333.25	390.47	411.37	186.82
4.92	35.401	20064	5029	12	1549.56	12	1546.92	12	1333.34	391.20	388.54	187.01
4.91	29.640	20035	5185	13	1549.50	13	1547.66	13	1333.73	391.14	367.34	184.58
4.92	20.600	20044	5189	14	1348.24	14	1548.95	14	1334.33	189.90	413.13	185.28
4.91	23.141	20072	5437	15	1334.95	15	1548.91	15	1334.22	176.57	412.59	179.64
4.93	21.451	20083	5362	16	1334.34	16	1548.65	16	1334.30	176.50	390.27	179.82
4.88	24.597	19892	5355	17	1334.18	17	1548.16	17	1333.60	175.82	367.64	173.58
4.91	31.899	20012	5384	18	1334.30	18	1547.92	18	1335.14	176.48	412.10	175.22
4.92	17.644	20124	5504	19	1335.90	19	1549.57	19	1335.62	177.76	413.23	151.02
4.91	28.993	20082	5465	20	1335.02	20	1549.90	20	1335.88	177.99	391.56	151.37
4.93	29.893	20208	5682	21	1334.17	21	1551.02	21	1334.57	178.25	370.70	147.22
4.95	20.780	20341	5895	22	1335.34	22	1550.45	22	1335.55	180.84	414.13	148.21
4.95	32.352	20349	5633	23	1344.95	23	1549.89	23	1334.57	190.90	391.55	147.22
4.96	28.521	20363	5724	24	1347.90	24	1551.11	24	1335.11	193.76	370.79	147.77
4.96	29.751	20341	5737	25	1360.18	25	1341.26	25	1335.28	206.12	205.44	147.91
4.97	33.568	20498	6073	26	1360.85	26	1340.50	26	1336.43	206.94	204.68	149.19
4.95	29.836	20330	6064	27	1361.56	27	1331.13	27	1336.17	207.92	195.31	148.91
4.95	21.196	20276	6306	28	1361.43	28	1341.49	28	1335.69	208.36	205.67	148.43
4.93	31.779	20173	6396	29	1361.56	29	1410.46	29	1336.37	208.51	274.16	149.15
4.90	30.268	20120	6037	30	1360.43	30	1336.07	30	1544.19	207.62	177.75	399.83
4.93	22.997	20319	6823	31	1360.82	31	1335.93	31	1549.70	208.87	155.61	399.34
4.95	18.231	20404	6149	32	1552.61	32	1339.79	32	1525.37	372.19	203.47	339.45
4.92	26.626	20307	6512	33	1552.59	33	1335.04	33	1546.00	372.23	176.72	401.64
4.96	20.546	20448	6227	34	1552.77	34	1336.13	34	1549.90	372.45	157.67	399.54
4.95	22.305	20424	7384	35	1553.00	35	1308.88	35	1516.03	372.72	172.66	330.11
4.98	28.668	20565	6189	36	1338.70	36	1331.74	36	1551.27	158.32	173.42	360.51
4.98	26.465	20553	6315	37	1336.66	37	1332.93	37	1335.40	156.28	156.86	146.27
4.98	24.127	20545	6032	38	1336.60	38	1335.14	38	1339.23	156.18	198.92	97.21
4.96	25.452	20543	6842	39	1335.88	39	1334.09	39	1338.07	155.46	158.17	125.50
5.00	29.243	20738	6698	40	1336.37	40	1339.58	40	1337.90	155.95	203.36	134.58
5.00	27.914	20704	7069	41	1551.32	41	1340.35	41	1335.59	414.96	182.03	141.52
4.98	28.569	20678	6706	42	1551.76	42	1338.07	42	1336.72	415.40	162.25	151.90
4.98	29.029	20616	6389	43	1544.94	43	1341.34	43	1336.19	408.58	205.52	154.17
4.99	22.022	20690	6903	44	1545.50	44	1338.36	44	1337.21	409.12	202.54	155.59
4.97	30.042	20584	6191	45	1432.73	45	1331.45	45	1338.56	296.37	195.63	157.54
4.96	32.569	20492	5863	46	1346.49	46	1551.23	46	1444.67	210.09	404.88	263.60
4.99	14.791	20617	6414	47	1328.37	47	1552.26	47	1495.55	191.95	410.71	313.40
4.96	29.193	20595	6505	48	1336.95	48	1552.93	48	1503.09	200.47	412.42	320.37
4.97	24.364	20600	6468	49	1342.89	49	1552.10	49	1512.33	206.49	412.68	329.01
5.00	29.856	20744	6844	50	1343.33	50	1552.87	50	1338.43	0.00	414.76	139.86
4.97	30.234	20653	6273	51	0.00	51	1552.14	51	1338.65	0.00	415.01	139.83
4.98	28.543	20659	6681	52	0.00	52	1552.70	52	1339.11	0.00	416.46	139.89
4.98	30.340	20642	6328	53	0.00	53	1343.07	53	1339.68	0.00	206.49	136.12
4.95	25.666	20468	6437	54	0.00	54	1341.12	54	1338.55	0.00	203.90	134.43
4.97	34.116	20583	6730	55	0.00	55	1339.09	55	1552.57	0.00	199.99	363.31
4.96	25.664	20525	7024	56	0.00	56	1340.49	56	1553.74	0.00	201.65	0.00
4.98	22.763	20676	6716	57	0.00	57	1336.36	57	1554.08	0.00	195.08	0.00

	4.99	26.583	20734	6493	58	0.00	58	1344.20	58	0.00	0.00	203.00	0.00
	4.97	24.828	20605	6338	59	0.00	59	1346.36	59	0.00	0.00	205.16	0.00
	4.98	27.291	20594	6356	60	0.00	60	1349.70	60	0.00	0.00	208.50	0.00
AVE	4.95	26.882	20326	STD. DEV. Q =		325.9							

CALCULATED VALUES.. RUN NO 110201 LEFT GATE (LOOKING DOWNSTREAM)

GATE OPENING = 11.000 PERCENT RESERVOIR ELEVATION = 1552.97

PRESSURE COEFFICIENTS					
PIEZ NO	BANK 1	PIEZ NO	BANK 2	PIEZ NO	BANK 3
1	.0192	1	.0250	1	1.0209
2	.0256	2	.0275	2	1.0183
3	.0241	3	.0295	3	1.0151
4	.0195	4	.0282	4	1.0202
5	.0182	5	1.0054	5	1.0547
6	.0164	6	1.0091	6	1.0427
7	.0193	7	1.0141	7	1.0397
8	.0199	8	1.0049	8	1.0745
9	.0173	9	.9616	9	1.0082
10	.0193	10	.0239	10	1.0096
11	.0191	11	.0242	11	1.0063
12	.0156	12	.0277	12	1.0059
13	.0159	13	.0243	13	1.0041
14	.9376	14	.0184	14	1.0013
15	.9985	15	.0186	15	1.0018
16	.9990	16	.0198	16	1.0015
17	1.0020	17	.0220	17	1.0047
18	.9992	18	.0231	18	.9976
19	.9942	19	.0155	19	.9954
20	.9982	20	.0140	20	.9942
21	1.0021	21	.0089	21	1.0002
22	.9944	22	.0115	22	.9958
23	.9527	23	.0141	23	1.0002
24	.9392	24	.0085	24	.9978
25	.8829	25	.9696	25	.9970
26	.8799	26	.9731	26	.9917
27	.8766	27	1.0160	27	.9929
28	.8772	28	.9685	28	.9951
29	.8766	29	.6526	29	.9920
30	.8818	30	.9934	30	.0402
31	.8800	31	.9940	31	.0149
32	.0016	32	.9763	32	.1264
33	.0017	33	.9981	33	.0319
34	.0009	34	.9931	34	.0141
35	-.0002	35	1.1179	35	.1692
36	.9813	36	1.0132	36	.0078
37	.9906	37	1.0078	37	.9964
38	.9909	38	.9976	38	.9789
39	.9942	39	1.0024	39	.9842
40	.9920	40	.9773	40	.9850
41	.0076	41	.9737	41	.9956
42	.0055	42	.9842	42	.9904
43	.0368	43	.9692	43	.9928
44	.0342	44	.9829	44	.9381
45	.5507	45	1.0145	45	.9820
46	.9457	46	.0080	46	.4960
47	1.0287	47	.0032	47	.2630
48	.9893	48	.0002	48	.2284
49	.9622	49	.0040	49	.1861
50	0.0000	50	.0005	50	.9826
51	0.0000	51	.0038	51	.9816
52	0.0000	52	.0012	52	.9794
53	0.0000	53	.9613	53	.9768
54	0.0000	54	.9703	54	.9820
55	0.0000	55	.9795	55	.0018

FORCE AT EACH LEFT GATE PIEZOMETER	
PIEZO NO	FORCE KIPS
1	-103.95
2	.61
3	-.58
4	-2.15
5	0.00
6	-.55
7	0.00
8	-5.04
9	0.00
10	0.00
11	0.00
12	0.00
13	0.00
14	0.00
15	0.00
16	0.00
17	-1.08
18	105.87
19	464.10
20	465.17
21	117.77
22	38.73
23	22.67
24	48.98
25	55.67
26	64.50
27	37.91
28	58.65
29	69.84
30	90.32
31	90.21
32	-79.64

FORCE ON EACH BEAM	
BEAM NO	FORCE KIPS
1	83.56
2	97.99
3	71.49
4	59.92
5	46.55
6	20.98
7	47.35
8	130.19
9	581.12
10	580.50
11	574.11
12	574.70
13	567.23
14	569.38
15	552.05
16	552.60
17	533.42
18	538.46

FORCE ON TOP SEAL = -79.642 KIPS

FORCE ON BOTTOM SEAL = 90.317 KIPS

NET HYDRAULIC FORCE = 3.80 KIPS

NET HYDRAULIC FORCE USING
TOP + BOTTOM + SEALS = 12.59

FORCE COEFFICIENT (FAVE) = .3742E-04

FORCE COEFFICIENT (NET) = .6260E-04

FORCE COEFFICIENT (TBS) = .7526E-04

GATE LEAKAGE = 750

FLOW UNDER GATE = 5071

FLOW THROUGH LEFT PASSAGE = 5821

VELOCITY UNDER GATE BASED ON CONTRACTION COEFFICIENT OF .640

VELOCITY = 118.58

VELOCITY HEAD AT VENA CONTRACTA = 218.35

VELOCITY HEAD IN TUNNEL = 2.54

56	0.0000	56	.9731	56	0.0000
57	0.0000	57	.9921	57	0.0000
58	0.0000	58	.9561	58	0.0000
59	0.0000	59	.9462	59	0.0000
60	0.0000	60	.9310	60	0.0000

DATA ANALYSIS FOR RUN NO 110201 FOR THE LEFT GATE HAS BEEN COMPLETED
THE DATA FOR THIS RUN IS ON DIGITAL TAPE NO Z0284

SKIPPED 3FILES. THERE WERE 0RECORDS IN THOSE FILF(S)

APPENDIX C

TABLE C-1. DATA FOR STEADY-STATE TESTS, GATE SUBMERGED

Run No.	Gate Position ft	Piezometric Levels				Piezometric Heads				
		U/S Tunnel	Bulkhead Well	Service Well	D/S Tunnel	H_1	H_2	H_3	H_4	H_5
112301*	0.25	------	1542.8	1235.0	------	407.0	99.2	52.4	307.8	-----
121301	1.00	1546.5	1545.7	1249.0	1257.5	409.9	113.2	65.7	296.7	289.0
110901	2.00	1535.0	1524.8	1272.0	1281.0	389.0	136.2	87.7	252.8	254.0
110201	4.95	1549.0	1550.0	1337.0	1361.5	414.2	201.2	149.8	213.0	187.5
91401	5.10	1503.0	1504.0	1235.0	1267.0	368.2	99.2	47.6	269.0	236.0
92502	9.00	1547.5	1549.0	1330.0	1371.5	413.2	194.2	138.7	219.0	176.0
91402	10.15	1529.0	1510.0	1233.0	1298.0	374.2	97.2	40.6	277.0	231.0
100201	15.00	1505.5	1506.0	1302.0	1360.5	370.2	166.2	104.7	204.0	145.0
91501	15.55	1555.0	1553.0	1232.0	1341.0	417.2	96.2	34.2	321.0	214.0
102301	20.00	1522.5	1512.5	1310.0	1391.0	376.7	174.2	107.7	202.5	131.5
91502	20.15	1548.0	1543.0	1235.0	1353.0	407.2	99.2	32.6	308.0	195.0
102302	24.93	1516.0	1509.0	1308.0	1388.0	373.2	172.2	100.8	201.0	128.0
91601	25.20	1525.0	1517.0	1228.0	1331.0	381.2	92.2	20.5	289.0	194.0
92402	30.10	1446.0	1430.0	1270.0	1326.0	294.2	134.2	57.6	160.0	120.0
91603	30.20	1495.0	1481.0	1221.0	1311.0	345.2	85.2	8.5	260.0	184.0
102303	35.00	1465.0	1444.0	1350.0	1381.0	308.2	214.2	132.7	94.0	84.0
92101	35.30	1489.0	1468.0	1293.0	1351.0	332.2	157.2	75.4	175.0	138.0
102601	40.00	1456.0	1405.0	1305.0	1332.0	269.2	169.2	82.7	100.0	124.0
92102	40.10	1505.5	1454.0	1335.0	1357.0	318.2	199.2	112.6	119.0	148.5
112302*	44.90	------	1264.9	1290.0	------	129.4	154.2	62.8	-25.1	-----
92103	48.00	1548.5	1460.0	1470.0	1492.0	324.2	334.2	239.7	-10.0	156.5
103001	48.00	1464.0	1400.5	1403.0	1324.0	264.7	267.2	172.7	- 2.5	118.0

*The left and right gates were not equal in opening.

TABLE C-2. CALCULATIONS FOR THE GATE SUBMERGED CONDITIONS - STEADY STATE TESTS

Run No.	Gate Position ft	Percent Gate Opening	Q_m	$V_{36}^2/2g$	$2gH_L/V^2_{36}$	$V_{45}^2/2g$	$V_c^2/2g$	$2gH_4/V_c^2$	H_{32}	C_{TS}	H_{30}	C_{BS}	H_{b1s}	H_{t1s}	C_{b1s}	C_{t1s}	C'_{b1s}	C'_{t1s}	H_{b1ss}	H_{t1ss}	C_{b1ss}	C_{t1ss}	F_M kips	F_C kips
112301	0.25	.56	-----	-----	-----	-----	309.5	.995	397	.030	401	.016	73.0	91	1.079	1.021	1.085	1.027	94.8	95.9	1.014	1.011	0.7	19.4
121301	1.00	2.22	3830	.220	1313.0	.02	297.2	.998	382	.095	408	.007	101.8	108	1.037	1.016	1.038	1.017	112.0	113.6	1.004	.999	0	17.5
110901	2.00	4.44	8112	.986	257.0	.40	258.5	.978	364	.098	385	.015	124.6	130	1.023	1.002	1.046	1.025	131.0	132.6	1.021	1.014	-47.1	9.5
110201	4.95	11.0	10900	1.781	104.7	.73	218.4	.975	389	.115	408	.026	187.0	194.5	1.040	1.006	1.067	1.031	199.0	200.1	1.010	1.005	-14.3	2.1
91401	5.10	11.3	13230	2.62	89.5	1.07	271.5	.991	324	.164	358	.037	83.2	93.6	1.050	1.011	1.059	1.021	96.6	98.2	1.010	1.004	- 8.4	6.1
92502	9.00	20.0	21190	6.73	25.6	2.76	226.4	.966	371	.192	403	.044	-----	-----	-----	-----	-----	-----	190.5	191.6	1.017	1.012	-41.0	-11.0
91402	10.15	22.6	25620	9.84	22.9	4.03	284.6	.973	304	.253	371	.011	91.0	93.6	.995	.986	1.022	1.013	94.6	95.7	1.009	1.005	-17.7	-10.8
100201	15.00	33.3	32540	15.9	8.53	6.50	217.3	.939	293	.352	361	.047	159.0	161.5	.972	.960	1.035	1.023	163.5	164.1	1.013	1.008	-27.9	- 3.5
91501	15.55	34.6	41760	26.1	7.61	10.7	343.5	.934	292	.396	403	.042	88.0	91	.958	.950	1.026	1.016	96.0	96.1	1.001	1.000	-11.5	- 0.9
102301	20.00	44.4	44160	29.2	3.91	12.0	226.6	.894	204	.854	373	.003	167.0	169.5	.925	.914	1.036	1.023	171.7	172.8	1.012	1.007	-29.6	3.9
91502	20.15	44.8	54534	44.6	3.78	18.3	340.5	.905	148	.840	406	.026	91.0	93.6	.929	.921	1.027	1.018	98.6	100.1	1.002	.997	-14.1	35.9
102302	24.93	55.4	57170	49.0	2.02	20.1	232.8	.863	187	.926	376	-.013	167.0	168.9	.886	.878	1.026	1.016	170.9	171.0	1.006	1.006	-11.3	16.9
91601	25.20	56.0	68680	70.7	2.04	29.0	338.4	.854	114	.925	385	-.012	84.0	87.7	.878	.867	1.028	1.016	92.1	92.2	1.000	1.000	14.5	36.8
92402	30.10	66.9	67253	67.8	1.18	27.8	211.8	.755	135	.993	312	-.120	127.0	128.0	.789	.785	1.045	1.039	131.1	131.2	1.019	1.019	-27.0	12.9
91603	30.20	67.1	83290	104.0	1.08	42.6	334.7	.780	92	.965	386	-.085	-----	-----	-----	-----	-----	-----	85.2	85.8	1.000	.998	31.7	41.3
102303	35.0	77.8	66900	67.1	0.66	27.5	136.7	.688	214	1.0	339	-.227	210.0	211.0	.718	.711	1.045	1.034	213.0	213.1	1.013	1.012	-19.3	1.3
92101	35.3	78.5	94182	133.0	0.45	54.5	265.5	.659	159	.989	398	-.248	144.0	145.8	.709	.702	1.075	1.065	157.3	157.4	.999	.999	-11.7	29.5
102601	40.0	88.9	98150	144.4	0.27	59.1	202.0	.495	169	1.0	332	-.300	162.0	166.5	.531	.508	1.072	1.027	169.5	169.6	.997	.996	-12.8	14.4
92102	40.1	89.1	108500	176.5	0.25	72.3	239.0	.498	195	1.02	390	-.311	192.0	196.1	.528	.511	1.061	1.026	196.6	196.7	1.022	1.021	-20.1	26.5
112302	44.9	99.7	-----	-----	-----	-----	270.8	-.111	154	1.0	148	-.070	105.9	131.4	.087	-.009	-0.936	0.080	153.9	155.0	.976	1.020	162.7	54.3
92103	48.0	106.7	109400	179.4	0.28	73.5	125.9	-.079	334	1.0	335	-.064	331.0	328.5	-.055	-.034	0.680	0.430	337.5	338.6	1.33	1.44	-19.0	-30.4
103001	48.0	106.7	105329	166.3	0.12	68.1	116.7	-.021	267	1.0	265	-.017	258.0	257.5	.057	.062	-2.680	-2.880	267.0	268.1	.920	1.36	-17.9	-33.3

TABLE C-3. DATA AND CALCULATIONS FOR THE GATE PARTIALLY SUBMERGED - STEADY STATE TESTS

		Piezo. Levels																				
Run No.	Gate Position ft	Bulkhead Gate Well	Service Gate Well	H_1	H_2	H_3	H_4	Percent Gate Opening	Q_G^*	$V_c^2/2g$	$2gH_4/V_c^2$	H_{32}	H_4'	C_{TP}	H_{30}	C_{BP}	H_{b1p}	H_{t1p}	C_{b1p}	C_{t1p}	F_M kips	F_C kips
110501	5	1484.9	1168	349.1	32	-19.5	317.1	11.1	6,300	311	1.02	310.5	299	.126	337.8	.036	18	27	1.065	1.035	31	35.1
110503	10	1502.2	1175	366.4	39	-17.5	327.4	22.2	12,800	336	.975	296.7	311	.221	351.6	.044	32	34	.995	.989	39	15.7
110505	15	1507.2	1173	371.4	37	-24.5	334.4	33.3	19,800	356	.950	271.6	311	.319	356.6	.042	26.5	28	.969	.965	23	36.1
110507	20	1509.8	1178	374.0	42	-24.5	332.0	44.4	27,000	368	.902	112.2	309	.845	366.4	.021	39	42	.910	.902	47	76.3
110510	25	1509.5	1177	373.7	41	-30.5	332.7	55.6	35,100	385	.864	102.1	303.5	.892	386.5	-.033	38.5	41	.870	.864	84	87.2
110511	30	1500.0	1186	364.2	50	-26.5	314.2	66.7	45,000	409	.768	85.8	289	.960	407.8	-.107	42	47	.787	.776	89	99.6
92401	30.1	1497.2	1205	361.4	69	- 7.6	292.4	66.9	43,500	380	.770	89.4	286	.950	396.3	-.920	60	64.5	.792	.780	42	69.1

*Calculated flow under the gate.

TABLE C-4. DATA AND CALCULATIONS FOR THE GATE UNSUBMERGED (FREE SURFACE) - STEADY STATE TESTS

		Piezo. Levels																	
Run No.	Gate Position ft	Bulkhead Gate Well	H_1	$H_2^\dagger$	H_4	Percent Gate Opening	Q_G^*	$V_c^2/2g$	$2gH_4/V_c^2$	H_{32}	H_4'	C_{TF}	H_{30}	C_{BF}	H_{b1p}	H_{t1p}	C_{b1p}	F_M kips	F_C kips
112303	.25	1535	400	.16	399.8	.56	366	397.0	1.007	397	354	.0056	398	.0025	-1.4	4.0	1.043	94.4	91.1
121302	1.0	1537	401	.68	400.3	2.22	1,470	400.2	1.00	339	355	.090	408	-.0175	-2.5	4.5	1.008	86	59.6
110902	2.0	1534	398	1.3	396.7	4.44	2,900	396.8	1.00	364	351	.097	393	.0126	2.5	3.5	0.997	33	53.1
110202	4.95	1561	425	3.3	421.7	11.0	7,220	423.0	.997	377	375	.128	408	.0402	1.5	4.5	1.001	56	48.2
92503	5.0	1555	419	3.3	415.7	11.1	7,240	417.1	.998	378	369	.111	405	.0335	5.5	5.5	.991	86	47.9
92501	9.0	1553	417	5.9	411.1	20.0	12,830	416.6	.986	362	363	.152	400	.0408	4.5	9.5	.990	67	53.2
100202	15.0	1545	409	9.6	399.4	33.3	21,360	415.6	.959	283	349	.361	395	.0336	13.0	16.0	.953	52	59.0
110601	15.05	1540	404	9.6	394.4	33.4	21,290	410.1	.960	311	344	.270	391	.0292	13.5	16.5	.952	21	58.6
91503	20.05	1476	340	13.0	327	44.5	26,550	352.7	.925	109	275	.840	336	.0113	20.5	22.5	.906	86	90.7
102602	19.98	1502	366	13.0	353	44.4	27,440	379.7	.930	114	301	.838	360	.0158	16.5	19.5	.920	99	94.9
91602	25.35	1513	377	16.5	360.5	56.3	36,990	412.2	.873	103	307	.892	390	-.0316	26.5	28.5	.850	146	105.8
110602	25.22	1510	374	16.5	357.5	56.0	36,570	407.5	.876	110	304	.865	390	-.0392	31.5	29.5	.840	132	104.3

TABLE C-2. CALCULATIONS FOR THE GATE SUBMERGED CONDITIONS - STEADY STATE TESTS

Run No.	Gate Position ft	Percent Gate Opening	Q_m	$V_{36}^2/2g$	$2gH_L/V^2_{36}$	$V_{45}^2/2g$	$V_c^2/2g$	$2gH_4/V_c^2$	H_{32}	C_{TS}	H_{30}	C_{BS}	H_{b1s}
112301	0.25	.56	-----	-----	-----	-----	309.5	.995	397	.030	401	.016	73.0
121301	1.00	2.22	3830	.220	1313.0	.02	297.2	.998	382	.095	408	.007	101.8
110901	2.00	4.44	8112	.986	257.0	.40	258.5	.978	364	.098	385	.015	124.6
110201	4.95	11.0	10900	1.781	104.7	.73	218.4	.975	389	.115	408	.026	187.0
91401	5.10	11.3	13230	2.62	89.5	1.07	271.5	.991	324	.164	358	.037	83.2
92502	9.00	20.0	21190	6.73	25.6	2.76	226.4	.966	371	.192	403	.044	-----
91402	10.15	22.6	25620	9.84	22.9	4.03	284.6	.973	304	.253	371	.011	91.0
100201	15.00	33.3	32540	15.9	8.53	6.50	217.3	.939	293	.352	361	.047	159.0
91501	15.55	34.6	41760	26.1	7.61	10.7	343.5	.934	292	.396	403	.042	88.0
102301	20.00	44.4	44160	29.2	3.91	12.0	226.6	.894	204	.854	373	.003	167.0
91502	20.15	44.8	54534	44.6	3.78	18.3	340.5	.905	148	.840	406	.026	91.0
102302	24.93	55.4	57170	49.0	2.02	20.1	232.8	.863	187	.926	376	-.013	167.0
91601	25.20	56.0	68680	70.7	2.04	29.0	338.4	.854	114	.925	385	-.012	84.0
92402	30.10	66.9	67253	67.8	1.18	27.8	211.8	.755	135	.993	312	-.120	127.0
91603	30.20	67.1	83290	104.0	1.08	42.6	334.7	.780	92	.965	386	-.085	-----
102303	35.0	77.8	66900	67.1	0.66	27.5	136.7	.688	214	1.0	339	-.227	210.0
92101	35.3	78.5	94182	133.0	0.45	54.5	265.5	.659	159	.989	398	-.248	144.0
102601	40.0	88.9	98150	144.4	0.27	59.1	202.0	.495	169	1.0	332	-.300	162.0
92102	40.1	89.1	108500	176.5	0.25	72.3	239.0	.498	195	1.02	390	-.311	192.0
112302	44.9	99.7	-----	-----	-----	-----	270.8	-.111	154	1.0	148	-.070	105.9
92103	48.0	106.7	109400	179.4	0.28	73.5	125.9	-.079	334	1.0	335	-.064	331.0
103001	48.0	106.7	105329	166.3	0.12	68.1	116.7	-.021	267	1.0	265	-.017	258.0

TABLE C-3. DATA AND CALCULATIONS FOR THE GATE PARTIALLY SUBMERGED - STEADY STATE TESTS

Run No.	Gate Position ft	Piezo. Levels: Bulkhead Gate Well	Piezo. Levels: Service Gate Well	H_1	H_2	H_3	H_4	Percent Gate Opening	Q_G^*	$V_c^2/2g$	$2gH_4/V_c^2$	H_{32}	H_4'
110501	5	1484.9	1168	349.1	32	-19.5	317.1	11.1	6,300	311	1.02	310.5	299
110503	10	1502.2	1175	366.4	39	-17.5	327.4	22.2	12,800	336	.975	296.7	311
110505	15	1507.2	1173	371.4	37	-24.5	334.4	33.3	19,800	356	.950	271.6	311
110507	20	1509.8	1178	374.0	42	-24.5	332.0	44.4	27,000	368	.902	112.2	309
110510	25	1509.5	1177	373.7	41	-30.5	332.7	55.6	35,100	385	.864	102.1	303.5
110511	30	1500.0	1186	364.2	50	-26.5	314.2	66.7	45,000	409	.768	85.8	289
92401	30.1	1497.2	1205	361.4	69	- 7.6	292.4	66.9	43,500	380	.770	89.4	286

*Calculated flow under the gate.

TABLE C-4. DATA AND CALCULATIONS FOR THE GATE UNSUBMERGED (FREE SURFACE) - STEADY STATE TESTS

Run No.	Gate Position ft	Piezo. Levels: Bulkhead Gate Well	H_1	$H_2^†$	H_4	Percent Gate Opening	Q_G^*	$V_c^2/2g$	$2gH_4/V_c^2$	H_{32}	H_4'	C_{TF}	H_{30}
112303	.25	1535	400	.16	399.8	.56	366	397.0	1.007	397	354	.0056	398
121302	1.0	1537	401	.68	400.3	2.22	1,470	400.2	1.00	339	355	.090	408
110902	2.0	1534	398	1.3	396.7	4.44	2,900	396.8	1.00	364	351	.097	393
110202	4.95	1561	425	3.3	421.7	11.0	7,220	423.0	.997	377	375	.128	408
92503	5.0	1555	419	3.3	415.7	11.1	7,240	417.1	.998	378	369	.111	405
92501	9.0	1553	417	5.9	411.1	20.0	12,830	416.6	.986	362	363	.152	400
100202	15.0	1545	409	9.6	399.4	33.3	21,360	415.6	.959	283	349	.361	395
110601	15.05	1540	404	9.6	394.4	33.4	21,290	410.1	.960	311	344	.270	391
91503	20.05	1476	340	13.0	327	44.5	26,550	352.7	.925	109	275	.840	336
102602	19.98	1502	366	13.0	353	44.4	27,440	379.7	.930	114	301	.838	360
91602	25.35	1513	377	16.5	360.5	56.3	36,990	412.2	.873	103	307	.892	390
110602	25.22	1510	374	16.5	357.5	56.0	36,570	407.5	.876	110	304	.865	390

H_{t1s}	C_{b1s}	C_{t1s}	C'_{b1s}	C'_{t1s}	H_{b18s}	H_{t18s}	C_{b18s}	C_{t18s}	F_M kips	F_C kips
91	1.079	1.021	1.085	1.027	94.8	95.9	1.014	1.011	0.7	19.4
108	1.037	1.016	1.038	1.017	112.0	113.6	1.004	.999	0	17.5
130	1.023	1.002	1.046	1.025	131.0	132.6	1.021	1.014	-47.1	9.5
194.5	1.040	1.006	1.067	1.031	199.0	200.1	1.010	1.005	-14.3	2.1
93.6	1.050	1.011	1.059	1.021	96.6	98.2	1.010	1.004	- 8.4	6.1
-----	-----	-----	-----	-----	190.5	191.6	1.017	1.012	-41.0	-11.0
93.6	.995	.986	1.022	1.013	94.6	95.7	1.009	1.005	-17.7	-10.8
161.5	.972	.960	1.035	1.023	163.5	164.1	1.013	1.008	-27.9	- 3.5
91	.958	.950	1.026	1.016	96.0	96.1	1.001	1.000	-11.5	- 0.9
169.5	.925	.914	1.036	1.023	171.7	172.8	1.012	1.007	-29.6	3.9
93.6	.929	.921	1.027	1.018	98.6	100.1	1.002	.997	-14.1	35.9
168.9	.886	.878	1.026	1.016	170.9	171.0	1.006	1.006	-11.3	16.9
87.7	.878	.867	1.028	1.016	92.1	92.2	1.000	1.000	14.5	36.8
128.0	.789	.785	1.045	1.039	131.1	131.2	1.019	1.019	-27.0	12.9
-----	-----	-----	-----	-----	85.2	85.8	1.000	.998	31.7	41.3
211.0	.718	.711	1.045	1.034	213.0	213.1	1.013	1.012	-19.3	1.3
145.8	.709	.702	1.075	1.065	157.3	157.4	.999	.999	-11.7	29.5
166.5	.531	.508	1.072	1.027	169.5	169.6	.997	.996	-12.8	14.4
196.1	.528	.511	1.061	1.026	196.6	196.7	1.022	1.021	-20.1	26.5
131.4	.087	-.009	-0.936	0.080	153.9	155.0	.976	1.020	162.7	54.3
328.5	-.055	-.034	0.680	0.430	337.5	338.6	1.33	1.44	-19.0	-30.4
257.5	.057	.062	-2.680	-2.880	267.0	268.1	.920	1.36	-17.9	-33.3

C_{TP}	H_{30}	C_{BP}	H_{b1p}	H_{t1p}	C_{b1p}	C_{t1p}	F_M kips	F_C kips
.126	337.8	.036	18	27	1.065	1.035	31	35.1
.221	351.6	.044	32	34	.995	.989	39	15.7
.319	356.6	.042	26.5	28	.969	.965	23	36.1
.845	366.4	.021	39	42	.910	.902	47	76.3
.892	386.5	-.033	38.5	41	.870	.864	84	87.2
.960	407.8	-.107	42	47	.787	.776	89	99.6
.950	396.3	-.920	60	64.5	.792	.780	42	69.1

C_{BF}	H_{b1p}	H_{t1p}	C_{b1p}	F_M kips	F_C kips
.0025	-1.4	4.0	1.043	94.4	91.1
-.0175	-2.5	4.5	1.008	86	59.6
.0126	2.5	3.5	0.997	33	53.1
.0402	1.5	4.5	1.001	56	48.2
.0335	5.5	5.5	.991	86	47.9
.0408	4.5	9.5	.990	67	53.2
.0336	13.0	16.0	.953	52	59.0
.0292	13.5	16.5	.952	21	58.6
.0113	20.5	22.5	.906	86	90.7
.0158	16.5	19.5	.920	99	94.9
-.0316	26.5	28.5	.850	146	105.8
-.0392	31.5	29.5	.840	132	104.3

TABLE C-5. OBSERVED MAXIMUM OSCILLATIONS AND CALCULATED FORCES

Gate Pos. ft	a_o ft	n Hz	V_1 fps	F_z kips
5	5.0	0.060	1.88	0.8
	11.5	0.090	6.50	9.7
	9.5	0.085	5.07	5.9
	7.5	0.069	3.25	2.4
	9.5	0.090	5.37	6.6
Ave.				5.1
10	11.5	0.043	3.11	2.1
	10.0	0.081	5.09	5.9
	12.0	0.043	3.24	2.4
Ave.				3.5
20	10.5	0.056	3.69	3.1
	11.0	0.065	4.49	4.6
	6.5	0.185	7.55	13.1
	12.5	0.045	3.53	2.9
	4.0	0.162	4.07	3.8
	9.0	0.130	7.35	12.4
Ave.				6.7
25	12.5	0.079	6.20	8.8
	1.8	0.286	3.14	2.3
	11.0	0.071	4.90	5.5
Ave.				5.5
30	15.0	0.090	8.48	16.5
	13.5	0.090	7.63	13.3
	12.5	0.104	8.16	15.3
	13.5	0.068	5.76	7.6
Ave.				13.2

TABLE C-6 DATA FOR FLOW COEFFICIENTS INTO AND OUT OF THE SERVICE GATE SHAFT, A_2 = .0199 FT^2 (MODEL)

Downward Flow

Gate Opening Percent	h_1 in.	h_2 in.	Q cfs	C_D	K_G
99.2	58.15	55.7	.0558	.773	
	57.05	53.0	.0747	.805	
	55.1	48.2	.0995	.822	
	53.0	43.0	.1212	.831	
	51.3	38.3	.1364	.821	
	46.0	29.05	.1556	.820	
			Ave	.820	.69
99.2	59.35	55.55	.0701	.780	
	57.8	51.35	.0939	.802	
	55.1	43.6	.1213	.776	
	53.7	39.6	.1413	.816	
	52.1	35.65	.1528	.817	
			Ave	.810	.72
75.0	60.25	58.6	.0488	.824	
	59.2	55.6	.0722	.825	
	57.65	51.55	.0971	.853	
	56.15	47.1	.1176	.848	
	54.65	43.1	.1337	.853	
	53.4	39.0	.1465	.862	
	51.95	35.8	.1580	.853	
			Ave	.855	.57
50.0	58.5	56.8	.0487	.810	
	57.6	54.9	.065	.858	
	55.8	50.3	.0917	.848	
	52.4	41.9	.1307	.875	
	49.7	35.5	.1465	.843	
			Ave	.860	.55

Gate Opening Percent	h_1 in.	h_2 in.	Q cfs	C_D	K_G
50.0	60.4	58.9	.0485	.858	
	59.1	55.4	.0763	.860	
	57.1	49.8	.1071	.860	
	55.2	44.7	.1294	.866	
	52.4	36.7	.1578	.864	
			Ave.	.865	.54
25.0	60.7	60.2	.0349	1.071	
	60.2	59.5	.0438	1.136	
	57.4	54.4	.0843	1.056	
	54.4	49.3	.1085	1.042	
	50.8	42.7	.1352	1.031	
	45.8	34.1	.1695	1.075	
			Ave	1.060	.23
0.0	59.7	59.4	.0315	1.245	
	58.0	51.4	.0694	1.944	
	56.5	55.5	.0843	1.829	
	53.6	52.3	.1057	2.010	
	49.4	46.6	.1318	1.696	
			Ave	1.85	.25*

Upward Flow

Gate Opening Percent	h_2 in.	h_1 in.	Q cfs	$\frac{V_2^2}{2g}$	K_G
99.2	60.6	59.9	.0482	.091	.64
	59.6	58.3	.0682	.183	.59
	57.9	55.4	.0951	.355	.585
	55.6	51.6	.1231	.595	.56
	55.3	51.1	.1258	.619	.555
				Ave	.56
75.0	60.8	60.25	.0422	.07	.66
	59.7	58.7	.0649	.165	.503
	57.45	55.0	.0990	.384	.531
	55.0	51.4	.1261	.625	.48
				Ave	.50
50.0	60.3	59.5	.0529	.11	.605
	57.8	55.2	.0941	.348	.625
	56.4	52.6	.1132	.505	.628
	55.35	50.9	.1254	.617	.60
				Ave	.61
25.0	60.45	59.4	.0504	.0995	.715
	59.4	57.45	.0708	.197	.595
	57.65	53.95	.0975	.373	.59
	55.1	49.0	.1257	.62	.55
				Ave	.59
0.0	61.05	60.75	.0339	.045	.555
	59.6	58.3	.0675	.178	.607
	58.3	56.2	.0864	.293	.596
	57.0	54.0	.1040	.424	.59
	55.3	51.1	.1231	.596	.587
				Ave	.59

*Calculated from $2gH_L/V_2^2$

TABLE C-7. SUBATMOSPHERIC PRESSURE HEADS.

Submerged Condition						Unsubmerged Condition									
Run No.	Percent Gate Opening	Piezo. No.	Pressure Head	Piezo. No.	Pressure Head	Run No.	Percent Gate Opening	Piezo. No.	Pressure Head	Piezo. No.	Pressure Head	Piezo. No.	Pressure Head	Piezo. No.	Pressure Head
112301	.55	3-47	-32.0*			112303	.55	None							
121301	2.22	3-47	-32.0*	3-48	-2.8	121302	2.22	1-46	- 9.2	2-35	- 1.1	3-47	-32.0	3-48	-32.0
110901	4.44	None						3-49	-19.6						
110201	11.0	None				110902	4.44	1-46	-32.0	1-47	- 6.6	2-35	-16.7	3-49	-32.0
91401	11.33	None				110202	11.0	1-47	- 5.6						
92502	20.0	None				92503	11.1	1-47	- 6.1	2-29	-32.0	2-35	-32.0		
91402	22.6	None				92501	20.0	2-29	-32.0	2-35	-32.0				
100201	33.3	None				100202	33.3	None							
91501	34.6	3-46	- 9.2			110601	33.4	2-27	-11.5	2-35	-32.0*	3-46	-32.0		
102301	44.4	3-46	-32.0*			102602	44.4	2-27	-16.6	2-35	-32.0	2-45	-11.3	2-59	-15.2
91502	44.8	3-46	-32.0*	3-47	-6.1			3-46	-32.0	3-47	-27.1				
102302	55.4	3-46	-32.0*			91503	44.6	2-27	-13.0	2-35	-32.0	2-59	-12.6	3-46	-32.0
91601	56.0	3-46	-32.0*					3-47	-32.0						
92402	66.9	3-46	-32.0*			110602	56.0	1-15	-32.0	2-27	-18.1	2-35	-32.0	3-46	-32.0
91603	67.1	3-46	-32.0*			91602	56.3	1-15	-13.6	2-27	-25.1	2-28	- 4.2	2-35	-32.0
102303	77.8	None						2-36	- 3.3	2-41	- 6.0	3-46	-32.0	3-47	- 5.1
92101	78.4	3-46	-32.0*			103002	106.7	2-27	-12.4	2-12	-32.0	2-13	-32.0	2-30	-15.4
102601	88.9	None						2-35	-32.0	2-36	-32.0	2-37	-26.0		
92102	89.1	None				92401‡	66.9	3-46	-32.0	3-47	- 4.0				
112302†	99.8	2-36	-10.2												
92103	106.7	None													
103001	106.7	None													

*Lowest subatmospheric pressure head possible.

†Unequal gate opening.

‡Gate partially submerged.